NOTICE

The quality of this microform is heavily dependent upon the quality of the original thesis submitted for microfilming. Every effort has been made to ensure the highest quality of reproduction possible.

If pages are missing, contact the university which granted the degree.

Some pages may have indistinct print especially if the original pages were typed with a poor typewriter ribbon or if the university sent us an inferior photocopy.

Reproduction in full or in part of this microform is governed by the Canadian Copyright Act, R.S.C. 1970, c. C-30, and subsequent amendments.

AVIS

La qualité de cette microforme dépend grandement de la qualité de la thèse soumise au microfilmage. Nous avons tout fait pour assurer une qualité supérieure de reproduction.

S'il manque des pages, veuillez communiquer avec l'université qui a conféré le grade.

La qualité d'impression de certaines pages peut laisser à désirer, surtout si les pages originales ont été dactylographiées à l'aide d'un ruban usé ou si l'université nous a fait parvenir une photocopie de qualité inférieure.

La reproduction, même partielle, de cette microforme est soumise à la Loi canadienne sur le droit d'auteur, SRC 1970, c. C-30, et ses amendements subséquents.

Canada

WAVE INDUCED RESPONSE OF SEA FLOOR DEPOSITS:

A SIMPLE MODEL FOR SANDS AND NONLINEAR ANALYSIS BY FEM.

Qingshi Yang

A Thesis

in

The Department

of

Civil Engineering

July 1990

Canada

CONCORDIA UNIVERSITY
Division of Graduate Studies

This is to certify that the thesis prepared

By: **Qingshi Yang**
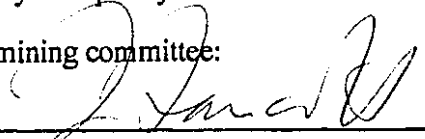
Entitled: **WAVE INDUCED RESPONSE OF SEA FLOOR DEPOSITS:**
A SIMPLE MODEL FOR SANDS AND NONLINEAR ANALYSIS BY FEM.

and submitted in partial fulfilment of the requirements for the degree of
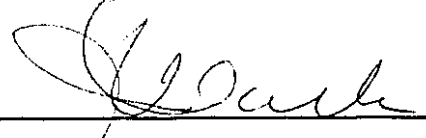
Doctor of Philosophy

complies with the regulations of this University and meets the accepted standards
with respect to originality and quality.
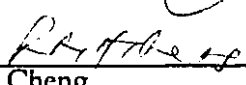
Signed by the final examining committee:
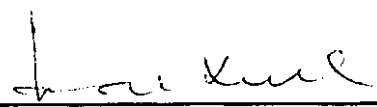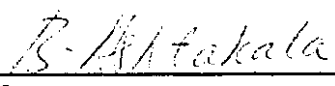
_____ Chair
Dr. T. Fancott

_____ External Examiner
Dr. J. I. Clark

_____ Examiner
Dr. R. Cheng
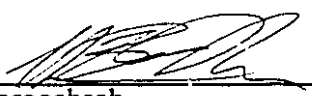
_____ Examiner
Dr. K. Ha-Huy

_____ Examiner
Dr. B. Ashtakala
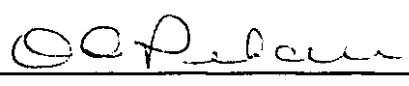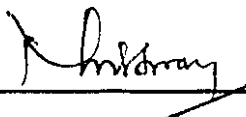
_____ Thesis Co-Supervisor
Dr. M. M. Douglass

_____ Thesis Co-Supervisor
Dr. H. B. Poorooshasb

Approved by _____ Chair of Department

_____Sept____ l(___1990___ _____ Dean of Faculty

ABSTRACT

WAVE INDUCED RESPONSE OF SEA FLOOR DEPOSITS:
A SIMPLE MODEL FOR SANDS AND NONLINEAR ANALYSIS BY FEM.

Qingshi Yang , Ph.D.
Concordia University, 1990

This dissertation analyzes the ocean wave-induced response of seafloor deposits. The linear wave theory is introduced for determination of the wave-induced pressure at the mud line. The seafloor deposit is assumed to be a saturated porous medium modelled by a two-phase system. The theory of mixture is used to derive the coupled governing equations.

A simple material constitutive model is proposed based on the generalized plasticity-bounding surface formulation. Some comparisons of the model tests with experimental results are made. The simple model is capable of simulating both loose and dense sand behavior under monotonic and cyclic loading, drained and undrained conditions.

A nonlinear finite element analysis procedure is presented. A fictitious freedom technique is used to treat the different nodal degrees of freedom due to the composition of coupled fields. A non-symmetric frontal solver subroutine is developed to accommodate the asymmetry due to the non-associated plastic flow rule. A simple artificial boundary is suggested to deal with the unbounded domain, which is easy to implement in the finite element program and universal to apply to nonlinear analysis.

One important conclusion obtained from the numerical analyses is the influence of the coefficient of permeability on the susceptibility of the sand mass to liquefaction; for high values of permeability even a loose sand mass need not liquefy. This is in direct contrast to the commonly held view that the liquefaction potential is a function of density only.

Two example cases are studied in detail. The first example examines the seabed response to the wave train at a pipeline site in Lake Ontario (Christian et al., 1974; Nataraja and Gill, 1983), where the deposit was measured to be loose and medium dense. The second example investigates the seafloor behavior under a storm wave at the Ekofisk tank site in the North Sea (Lee and Focht, 1975; Nataraja and Gill, 1983). Here the deposit was reported to be dense. The numerical analyses predict the susceptibility of the two sites to liquefaction which reflects the real situations. It helps build confidence in the numerical procedure adopted in this study and lends it credibility.

To

My Father

And

My Mother

ACKNOWLEDGEMENTS

CONTENTS

LIST OF FIGURES AND TABLES

1

INTRODUCTION

1.1 GENERAL

The solution of geotechnical engineering problems is complicated for several reasons. First, geotechnical problems generally involve large scale structures and/or unbounded domain. Second, soil exists in general as a nonhomogeneous multi-phase, solid-fluid interative system. Third, the behaviour of the soil skeleton is highly nonlinear, anisotropic and hysteretic. Under these conditions, the analytical solutions of geotechnical problems have necessarily involved many simplifying assumptions. However, the development of computing facilities has now made it possible to solve these complicated problems more exactly using numerical methods.

One problem which has received considerable attention in geotechnical and marine foundation engineering is the ocean wave induced response of seafloor deposits. The stability and deformation of the seafloor under the action of storm waves are important considerations in the design of pipelines, anchors and offshore structures such as gravity and pile supported platforms.

Various methods including empirical, analytical and numerical procedures for predicting the response of marine deposits have been proposed. Noticeably different methods can be categorized as the total stress approach and the effective stress approach.

1

In all cases, the seafloor is considered as being subjected to an ocean wave induced plane pressure wave, travelling across the surface of the underlying deposits. In wave response studies, it is customary to neglect the effects of inertia and damping (pseudo-static analysis).

Henkel (1970) was one of the first to carry out a total stress analysis for one-phase system seafloor under wave loads following the classical procedure of limit equilibrium slope stability analysis. Generally the total stress method does not account for the changes in pore water pressure explicitly. The pore water flow in a rigid porous bed is governed by the Laplace equation (Putnam, 1949 and Lin, 1977).

Analytical solutions of effective stress analysis for two-phase coupled response of a poro-elastic bed to water wave were provided by Madsen (1978) and Yamamoto (1978) applying the Biot theory of consolidation.

Assuming linear elastic behavior Seed and Rahman (1978) developed a methodology for wave induced liquefaction analysis using an uncoupled scheme. This was accomplished by solving the usual continuity equation of flow in conjunction with a pore-water pressure generation model proposed by Seed et al. (1976). The combined effects of the pore pressure generation and dissipation cause the pore pressure build-up which depends on the storm characteristics, i.e. wave height, period and duration, and the drainage and compressibility characteristics of the seafloor deposits.

The needs grow for numerical techniques and material constitutive relations which efficiently and accurately model the complex behavior of soil systems. Over the past decades much effort has been devoted to constitutive modelling of the soil behavior under cyclic and transient loading conditions such as that caused by earthquake, traffic and ocean waves.

The observation of the behaviour of sand from experimental results such as accumulation of permanent deformation, existence of hysteresis loops, etc., suggests that

2

the behavior of soil can be modelled by means of plasticity theory. Moreover, the observation of the dissipation of energy, even at low stress levels, implies that the soil behavior within a classical yield surface cannot be treated as purely elastic. A more sophisticated material model should be adopted such as the bounding surface model (Krieg, 1975; Dafalias and Popov, 1975; Dafalias and Herrmann, 1982) and the two-surface model (Mroz et al., 1978,1979; Poorooshasb and Pietrusczcak, 1985, 1986) where the attention has been focused on the progressive build up of excess pore water pressure during cyclic or transient loading. The developed pore pressure may become almost equal to the confining pressure and this phenomenon is referred to as liquefaction (for loose sand) or cyclic mobility (for dense sand). So far, the realistic modelling of the non-linear transient dynamic behaviour of soils is still an active field which calls for further experimental and theoretical research.

Transient analyses of the response of seafloor deposits to ocean waves have until recently been solved by very simple models. Traditionally, the finite element method is used assuming elastic soil behaviour (e.g. Dunham et al., 1971; Gatmiri, 1990). An equivalent linear method has been developed (Seed et al., 1973; Siddharthan, 1987) in which the nonlinear characteristics of the soil skeleton are accounted for by using equivalent linear soil properties, and an iterative procedure is used to obtain modulus and damping values compatible with the effective strains computed in each zone of the soil mass.

Some simplified procedures were proposed for wave-induced liquefaction analysis. (Seed and Rahman, 1978; Finn and Lee, 1979; Nataraja and Gill, 1979, 1983). These approximate procedures actually are modifications of those for seismic response analyses (Seed and Idriss, 1971). The seismic shear strength curve developed by Seed (1979) was extrapolated to ocean wave problems. The fairly simple step-by-step procedures can be used in ocean wave-induced liquefaction problems as a first check if a sophisticated

3

analysis is required. It is worth noting that certain differences exist between earthquake excitation and wave loading although both are cyclic in nature. Ocean wave periods and duration are considerably longer than the earthquake periods and duration. Ocean wave loadings are imposed at the surface of the seafloor as a pressure load rather than earthquake excitation at some lower boundaries as base shaking. Ishihara (1983) has indicated that the ground motion developed in soil deposits during an earthquake is attributed to the upward propagation of shear waves from an underlying rock formation. A soil element is deformed in the simple shear mode. However, the soil element under the seabed is stressed in a more complicated manner during the passage of a wave train. Therefore, the cyclic stresses induced in the seabed deposits due to water wave travelling overhead are characterized by a continuous changing of the principal stress values and their directions. Therefore, one must be cautious in using these procedures.

It is possible to develop a more rigorous nonlinear transient analysis procedures. In an attempt to analyze the liquefaction susceptibility of the seafloor deposits to wave action, Poorooshasb, Ishihara and Yang (1987), Poorooshasb, Yang and Clark (1990) have carried out the finite element nonlinear transient analyses, in which the soil was considered as a coupled two phase system modelled by a two-surface plastic constitutive law.

1.2 PURPOSE OF STUDY

For many constitutive models currently available for soils, a common drawback is that they are applicable only to a specific boundary condition. Monotonic and cyclic loading are usually treated separately so that an artificial distinction is made between the two types of loading in order to suit the specific requirements of the boundary value problems which are to be solved.

4

For a genuine representation of saturated soil the single phase theory is inadequate. Two phase theory for consolidation was first introduced by Terzaghi. Subsequently Biot generalized Terzaghi's work to three dimensions, and the so-called Biot theory has been further extended to accommodate the different nonlinear constitutive relations for soil by Zienkiewicz and Bettess (1982).

The primary purposes of this study are to

(1) develop a simple constitutive model in terms of effective stress within a more fundamental framework of the generalized plasticity-bounding surface formulation such that the same model could be applicable to monotonic or cyclic, drained or undrained, or any other form of loading condition in three dimensions.

(2) develop a numerical procedure incorporating the proposed constitutive model for nonlinear transient analyses of two phase coupled problems of effective stress and pore pressure interaction under wave loads. The finite element method is employed.

(3) work out examples relevant to wave induced response of seafloor deposits. Standing waves and two example cases of travelling waves passing over homogeneous seafloor deposits are studied in detail.

1.3   STRUCTURE OF THE THESIS

1. The general coupled transient, dynamic field equations for a two-phase soil system based on the theory of mixture are presented. Then they are reduced to the nonlinear transient consolidation equations for analysis of the ocean wave induced response of sea floor deposits. (Chapter 2)

5

2. The soil plasticity is historically reviewed. First, the general formulation of classical plasticity is derived, then the concepts of isotropic, kinematic and mixed hardening and their generalizations on the cap models, the nested yield surface models and the bounding surface models are briefly illustrated. (Chapter 3)

3. Zienkiewicz's generalized plasticity concept is introduced to develop a simple constitutive model for sands. The proposed model is first derived in the triaxial configuration based on the generalized plasticity-bounding surface formulation. (Chapter 4)

4. The proposed material model is also a simplified version of the two-surface elasto-plastic model developed by Poorooshasb and Pietruszczak (1985, 1986). Non-associative flow rule is adopted in the simple model. The global plastic potential is similar to that used in the two-surface model. The idea of reflecting local plastic potential is retained implicitly by a vanishing yield surface which significantly reduces the numerical complexity of the model. (Chapter 4)

5. The formulations of the proposed model are generalized from the triaxial configuration to the full effective stress space to describe the soil behaviour along any possible stress path. (Chapter 4)

6. The computer program MDTEST is developed for numerical implementation of the model. There are three different versions: MDTEST 1, MDTEST 2 and MDTEST 3 serve for stress controlled drained path, stress controlled undrained path and strain controlled path, respectively. The algorithm for the stress controlled drained path is straightforward. The effective stress increment can be controlled as an independent variable. However, for stress controlled undrained path, the internal constraint of undrained

condition must be satisfied. Thus, the effective stress increment cannot be controlled independently. A modified constitutive relation in terms of the total stress increment and strain increment should be derived.

The state variables are computed for a given deformation history in the displacement type finite element method. The precision of the integration at a local level of the constitutive equations for the strain controlled path has a direct impact on the overall accuracy of the analysis. Most of the algorithms can be considered as particular cases of the generalized trapezoidal rule or midpoint rule (Ortiz and Popov, 1985) in which the update process splits into an elastic predictor of trial state and a plastic corrector of return mapping that restores incremental plastic consistency. (Chapter 4)

7. The loose and the dense sand behaviour under monotonic and cyclic loading, drained and undrained conditions are simulated by a number of numerical model tests. Comparison is made with experimental results whenever possible to establish confidence in applying this simple model to initial-boundary value problems. (Chapter 4).

8. The methods of finite element spatial discretization of the field equations are described. The virtual principle and the weighted residual method are used to derive the semi-discrete finite element equations. Time integration schemes such as field elimination, staggered method and direct integration of the resulting coupled nonlinear system are discussed. A fictitious freedom technique is proposed to treat the different nodal degrees of freedom. Based on Iron's symmetric frontal solver, a non-symmetric frontal solver subroutine is developed to accommodate the asymmetry due to the non-associated plastic flow rule adopted in the material model. (Chapter 5)

9. The sea floor is considered as being subjected to an ocean wave induced, plane pressure wave travelling across the surface of the underlying deposits. The linear wave theory is introduced for determining the wave-induced pressure at sea bottom (mud line). (Chapter 6)

10. Numerical methods for an unbounded domain are investigated. A simple artificial boundary is applied in dealing with the wave-induced response of seafloor deposits. The suggested artificial boundary is derived from the Taylor series without any problem dependence. It simply states that the boundary values at current time could be predicted by extrapolation of the values of the variable in the vicinity of the boundary at past time. Thus, it is universal and can be used for nonlinear analysis. It is also very easy to implement in finite element programs. (Chapter 7)

11. Finite element nonlinear transient analysis program PCPSTAD and PCPTRAV are developed. An incremental iteration procedure is used for the solution of the global nonlinear system.The numerical formulation of the proposed simple constitutive model and the suggested simple artificial boundary are implemented into the computer program to solve the two-phase coupled, nonlinear, unbounded domain problem.

Two relevant examples are worked out. The standing wave and the travelling wave train passing overhead the homogeneous seabed are studied and the wave-induced responses of seafloor deposits are analyzed. The effects of various factors involved, especially the coefficient of permeability, are examined. (Chapter 8)

12. Concluding remarks are made and further work is suggested. (Chapter 9)

2

MECHANICS OF SATURATED POROUS MEDIA

2.1 INTRODUCTION

The analysis of dynamic transient phenomena in fluid-saturated porous media is of great interest in geophysics and geotechnical engineering. Fluid saturation of a porous solid skeleton introduces a time dependence into the response to applied loads. The classical early work of Terzaghi (1943) on soil consolidation was followed by the more explicit work of Biot (1941, 1955, 1956, 1962, 1963). Biot first formulated linear governing equations for the interaction of the fluid and solid phases. It was later extended, by himself, to the dynamic range using a mechanistic modelling approach. Since then his theory and results have been the standard reference and the basis for most subsequent investigations in acoustics, geophysics and geomechanics.

Modern treatment of mixture was first tried by Truesdell (1960). He introduced three principles:

(1) All properties of the mixture must be mathematical consequences of properties of the constituents.

(2) So as to describe the motion of the constituent, one may imagine it isolated from the rest of mixture, provided one will allow properly for the actions of the other constituents upon it.

(3) The motion of the mixture is governed by the same equations as is a single phase body.

The development of general nonlinear equations has later become fashionable using the theory of mixtures, such as Eringen and Ingram (1965, 1967), Green and Naghdi (1965), Bowen (1976, 1982) and Prevost (1980). A physical derivation of the full formulation and the validity of various simplifying approximations have been given by Zienkiewicz et al. (1977, 1980, 1982, 1984).

In the following sections, the general coupled transient, dynamic field equations for a two-phase soil system based on the theory of mixture are presented. Then they are reduced to the nonlinear transient consolidation equation for analysis of the ocean wave induced response of seabed deposits.

2.2 EFFECTIVE STRESS AND CONSTITUTIVE EQUATION

Saturated soil is a two-phase mixture consisting of solid particles and water in the pores which is idealized in Figure 2.1.

Saturated Soil   Solid Phase   Fluid Phase
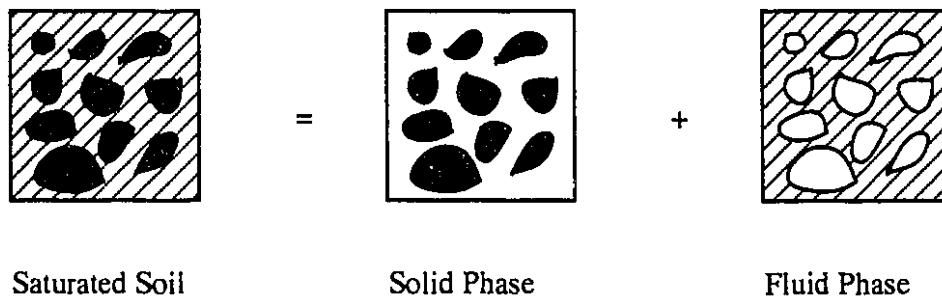
Figure 2.1 Saturated soil as a two-phase mixture.

10

For each constituent α ($\alpha = s, f$ for solid and fluid phases respectively):

$n^\alpha = n^\alpha (x_i, t) = dV^\alpha / dV$ = volume fraction occupied by the α phase.

ρ_α = microscopic mass density

$\rho^\alpha = n^\alpha \rho_\alpha$ = macroscopic average mass density (no summation involved)

u^α_i = displacement of the α phase

v^α_i = velocity of the α phase

σ^α_{ij} = partial (Cauchy) stress of the α phase

Thus,

$$n^s + n^f = 1$$

$$n^f = n = \text{porosity} \tag{2.1}$$

$$n^s = 1 - n$$

$$\rho = \rho^s + \rho^f = (1-n)\,\rho^s + n\rho^f \tag{2.2}$$

The relative displacement, velocity and acceleration of the fluid vis-a-vis the solid skeleton are

$$w_i = n\,(u^f_i - u^s_i)$$

$$\dot{w}_i = n\,(v^f_i - v^s_i) = n\,(\dot{u}^f_i - \dot{u}^s_i) \qquad \text{(filter velocity)} \tag{2.3}$$

$$\ddot{w}_i = n\,(a^f_i - a^s_i) = n\,(\dot{v}^f_i - \dot{v}^s_i) = n\,(\ddot{u}^f_i - \ddot{u}^s_i)$$

The partial stress tensor σ^f_{ij} corresponding to the fluid phase is assumed to be

$$\sigma^f_{ij} = n^f\,p\,\delta_{ij} = n\,p\,\delta_{ij} \tag{2.4}$$

11

where p is the pore water pressure, δ_{ij} is the Kronecker delta and compressive stress and strain are taken as positive. However, with the total stress σ_{ij} given by

$$\sigma_{ij} = \sigma^s_{ij} + \sigma^f_{ij} \tag{2.5}$$

the partial stress tensor σ^s_{ij} corresponding to the solid phase is not the effective stress σ'_{ij} of classical soil mechanics (Terzaghi, 1943), which is defined as

$$\sigma'_{ij} = \sigma_{ij} - p\,\delta_{ij} \tag{2.6}$$

from (2.4), (2.5) and (2.6)

$$\sigma^s_{ij} = \sigma'_{ij} + (1-n)\,p\,\delta_{ij} \tag{2.7}$$

$$\sigma_{ij} = \sigma^s_{ij} + \sigma^f_{ij} = \sigma'_{ij} + p\,\delta_{ij} \tag{2.8}$$

Terzaghi (1943) showed that the definition of effective stress allows a rational treatment of the stress-strain behavior. Terzaghi's principle of effective stress states that all measurable effects of a change in strain in soils (such as compression, distortion) are due to changes in effective stress. The consequence is that the constitutive laws which describe soil behavior must refer to effective stress (rather than total stress). A rate-type constitutive equation is assumed to describe the behavior of the porous solid skeleton, of the following form (the summation convention over repeated indices applies hereafter):

$$-D^s_t\,(\sigma'_{ij}) = D_{ijkl}\,\nabla_l v^s_k = D^s_{ijkl}\,\nabla_{(l}\,v^s_{k)} + D^G_{ijkl}\,\nabla_{[l}\,v^s_{k]} \tag{2.9}$$

where

$$D^\alpha_t = \frac{D^\alpha}{Dt} = \frac{\partial}{\partial t} + v^\alpha_j\,\nabla_j = \text{material derivative following the } \alpha \text{ constituent}$$

$\nabla_{(l}\,v^s_{k)}$ = symmetric part of solid relocate gradient

12

$\nabla_{[l} v^s{}_{k]}$ = skew-symmetric part of solid velocity gradient

$D^G{}_{ijkl}$ is the constitutive tensor for the rotational component of the stress rate:

$$D^G{}_{ijkl} = - (\sigma'_{il} \delta_{jk} + \sigma'_{jl} \delta_{ik} - \sigma'_{ik} \delta_{jl} - \sigma'_{jk}\delta_{il}) / 2 \qquad (2.10)$$

This tensor plays a role in finite deformation theory only and is ignored in the following. $D^s{}_{ijkl}$ is an objective, material constitutive tensor. For linear isotropic elastic material

$$D^s{}_{ijkl} = \lambda^s \delta_{ij} \delta_{kl} + \mu^s (\delta_{ik} \delta_{jl} + \delta_{il} \delta_{jk}) \qquad (2.11)$$

where λ^s, μ^s = Lame elastic constants.

The strain is given for small deformation by

$$\varepsilon_{ij} = - (u^s{}_{i,j} + u^s{}_{j,i}) / 2$$

$$\dot{\varepsilon}_{ij} = - (v^s{}_{i,j} + v^s{}_{j,i}) / 2 = - \nabla_{(i} v^s{}_{j)} \qquad (2.12)$$

where $u^s{}_{i,j} = \partial u^s{}_i / \partial x_j$, etc.

Thus, the constitutive equation is

$$\dot{\sigma}'_{ij} = D^s{}_{ijkl} \dot{\varepsilon}_{ij} \qquad (2.13)$$

For a rate-independent plastic model, it is appropriate to write in the incremental form

$$d \sigma'_{ij} = D^s{}_{ijkl} d\varepsilon_{kl} \qquad (2.14)$$

where $D^s{}_{ijkl}$ is the tangent modulus tensor.

13

2.3 BALANCE LAWS AND SYSTEM OF GOVERNING EQUATIONS

2.3.1 Balance of Mass

$$D^\alpha_t \rho^\alpha + \rho^\alpha \nabla_j v_j{}^\alpha = \partial_t \rho^\alpha + \nabla_j (\rho^\alpha v_j{}^\alpha) = 0 \qquad (\alpha = s, f) \quad (2.15)$$

2.3.2 Balance of Linear Momentum

$$-\nabla_j \sigma^\alpha{}_{ij} + \rho^\alpha b_i + R^\alpha{}_i = \rho^\alpha a^\alpha{}_i \qquad (\alpha = s, f) \quad (2.16)$$

In the above set of equations the notation is as those in section 2.2 and

b_i = body force per unit mass

$a^\alpha{}_i$ = acceleration of the α phase

$R^\alpha{}_i$ = momentum supply to the α phase from the other phase

The momentum interaction is assumed to consist of diffusion and dilatation contributions,

$$R^s{}_i = -R^f{}_i = -d_{ij}(v^s{}_j - v^f{}_j) - p \nabla_j n \qquad (2.17)$$

Where d_{ij} is a symmetric, positive definite second-order tensor. The first term in (2.17) is sometimes called the 'Stokes drag', (See e.g. Bowen, 1976).

2.3.3 Full System of Equations

The problem of the dynamic transient response of a two-phase soil system can be represented as the following initial-boundary-value problem:

Let Ω denote the domain occupied by the two phase structure and Γ its boundary.

Find the soil displacement field $u^s{}_i$ (x_i, t) and fluid velocity field $v^f{}_i$ (x_i, t) in the domain

14

$\Omega \in R^{NSD}$ (NSD= number of space dimensions), such that they both satisfy equilibrium equation (2.16), continuity equation (2.15) and constitutive equation (2.13), together with the boundary conditions

$$u^s_i = u^s_i \big|_\gamma \qquad \text{on } \Gamma_{su}$$

$$v^f_i = v^f_i \big|_\gamma \qquad \text{on } \Gamma_{fv}$$

$$(\sigma'_{ij} + (1 - n) p \, \delta_{ij}) \, n_j = h^s_i \big|_\gamma \qquad \text{on } \Gamma_{sh}$$

$$n \, p \, \delta_{ij} \, n_j = h^f_i \big|_\gamma \qquad \text{on } \Gamma_{fh} \qquad (2.18)$$

and the initial conditions

$$u^s_i (0) = u^s_{i0}$$

$$v^s_i (0) = v^s_{i0}$$

$$v^f_i (0) = v^f_{i0} \qquad (2. 19)$$

Γ_{su}, Γ_{fv}, Γ_{sh}, Γ_{fh} are the parts of the boundary on which the displacement and traction for the solid and fluid respectively are prescribed. They satisfy the following conditions:

$$\Gamma_{su} \cup \Gamma_{sh} = \Gamma \qquad , \qquad \Gamma_{su} \cap \Gamma_{sh} = 0$$

$$\Gamma_{fv} \cup \Gamma_{fh} = \Gamma \qquad , \qquad \Gamma_{fv} \cap \Gamma_{fh} = 0 \qquad (2.20)$$

15

2.4 SOME REDUCED SYSTEMS OF APPROXIMATIONS

2.4.1 The u-w Formulation (Biot theory)

Substituting equation (2.4) and (2.7) in equation (2.16) and (2.17) for the solid phase and fluid phase respectively two equilibrium equations are obtained.

$$- \nabla_j \sigma'_{ij} - (1\text{-}n) \nabla_i p + \rho^s b_i - d_{ij} (v^s_j - v^f_j) = \rho^s a^s_i \tag{2.16s}$$

$$- n\nabla_i p + \rho^f b_i + d_{ij} (v^s_j - v^f_j) = \rho^f a^f_i \tag{2.16f}$$

The overall equilibrium equation is derived by adding equation (2.16s) and (2.16f) and using equation (2.2) and (2.3)

$$- \nabla_j \sigma'_{ij} - \nabla_i p + \rho b_i = - \nabla_j \sigma_{ij} + \rho b_i = \rho \ddot{u}^s_i + \rho_f \ddot{w}_i \tag{2.21}$$

The fluid equilibrium equation (2.16f) could be rearranged with the notation

$$d_{ij} / n^2 = \gamma_f k^{-1}_{ij} \tag{2.22}$$

as

$$- \nabla_i p + \rho_f b_i = \gamma_f k^{-1}_{ij} \dot{w}_j + \rho_f \ddot{u}^s_i + \rho_f \ddot{w}_i / n \tag{2.23}$$

Rewriting equation (2.15) for the solid and fluid phases respectively,

$$(1\text{-}n) \partial_t \rho_s + \rho_s \partial_t (1\text{-}n) + \rho_s \nabla_i ((1\text{-}n) v^s_i) + (1\text{-}n) v^s_i \nabla_i \rho_s = 0 \tag{2.15s}$$

$$n \partial_t \rho_f + \rho_f \partial_t n + \rho_f \nabla_i (n v^f_i) + n v^f_i \nabla_i \rho_f = 0 \tag{2.15f}$$

Dividing equation (2.15s) and (2.15f) by f_s and f_f respectively, and adding them results in

$$\nabla_i v^s_i + \nabla_i (n (v^f_i - v^s_i)) + (\partial_t \rho_f + v^f_i \nabla_i \rho_f)n / \rho_f + (\partial_t \rho_s + v^s_i \nabla_i \rho_s) (1\text{-}n) / \rho_s = 0$$

that is

$$- \dot{\varepsilon}_{ii} + \dot{w}_{i,i} + n \dot{\rho}_f / \rho_f + (1\text{-}n) \dot{\rho}_s / \rho_s = 0 \tag{2.24}$$

The solid grains may be assumed to be incompressible, i.e. $\dot{\rho}_s = 0$.

According to conservation of mass,

$$\frac{D(\rho_f V^f)}{Dt} = \dot{\rho}_f V^f + \rho_f \dot{V}^f = 0 \qquad (2.25)$$

$$\dot{\rho}_f / \rho_f = - \dot{V}^f / V^f = \dot{p} / K_f$$

where K_f defining the bulk modulus of the fluid, represents the rate of fluid contraction.
Therefore, the continuity equation (2.24) yields

$$- \dot{w}_{i,i} = - \dot{\varepsilon}_{ii} + \dot{p} \, n / K_f \qquad (2.26)$$

Thus the generalized Biot's equations (2.8), (2.12), (2.14), (2.21), (2.23) and (2.26) have been derived from the theory of mixture. For easy reference, this system is renumbered in the set of equations (2.27) where u^s_i and D^s_{ijkl} have been replaced by u_i and D_{ijkl}, respectively.

$$\sigma_{ij} = \sigma'_{ij} + p \, \delta_{ij} \qquad (2.27a)$$

$$d\varepsilon_{ij} = - (du_{i,j} + du_{j,i}) / 2 \qquad (2.27b)$$

$$d \, \sigma'_{ij} = D_{ijkl} \, d\varepsilon_{kl} \qquad (2.27c)$$

$$- \nabla_j \sigma_{ij} + \rho b_i = \rho \, \ddot{u}^s_i + \rho_f \ddot{w}_i \qquad (2.27d)$$

$$- \nabla_i p + \rho_f b_i = \gamma_f k^{-1}{}_{ij} \, \dot{w}_j + \rho_f \ddot{u}_i + \rho_f \ddot{w}_i / n \qquad (2.27e)$$

$$- \dot{w}_{i,i} = - \dot{\varepsilon}_{ii} + \dot{p} \, n / K_f \qquad (2.27f)$$

It may be noted that equation (2.27 a,b,c,f) can be used to eliminate σ_{ij}, σ'_{ij}, ε_{ij} and p , leaving two sets of equations, (2.27d) and (2.27e), for the determination of the primary set of variables u_i and w_i . The solution of its discretized equations in the linear case has been adopted as the basic formulation used by Ghaboussi and Wilson (1972).

17

2.4.2 The u-p Formulation (medium-speed phenomena)

The use of **u-w** formulation requires six variables in three dimensions (or four in two dimensions). It is often preferable to reduce the problem by retaining u_i and p as basic variables. If $\ddot{w}_i$ terms are negligible in dealing with medium-speed phenomena, the elimination of the variable w_i is simple. Now solving equation (2.27e) for w_i with $\ddot{w}_i$ term dropped, results in

$$-\dot{w}_i = (k_{ij} / \gamma_f) (\nabla_j p - \rho_f b_j) + (k_{ij} / \gamma_f) \rho_f \ddot{u}^s_i \tag{2.28}$$

which upon substitution in Equation (2.27f), yields;

$$\sigma_{ij} = \sigma'_{ij} + p\, \delta_{ij} \tag{2.29a}$$

$$d\varepsilon_{ij} = - (du_{i,j} + du_{j,i}) / 2 \tag{2.29b}$$

$$d\,\sigma'_{ij} = D_{ijkl}\, d\varepsilon_{kl} \tag{2.29c}$$

$$- \nabla_j \sigma_{ij} + \rho b_i = \rho\, \ddot{u}_i \tag{2.29d}$$

$$\nabla_i (k_{ij} / \gamma_f) (\nabla_j p - \rho_f b_j) + \dot{\varepsilon}_{ii} = - \nabla_i ((k_{ij} / \gamma_f) \rho_f \ddot{u}_i) + \dot{p}\, n / K_f \tag{2.29f}$$

2.4.3 Consolidation Equation (slow phenomena)

If the process is so slow that all the acceleration forces are found to be negligible, i.e.

$$\ddot{w}_i \rightarrow 0 , \qquad \ddot{u}^s_i \rightarrow 0 , \qquad \ddot{u}^f_i \rightarrow 0$$

then the fluid equilibrium equation (2.16f) or (2.28) reduces to Darcy's law (1856) as

$$\dot{w}_i = n\, (v^f - v^s) = - (k_{ij} / \gamma_f) (\nabla_j p - \rho_f b_j) \tag{2.30}$$

with

$$k_{ij} = n^2\, \gamma_f\, d^{-1}_{ij} = \text{Darcy permeability tensor.}$$

18

$k_{ij} = k \, \delta_{ij}$ for an isotropic medium, k is the permeability coefficient (unit : L / T).

$\gamma_f = \rho_f \, g$ = unit weight of the fluid.

g = acceleration of gravity.

By omitting terms containing $\ddot{u}_i$ from **u-p** formulation (2.29), the well-known equations of consolidation are obtained,

$$\sigma_{ij} = \sigma'_{ij} + p \, \delta_{ij} \qquad\qquad (2.31a)$$

$$d\varepsilon_{ij} = - (du_{i,j} + du_{j,i}) / 2 \qquad\qquad (2.31b)$$

$$d \, \sigma'_{ij} = D_{ijkl} \, d\varepsilon_{kl} \qquad\qquad (2.31c)$$

$$- \nabla_j \, \sigma_{ij} + \rho b_i = 0 \qquad\qquad (2.31d)$$

$$\nabla_i \, (k_{ij} / \gamma_f) (\nabla_j \, p - \rho_f b_j) + \dot{\varepsilon}_{ii} = \dot{p} \, n / K_f \qquad\qquad (2.31f)$$

Equation (2.31f) represents the transient seepage of the fluid, coupled with the deformation of the solid skeleton. The incremental form of this system of equations also allows dealing with the nonlinear consolidation problems.

2.4.4. Undrained Behavior (rapid phenomena)

When the speed of the phenomena is very fast so that $\dot{w}_i$, $\ddot{w}_i$ and w_i never reach significant values, one obtains the limiting case of undrained behavior. It is equivalent to the case of very small permeability k_{ij} . On making $k_{ij} = 0$, equation (2.29f) gives

$$\dot{\varepsilon}_{ii} = \dot{p} \, n / K_f$$

or incrementally

$$dp = (K_f / n) \, d\varepsilon_{ii} \qquad\qquad (2.32)$$

19

Thus we can readily express the constitutive equation in terms of total stress. The system can be written as

$$d\varepsilon_{ij} = -(du_{i,j} + du_{j,i}) / 2 \tag{2.33b}$$

$$d\sigma_{ij} = \underline{D}_{ijkl}\, d\varepsilon_{kl} \tag{2.33c}$$

$$-\nabla_j\, \sigma_{ij} + \rho b_i = \rho\, \ddot{u}_i \tag{2.33d}$$

with

$$\underline{D}_{ijkl} = D_{ijkl} + \delta_{ij}\, \delta_{kl}\, K_f / n \tag{2.33e}$$

which is identical to the behavior of a single-phase system with a redefined total stress tangent modulus $\underline{D}_{ijkl}$.

2.4.5. Fully Drained Behavior (steady flow)

If all transient behavior has ceased, i.e. if $\dot{w}_i = 0$, $\dot{u}_i = 0$, $\ddot{w}_i = 0$, $\ddot{u}_i = 0$ and $p = 0$, complete uncoupling of equations occurs. Equation (2.29f) becomes

$$\nabla_i\, (k_{ij} / \gamma_f)\, (\nabla_j\, p - \rho_f b_j) = 0 \tag{2.34}$$

which can be solved independently to determine the pore fluid pressure p.

The remaining equations are

$$d\varepsilon_{ij} = -(du_{i,j} + du_{j,i}) / 2 \tag{2.35b}$$

$$d\sigma'_{ij} = D_{ijkl}\, d\varepsilon_{kl} \tag{2.35c}$$

$$-\nabla_j\, \sigma'_{ij} - \nabla_i\, p + \rho b_i = 0 \tag{2.35d}$$

Thus one may determine u_i using the known values of p.

2.5. SUMMARY OF BASIC EQUATIONS IN MATRIX FORM

Defining displacements as $u^T = [\ u_1, u_2, u_3\ ]$, stresses and strains as $\sigma^T =$ $[\sigma_{11}, \sigma_{22}, \sigma_{33}, \sigma_{12}, \sigma_{23}, \sigma_{31}]$, $\mathbf{D}$ as a 6 x 6 matrix of stiffness coefficients, $\mathbf{m}^T = [1,1,1,0,0,0]$, and $\mathbf{L}$ as a 6 x 3 matrix operator equivalent to the strain definition, such as (2.12), the basic equations may be written in a form more suitable for the finite element discretization.

Thus the equivalent of the generalized Biot's equations (2.27) is

$$\sigma = \sigma' + \mathbf{m}p$$

$$d\varepsilon = \mathbf{L}\ du$$

$$d\sigma' = \mathbf{D}\ d\varepsilon$$

$$\mathbf{L}^T \sigma + \rho\ \mathbf{g} = \rho\ \ddot{\mathbf{u}} + \rho_f\ \ddot{\mathbf{w}} \qquad\qquad \textbf{(B)}$$

$$-\nabla p + \rho_f \mathbf{g} = (\ k^{-1}/\gamma_f\ )\ \dot{\mathbf{w}} + \rho_f \ddot{\mathbf{u}} + \rho_f\ \ddot{\mathbf{w}}/n$$

$$-\mathbf{m}^T \mathbf{L}^T \dot{\mathbf{w}} + \mathbf{m}^T\ \dot{\varepsilon} = \dot{p}n/K_f$$

The approximate dynamic equation (2.29) becomes

$$\sigma = \sigma' + \mathbf{m}p$$

$$d\varepsilon = \mathbf{L}\ du$$

$$d\sigma' = \mathbf{D}\ d\varepsilon \qquad\qquad \textbf{(Z)}$$

$$\mathbf{L}^T \sigma + \rho \mathbf{g} = \rho\ \ddot{\mathbf{u}}$$

$$\nabla^T (\ (k/\gamma_f)\ (\nabla p - \rho_f\ \mathbf{g})\ ) + \mathbf{m}^T\ \dot{\varepsilon} = -\nabla^T (\ (k/\gamma_f)\ \rho_f \ddot{\mathbf{u}}\ ) + \dot{p}\ n/K_f$$

The consolidation equation (2.31) will be

$$\sigma = \sigma' + mp$$

$$d\varepsilon = L\, du$$

$$d\sigma' = D\, d\varepsilon$$

$$L^T \sigma + \rho g = 0 \qquad\qquad\qquad (C)$$

$$\nabla^T ((k / \gamma_f) (\nabla p - \rho_f\, g)) + m^T \dot{\varepsilon} = \dot{p}\, n / K_f$$

Finally the system of equations for the undrained case (2.33) is reduced to:

$$d\sigma = \underline{D}\, d\varepsilon$$

$$d\varepsilon = L\, du$$

$$L^T \sigma + \rho g = \rho\, \ddot{u} \qquad\qquad\qquad (U)$$

with

$$\underline{D} = D + m\, (K_f / n)\, m^T$$

Zienkiewicz, Chang and Bettess (1980) stated the basic conclusions taken from the examination of many computational results, in which zones (Figure 2.2) of applicability of various assumptions hold for determination of pressure fluctuations.

Extrapolating the conclusions of this simple elastic analysis to other real problems one now has a useful guide as to the applicability of the various assumptions.

Zone I   B = Z = C   Slow phenomena ($\ddot{w}$ and $\ddot{u}$ can be neglected)
Zone II B = Z ≠ C   Moderate speed ($\ddot{w}$ can be neglected)
Zone III B ≠ Z ≠ C Fast phenomena ($\ddot{w}$ can not be neglected) only
                           full Biot equation valid
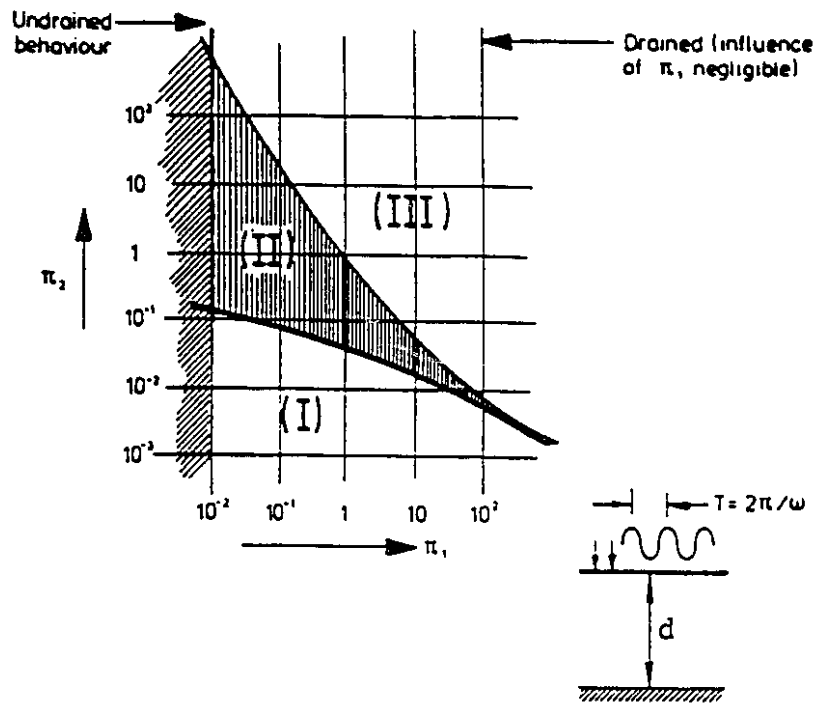
$$\pi_1 = \frac{k\rho V_c^2}{\omega d^2} = \frac{2k\rho T}{\pi \hat{T}^2} = \left(\frac{2}{\beta\pi}\right)\frac{\bar{k}}{g}\frac{T}{\bar{T}^2}$$

$$\pi_2 = \frac{\omega^2 d^2}{V_c^2} = \pi^2\left(\frac{\hat{T}}{T}\right)^2$$

$\bar{k} = \rho_f g k$ $\bar{k}$—kinematic permeability

$\hat{T} = 2d/V_c$ $V_c^2 = (D + K_f/n)/\rho$

               $\approx \beta K_f/\rho_f n$

$\approx K_f/\rho_f$ (speed of sound in water)

     $\beta = \rho_f/\rho$ $n \approx 0.33$ $\beta = 0.33$

Figure 2.2 Zones of applicability of various assumptions

(after Zienkiewicz and Bettess, 1982)

23

Thus for a typical seabed response problem on which waves of a period of seconds are acting and in which the length of interest, (say the depth below surface), is of the order of 10m

$$\widehat{T} = 10^{-2}\,s$$

hence,

$$\Pi_2 < 10\,(\frac{10^{-2}}{1})^2 = 10^{-3}$$

so the dynamic terms may be entirely neglected.

In wave response studies it is customary to neglect the effects of inertia. The nonlinear transient consolidation equations (2.31), or the set of equations (C) will be used to study the ocean wave induced response of sandy sea floor deposits and liquefaction analysis.

3

SOIL PLASTICITY — A HISTORICAL REVIEW

3.1 INTRODUCTION

For a long time, soil mechanics has been based on Hooke's law of linear elasticity for stress and deformation analysis of a soil mass under a footing, or behind a retaining wall, when no failure of the soil is involved. These are classed as elasticity problems in soil mechanics. On the other extreme, the theory of perfect plasticity is used to deal with the conditions of ultimate failure of a soil mass. Problems of earth pressure, retaining walls, bearing capacity of foundations, and stability of slopes are all considered in the realm of perfect plasticity. These are called stability problems.

Partly for simplicity in practice and partly because of the historical development of mechanics of solids, elasticity problems and stability problems in soil mechanics are treated separately in unrelated ways. The essential connection between elasticity problems and stability problems are problems known as progressive failure problems. Progressive failure problems deal with the elastic-plastic transition from the initial linear elastic state to the ultimate state of the soil by plastic flow. The essential set of equations for the solutions of progressive failure problems is the set of constitutive equations of soils.

In fact, the actual behavior of soils is very complicated and varies greatly when soils are subjected to different conditions. Drastic idealizations are therefore essential in order to develop simple mathematical models for practical applications. Each soil model

targets a certain class of phenomena, captures their essential features, and disregards what is considered to be of minor importance in the class of application.

The development of the modern theory of soil plasticity was strongly influenced by the well-established theory of metal plasticity. Soil mechanics specialists have been preoccupied with extending these concepts to answer the complex problems of soil behavior. Tresca's yield condition, used widely in metal plasticity, can be regarded as a special case of the condition of Coulomb on which the important concept of the limiting equilibrium of a soil media had been firmly established in soil mechanics (Terzaghi, 1943).

It is a relatively straightforward matter to extend the method of characteristics to cover Coulomb material where c and ϕ can either remain constant (Sokolovsky, 1965) or vary throughout the stress field in some specified manner (Booker and Davis, 1972).

The general theory of limit analysis, developed in the early 1950's considers the stress-strain relation of a soil in an idealized manner. This idealization, termed normality or the associated flow rule, establishes the limit theorems on which limit analysis is based. Although the applications of limit analysis to soil mechanics are relatively recent, there have been an enormous number of practical solutions available (Chen, 1975). As a result of this development, the meaning of the limit equilibrium solutions in the light of the upper- and lower-bound theorems of limit analysis becomes clear.

The first major advance in the extension of metal plasticity to soil plasticity was made in the paper "Soil Mechanics and Plastic Analysis or Limit Design" by Drucker and Prager (1952). In this paper, the authors extended the Coulomb criterion to a three-dimensional soil mechanics problem. The Coulomb criterion was interpreted by Drucker (1953) as a modified Tresca, and by Drucker and Prager (1952) as an extended von Mises yield criterion. The yield criterion obtained by Drucker and Prager for the latter case is now known as the Drucker-Prager model or the extended von Mises model. Shield

(1955) following the related work of Drucker and Prager (1952), extended uniquely and correctly the Coulomb criterion into the three-dimensional stress space.

One of the main stumbling blocks in the further development of the stress-strain relations of soil based on the Drucker-Prager type or Coulomb type of yield surface to define the limit of elasticity and beginning of a continuing irreversible plastic deformation was the excessive prediction of dilation, which was the result of the use of the associated flow rule. It became necessary, therefore, to extend the classical plasticity ideas to a non-associated form in which the plastic potential and yield surface are defined separately (Poorooshasb, Holubec and Sherbourne 1966, 1967).

In 1957 an important advance was made in the paper "Soil Mechanics and Work-Hardening Theories of Plasticity" by Drucker, Gibson and Henkel. In this paper the authors introduced the concept of work-hardening plasticity into soil mechanics. There are two important innovations in this paper. The first is the introduction of the idea of a work-hardening cap to the perfectly plastic yield surface such as the Coulomb type or Drucker-Prager type of yield criterion. The second innovation is the use of current soil density (or void ratio, or plastic compaction) as the state variable or the strain-hardening parameter to determine the successive loading cap surfaces.

These ideas have led in turn to the generation of many soil models, most notably the development of the critical state soil mechanics at Cambridge University, U. K. These new soil models have grown increasingly complex as additional experimental data has been gathered, interpreted, and matched. This extension marks the beginning of the modern development of a consistent theory of soil plasticity.

It is important to note here that the path to reach the present state-of-the-art in the soil plasticity is by no means easy and that much of the classical theory of plasticity for metal has been considerably modified in order to obtain rational results for soils. These achievements have been summarized in two earlier symposia (Parry, 1972; Palmer, 1973),

27

as well as in ASCE workshop and symposium proceedings (Pande and Zienkiewicz, 1980; Yong and Ko., 1981; Yong and Selig, 1982). An up-to-date summary is given in the books "Constitutive Laws for Engineering Materials" by Desai (1984), "Constitutive Equations for Engineering Materials, Vol. 2, Plasticity and Modelling" by Chen and Saleeb (1986) and the Proceeding on "Constitutive Laws for Engineering Materials: Theory and Application" edited by Desai et al. (1987).

The use of strain- or work - hardening plasticity theories in soil mechanics has been developed for about three decades. Most research has been conducted in the area of soil statics. In recent years, attention has been focused on the modelling of soil behavior under cyclic loading conditions encountered in soil transient and dynamic problems. In the following sections, the general formulation of classical plasticity is first derived, then the concepts of isotropic, kinematic and mixed hardening and their generalizations on the cap models, the nested yield surface models and the bounding surface models are briefly illustrated.

3.2 CLASSICAL PLASTICITY

In the 1950's major advances were made in the theory of metal plasticity by the development of (a) the fundamental theorems of limit analysis of perfect plasticity (Drucker and Prager, 1952), (b) Drucker's postulate for stable material or definition of work-hardening material (see for example, Drucker, 1951, 1960), and (c) the formalization of the concept of normality condition or associated flow rule. The theory of limit analysis of perfect plasticity leads to practical methods that are needed to estimate the load-carrying capacity of structures in a more direct manner. The concept of a stable material provides a unified treatment and broad point of view of the stress-strain relations of plastic solids. The idea of normality condition provides the necessary connection between the yield criterion or

28

loading function to the plastic stress-train relations. All these have led to a rigorous basis for the theory of classical plasticity.

The general formulation of elastoplasticity could be derived from three fundamental assumptions (see e.g. Yang, Poorooshasb and Yong, 1987):

(1) Additive

The total strain increment $d\varepsilon_{ij}$ is assumed to be decomposed into elastic strain increment $d\varepsilon^e_{ij}$ and plastic strain increment $d\varepsilon^P_{ij}$. (In the following, both the indicial and matrix notation will be used whenever it is convenient.)

$$d\varepsilon_{ij} = d\varepsilon^e_{ij} + d\varepsilon^P_{ij} \quad , \quad d\varepsilon = d\varepsilon^e + d\varepsilon^P \qquad (3.1)$$

The elastic part is usually assumed to be governed by an incremental form of the generalized Hooke's law. i.e.

$$d\varepsilon^e_{ij} = C^e_{ijkl}\, d\sigma_{kl} \quad , \qquad d\varepsilon^e = C^e\, d\sigma$$

$$d\sigma_{ij} = D^e_{ijkl}\, d\varepsilon^e_{kl} \quad , \qquad d\sigma = D^e\, d\varepsilon^e \qquad (3.2)$$

where C^e, D^e are the tensor of elastic compliance and moduli respectively with

$$D^e_{ijkl}\, C^e_{klmn} = (\delta_{im}\, \delta_{jn} + \delta_{in}\, \delta_{jm}\,)\, /\, 2 \qquad (3.3)$$

(2) Existence of a scalar valued yield function $F\,(\sigma\,,\, \varepsilon^P\,,\, \kappa\,)$.

The previous loading history, expressed quantitatively by means of the plastic strain tensor ε^P and a scalar function $\kappa = \kappa\,(\,\varepsilon^P\,)$, determines the current yield surface in the stress space. It is evident that stress σ here stands for the effective stress. Since the constitutive relations refer to the deformation of the soil skeleton, the state of the material is defined in terms of the effective stress and plastic internal variables, such as ε^P and $\kappa(\varepsilon^P)$.

29

If $F < 0$, the material is in the elastic range. If σ satisfies $F=0$, the material is at the plastic state. Therefore, the so-called "consistency condition" is introduced which states that during loading each stress increment leads from one plastic state to another, the condition $F=0$ holding both before and after, that is

$$dF=0 \qquad (3.4)$$

(3) Drucker postulate (1951): Non-negative dissipation of mechanical energy.

The work done by the added stress over any step cycle starting at σ^0 and involving infinitesimal plastic straining is

$$W_D = \int_\sigma (\sigma - \sigma^0)^T \, d\varepsilon \geq 0 \qquad (3.5)$$

It may be expanded to Taylor series at point b which satisfies $F=0$,

$$W_D = (\sigma^b - \sigma^0)^T \, d\varepsilon^P + [\, d\sigma^T d\varepsilon^P + (\sigma^b - \sigma^0)^T (d\varepsilon^P)^2 \,] / 2 + 0 [\, (d\varepsilon^P)^2 \,] \geq 0$$

If σ^0 is inside the elastic domain, then

$$(\sigma^b - \sigma^0)^T \, d\varepsilon^P \geq 0 \qquad (3.6)$$

If $\sigma^0 = \sigma^b$, then

$$d\sigma^T d\varepsilon^P / 2 \geq 0 \qquad (3.7)$$

Thus the yield surface must be convex and $d\varepsilon^P$ must be normal to the yield surface according to inequality (3.6). So that the associated flow rule results in the form

$$d\varepsilon^P = d\lambda \, (\, \partial F / \partial \sigma)^T \qquad d\lambda \geq 0 \qquad (3.8)$$

The scalar parameter $d\lambda$ in (3.8) is determined by the consistency condition

$$dF = \frac{\partial F}{\partial \sigma} d\sigma + \frac{\partial F}{\partial \varepsilon^P} d\varepsilon^P + \frac{\partial F}{\partial \kappa} \frac{\partial \kappa}{\partial \varepsilon^P} d\varepsilon^P = 0 \qquad (3.4)'$$

Substituting (3.8) into (3.4)' , and solving for $d\lambda$

$$d\lambda = L / K_p \qquad (3.9)$$

where

$$L = (\partial F / \partial \sigma) \, d\sigma = \text{loading function}$$

$$K_p = - \left(\frac{\partial F}{\partial \varepsilon^P} + \frac{\partial F}{\partial \kappa} \frac{\partial \kappa}{\partial \varepsilon^P}\right) \left(\frac{\partial F}{\partial \sigma}\right)^T = \text{hardening parameter}$$

Substituting (3.9), (3.8) into inequality (3.7), the condition of stability results

$$d\sigma^T d\varepsilon^P = L^2 / H \ge 0$$

i.e.

$$K_p \ge 0 \qquad (3.10)$$

This means that the non-negative hardening modulus is required by the material stability.

If $K_p < 0$, the material is said to be unstable. For $K_p > 0$, it is a hardening material, and $K_p = 0$, an ideal (perfect) plastic material.

For a hardening material ($K_p > 0$), the loading criteria is

$$h(L) = \begin{cases} 1, & L > 0 \ \& \ F = 0 & \text{loading} \\ 0, & L = 0 \ \& \ F = 0 & \text{neutral loading} \\ 0, & L < 0 \ \& \ F = 0 & \text{unloading} \\ 0, & F < 0 & \text{elastic state} \end{cases} \qquad (3.11)$$

The plastic strain increment is obtained as

$$d\varepsilon^P = \frac{h(L)}{K_p} \left(\frac{\partial F}{\partial \sigma}\right)^T \frac{\partial F}{\partial \sigma} d\sigma = C^P d\sigma \qquad (3.12)$$

31

Therefore, the elastoplastic constitutive equation is

$$d\varepsilon = \mathbf{C}^{ep} \, d\sigma = (\, \mathbf{C}^e + \mathbf{C}^p \,) \, d\sigma \tag{3.13}$$

$$\mathbf{C}^{ep} = \mathbf{C}^e + \frac{h(L)}{K_p} \left(\frac{\partial F}{\partial \sigma} \right)^T \frac{\partial F}{\partial \sigma} \, d\sigma$$

Combining equation (3.1) with (3.2), (3.8),(3.9)

$$\frac{\partial F}{\partial \sigma} \mathbf{D}^e \, d\varepsilon = \frac{\partial F}{\partial \sigma} \mathbf{D}^e \, d\varepsilon^e + \frac{\partial F}{\partial \sigma} \mathbf{D}^e \, d\varepsilon^p$$

$$= \frac{\partial F}{\partial \sigma} \, d\sigma + \frac{\partial F}{\partial \sigma} \mathbf{D}^e \left(\frac{\partial F}{\partial \sigma} \right)^T d\lambda$$

$$= K_p \, d\lambda + \frac{\partial F}{\partial \sigma} \mathbf{D}^e \left(\frac{\partial F}{\partial \sigma} \right)^T d\lambda$$

yields

$$d\lambda = \frac{1}{K_{2p}} \frac{\partial F}{\partial \sigma} \mathbf{D}^e \, d\varepsilon \tag{3.14}$$

where

$$K_{2p} = K_p + \frac{\partial F}{\partial \sigma} \mathbf{D}^e \left(\frac{\partial F}{\partial \sigma} \right)^T$$

Therefore

$$d\varepsilon^p = h\,(L) \left(\frac{\partial F}{\partial \sigma} \right)^T d\lambda = \frac{h(L)}{K_{2p}} \left(\frac{\partial F}{\partial \sigma} \right)^T \frac{\partial F}{\partial \sigma} \mathbf{D}^e \, d\varepsilon$$

The inversion of the constitutive equation is

$$d\sigma = \mathbf{D}^e \, d\varepsilon^e = \mathbf{D}^e (\, d\varepsilon - d\varepsilon^p \,) = \mathbf{D}^{ep} \, d\varepsilon \tag{3.15}$$

where

$$\mathbf{D}^{ep} = \mathbf{D}^e - \frac{h(L)}{K_{2p}} \mathbf{D}^e \left(\frac{\partial F}{\partial \sigma} \right)^T \frac{\partial F}{\partial \sigma} \mathbf{D}^e$$

32

3.3 ISOTROPIC HARDENING AND CAP MODEL

(Concept of Critical State)

The introduction of isotropic hardening plasticity into soil mechanics led in turn to the generation of the family of soil models of the strain-hardening cap type developed at Cambridge University by Professor Roscoe and his co-workers. Two of these models are now widely used. The first is known as the Cam-clay model (Schofield and Wroth. 1968) and was originally formulated by Roscoe et al. (1963) for normally and lightly over-consolidated clays in the triaxial test. The second, known as the Modified Cam-clay model, was developed by Roscoe and Burland (1968) as a modification and extension of the Cam-clay model to the general three-dimensional stress state. In both models, the associated flow rule was used. The modified Cam-clay model is an isotropic, nonlinear elastic-plastic strain-hardening model. Only the volumetric strain is assumed to be partially recoverable; i. e. elastic shearing strain is assumed to be identically zero. The elastic volumetric strain is nonlinearly dependent on the hydrostatic stress and is independent of the deviatoric (shear) stresses. For certain stress histories, strain-softening may occur. Extensive reviews of various types of Cambridge models have been given in two symposia (Parry, 1972; Palmer, 1973).

The important feature that has been the integral part of all Cambridge models is the concept of critical state proposed by Poorooshasb (1961) which had previously been referred to as the critical void ratio (Roscoe et al., 1958). The critical state line is the locus of the failure points of all shear tests under both drained and undrained conditions. Its crucial property is that failure of initially isotropically compressed samples will occur once the states of stress in the samples reach the line, irrespective of the test path followed by the samples on their way to the critical state line (Atkinson and Bransby, 1978). At the critical state, large shear deformations occur with no change in stress or plastic volumetric strain.

33

Experimental results have indicated that at failure the behavior of soil is governed by the Mohr-Coulomb failure criterion (Bishop, 1966). The failure (yield) surface corresponding to the Mohr-Coulomb criterion in principal stress space is an irregular hexagonal pyramid whose apex lies on the space diagonal as shown in Figure 3.1. A strain-hardening cap intersects with the Coulomb surface in line ABCDEFA. This line is called the critical state locus, and it is simply a line which separates the two surfaces corresponding to one fixed value of the specific volume (or void ratio). The complete failure surface is termed a state boundary surface (e.g. Roscoe and Burland, 1968; Atkinso and Bransby, 1978). There will be similar surfaces of different sizes, but of the same shape, corresponding to different values of the specific volume. The geometric representation of the shape of the generalized state boundary surface requires four dimensions (i.e., three principal stress and one specific volume).

DiMaggio and Sandler (1971) proposed a generalized cap model. The yield function they used consists of a perfectly-plastic (failure) portion fitted to a strain-hardening elliptical cap. The associated flow rule was employed for the failure and cap functions. In this model, the functional forms for both the perfectly-plastic and the strain-hardening portions may be quite general and would allow for the fitting of a wide range of material properties.

The movement of the cap is controlled by the increase or decrease of the plastic volumetric strain. Strain-hardening in this model can therefore be reversed. It is this mechanism that leads to an effective control of dilation, which can be kept quite small (effectively zero) as required for many soils.
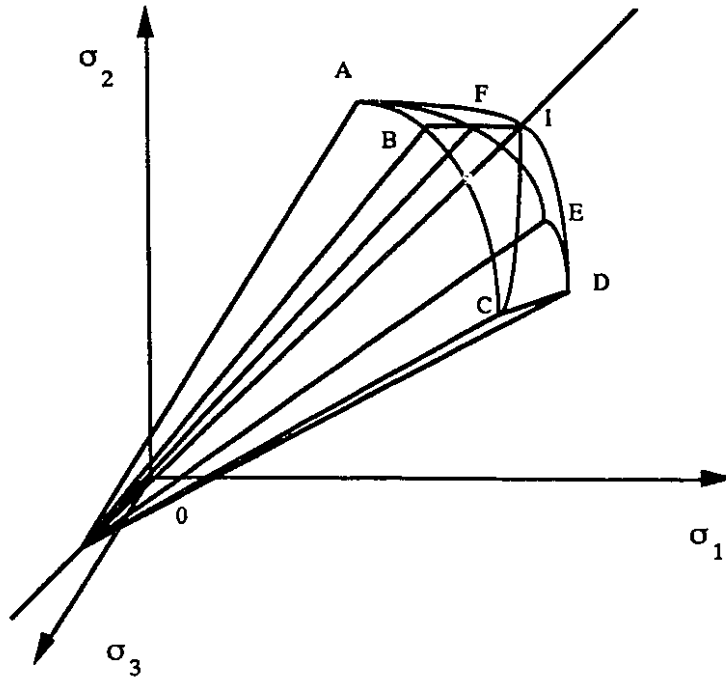
Figure 3.1 A Cambridge type of strain-hardening cap model.

Using the idea of a cap fitted to the yield surface, Lade (1977, 1979) has developed a strain-hardening model to describe the behavior of different sands and normally consolidated clays. He used a spherical cap together with a modified version of the conical yield surface suggested earlier by Lade and Duncan (1975). In this model, both the conical yield surface and the cap are allowed to harden isotropically. However, for the cap, the associated flow rule was employed, while the nonassociated rule was used in connection with the conical portion.

3.4 KINEMATIC HARDENING AND NESTED YIELD SURFACE MODEL

An alternative approach to the isotropic hardening type of models described above is provided by the kinematic type of strain-hardening rules. This approach has been employed by several researchers to provide a more realistic representation of soil behavior under reversed, and particularly cyclic, loading conditions.

Iwan (1967), following the earlier work of Masing (1926), proposed one-dimensional plasticity models which consist of a collection of perfectly elastic and rigid-plastic or slip elements arranged in either a series-parallel or a parallel-series combination. The model can contain a large number of elements and the properties of these elements which can be distributed such that they can match the particular form of hysteretic behavior of certain types of soils. This is known as the overlay or mechanical sublayer model (e.g. Zienkiewicz, Norris and Naylor,1977). The concept of a sublayer model was originally introduced by Duwez (1953) and further developed by Besseling (1958).

In order to extend the one-dimensional model to the three-dimensional situation, an extended formulation of the classical incremental theory of plasticity has been proposed by Iwan (1967). Instead of using a single yield surface in stress space, he postulated a family (nest) of yield surfaces (Figure 3.2) with each surface translating independently in a pure kinematic manner, or individually obeying a linear work-hardening model. Their combined action, in general, gives rise to piecewise linear work-hardening behavior for the material as a whole. The approach leads to a realistic Bauschinger effect of a type that could not be obtained by using a single yield surface and a nonlinear work-hardening rule even with kinematic hardening. The same concept of using a field of nested yield surfaces was also proposed independently by Mroz (1967). All the nested yield surface models have a feature common to the early sublayer models: namely, a piecewise linear stress-strain behavior under proportional loading. These models used for soils are usually known as nested yield surface or multisurface plasticity models.

36

X Current Stress Point
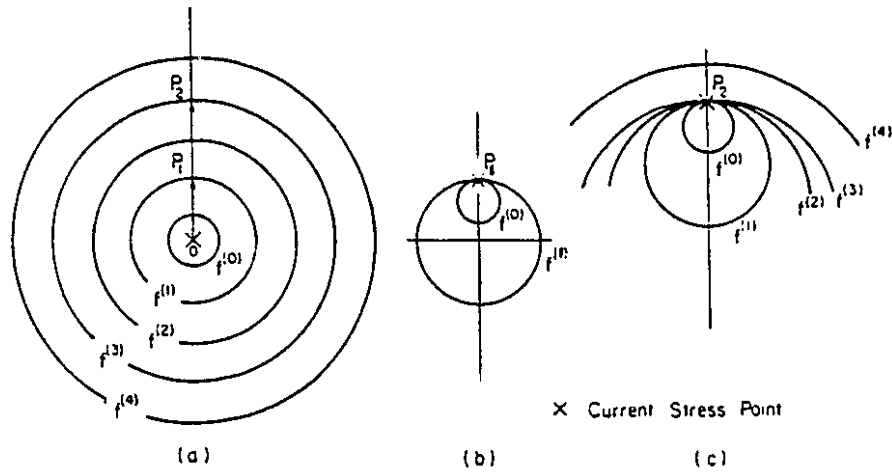
Figure 3.2 Nested yield surfaces in Mroz-Iwan type of strain hardening models.

Figure 3.2 demonstrates the qualitative behavior of a multisurface model with pure kinematic hardening. The initial positions of the yield surfaces $f^{(0)}$, $f^{(1)}$, $f^{(2)}$, and $f^{(3)}$ are shown in Figure 3.2a. When the stress point moves from O to P1, elastic strains first occur until the surface $f^{(0)}$ is reached, where the plastic flow begins and the surface $f^{(0)}$ starts to move towards the surface $f^{(1)}$. Before their contact, the hardening modulus $H^{(0)}$ associated with $f^{(0)}$ governs the plastic flow according to the normality flow rule. However, when $f^{(0)}$ engages $f^{(1)}$ at P1 (Figure 3.2b), the first nesting surface $f^{(1)}$ becomes the active surface and , upon further loading, the hardening modulus $H^{(1)}$ applies in the flow rule. Both $f^{(0)}$ and $f^{(1)}$ are then translated by the stress point, and they remain tangent to each

37

other along with the stress path until they touch the yield surface $f^{(2)}$ which then becomes the active surface. For subsequent contacts of consecutive surface, the process is repeated with new corresponding values of hardening moduli applied. The situation when $f^{(3)}$ is reached is illustrated in Figure 3.2c. Prevost (1977, 1978a, b) has extended the Iwan / Mroz model for the undrained behavior of clays under monotonic and cyclic loading conditions. In this development, the basic work-hardening rule is still of the kinematic type but a simultaneous isotropic hardening (or softening) is allowed.

3.5 MIXED HARDENING AND BOUNDING SURFACE MODEL

Various types of work-hardening plasticity models have been recently employed for soils based on the bounding (consolidation or limiting) surface concept introduced earlier for metals (e.g. Dafalias and Popov, 1975; Krieg, 1975). A two-surface model of this type was proposed by Mroz et al. (1978, 1979) for clays. A bounding surface, F=0, representing the consolidation history of the soil, and a yield surface, f=0, defining the elastic domain within the bounding surface (Fig. 3.3) were employed in the model.

The bounding surface was assumed to expand or contract isotropically, but the yield surface was allowed to translate, expand or contract within the domain enclosed by the bounding surface. The translation of the yield surface is governed by the same rule as the multisurface models described earlier (i.e., F will translate towards the bounding surface along PR in Fig. 3.3).

38
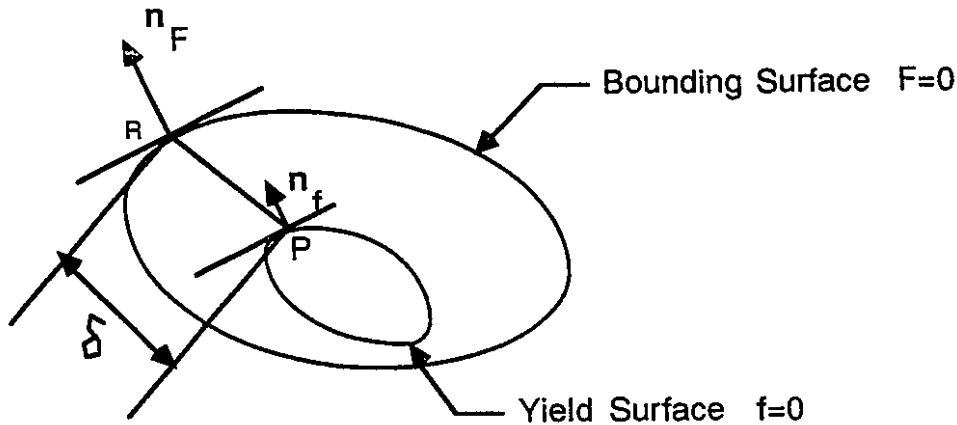
Figure 3.3 Yield and bounding surfaces in stress space.

The hardening modulus on the yield surface is assumed to vary depending on the relative configuration of the yield and bounding surfaces. It was this last assumption that distinguished the present formulation from the previous multisurface models. Here, instead of using a field of nested yield surfaces with associated hardening moduli, an interpolation rule is utilized to define the variation of the hardening moduli between the yield and the bounding surfaces. In the interpolation rule used by Mroz et al. (1978, 1979), the hardening modulus, H, was taken as a function of the distance d (Fig. 3.3) between the current stress point, P, on the yield surface and its conjugate point, R, on the bounding surface. Very detailed discussions of the present model and its application to represent the behavior of clays under monotonic and cyclic triaxial test conditions have been given by Mroz et al. (1979).

39

Dafalias and Herrmann (1980) have also used the bounding surface formulation to describe the behavior of clay under cyclic loadings. However, no explicit yield surface was postulated. The associated flow rule was utilized for the bounding surface. In this model, the variation of the plastic (hardening) modulus within the bounding surface is defined on the basis of a very simple radial mapping rule. For each actual stress point within (or on) the bounding surface, a corresponding "image" point on the surface is specified as the intersection of the surface with the straight (radial) line connecting the origin with the current stress point (the origin was assumed to be always within the bounding surface). The actual hardening modulus is then assumed to be a function of the hardening modulus on the bounding surface at the "image" point and the distance between the actual stress point and its "image".

Unlike the nested yield surface models, the bounding surface models have the definite advantage of smooth transition from elastic to fully plastic state for general reversed loading which is generally observed experimentally on soils. In fact, the bounding surface model can be considered as a smooth extension of the nested yield surface model with an analytical function to replace the nest of several loading surfaces.

4

A SIMPLE CONSTITUTIVE MODEL FOR SANDS

4.1 INTRODUCTION

The classical concept of a yield surface implies a purely elastic stress range contrary to the reality for many soils. Some very important aspects of soil behavior, mainly relating to the cyclic response such as strain accumulation for drained cyclic loading or pore water pressure build up for undrained cyclic deviatoric loading, cannot be adequately described. A feature of many stress-strain laws for soils is that they are applicable only to loading conditions of a rather specific nature. When an artificial distinction is made, for example, dealing primarily with gross overall soil behavior under specifically chosen cyclic conditions, the corresponding constitutive relations are useless for monotonic, or interchange of monotonic and cyclic loading. This shows the necessity to develop constitutive laws within a more fundamental framework, such that they are applicable to monotonic or cyclic, drained or undrained, or any other form of loading conditons which may occur in earthquake response of large dams, nuclear power stations or in off-shore structures subject to wave action. Eisenberg and Phillips (1969) introduced the concept of loading surfaces distinct from the yield surface. Mroz (1967) introduced the field of work-hardening moduli which was originally applied to metal plasticity and subsequently to soils by Mroz, Norris and Zienkiewicz (1978) and Prevost (1978). Among the new concepts is that of the bounding surface originally introduced by Dafalias and Popov (1975, 1976) and

41

independently by Krieg (1975) in conjunction with an enclosed yield surface for metal plasticity. The salient features of a bounding surface formulation are that plastic deformation may occur for stress states within the surface and the possibility of having a very flexible variation of the plastic modulus. These features yield definite advantages over a classical yield surface formulation, particularly with regard to soil plasticity.

A bounding/yield surface plasticity formulation for soils was fully developed by Mroz et al. (1979) and Mroz and Pietruszczak (1983) within the triaxial space of critical state soil mechanics. Poorooshasb and Pietruszczak (1985, 1986) developed a two-surface model for sand extended to the general effective stress space which is based on the bounding surface concept incorporating a non-associative flow rule and the idea of reflected plastic potential (Pande, 1982). A computer program, called CARIBOU (Yang, 1986), was also developed for numerical simulation of the model behavior. This model has been proved to be applicable for both loose and dense sands, in particular, liquefaction and cyclic mobility can adequately be simulated. Also it has been applied to analysis of earthquake excitation (Pietruszczak and Stolle, 1987) and wave action (Poorooshasb, Ishihara and Yang, 1987; Poorooshasb, Yang and Clark, 1990). The model is fairly complicated mainly because of the kinematics of the yield surface.

A relatively simple constitutive model within the framework of the generalized plasticity / bounding surface formulation is proposed. The idea of reflecting plastic potential is retained implicitly by a vanishing yield surface which significantly reduces the numerical complexity of the model. For a number of tests, the performance of the model is compared with experimental results (Castro, 1969; Ishihara and Tatsuoka, 1974, 1975, 1982). The predictions indicate that the model is capable of appropriate simulation of several fundamental aspects of sand behaviour which have already been recognized through laboratory investigations. Therefore, this simple constitutive model may be applied to initial-boundary value problems with confidence.

4.2 THE GENERALIZED PLASTICITY FORMULATION

In generalized plasticity formulation, the unit vector n at the effective stress space which determines both loading and unloading direction is required. The incremental stress-strain relations could be written in compact matrix notation in which the subscripts l and u refer to loading and unloading respectively,

$$d\sigma' = D_l \, d\varepsilon \qquad \text{if } n^T d\sigma' > 0 \text{ loading}$$

$$d\sigma' = D_u \, d\varepsilon \qquad \text{if } n^T d\sigma' < 0 \text{ unloading} \qquad (4.1)$$

where the tangent matrices are related (Zienkiewicz and Mroz, 1984) by

$$(D_l)^{-1} = (D^e)^{-1} + n_{gl} \, n^T / H_l \qquad (4.2)$$

$$(D_u)^{-1} = (D^e)^{-1} + n_{gu} \, n^T / H_u \qquad (4.3)$$

in which H_l and H_u are scalar parameters known as plastic loading and unloading moduli. D^e is the eastic matrix. This relation simply ensures the uniqueness of strain increments when $n^T d\sigma' = 0$. n_{gl} and n_{gu} are arbitrarily specified unit vectors which define the flow rule. If they differ from n then the flow is non-associative and will lead to non-symmetric tangent matrices D_l and D_u.

It is easy to convert equation (4.2) in the same way as used in section 3.2, to the standard form of the so-called elasto-plastic matrix,

$$D_{l/u} = D^e - \frac{D^e \, n_{gl/u} \, n^T \, D^e}{H_{l/u} + n^T \, D^e \, n_{gl/u}} \qquad (4.4)$$

The material behaviour can be fully described if we prescribe D^e, n, $n_{gl/u}$ and $H_{l/u}$ for all states of the material.

43

For comparison, a yield surface $F(\sigma', q_n)$ is used in classical plasticity. The state of the soil skeleton is defined in terms of the effective stress σ' and the plastic internal variable q_n accounting for the past loading history. The q_n are usually scalar or second-order tensor quantities such as the plastic work, the plastic strain, etc. From the point of view of the generalized plasticity, $\mathbf{n}$ is defined by the unit normal vector of the yield surface.

$$\mathbf{n}^T = \frac{\partial F}{\partial \sigma'} / [(\frac{\partial F}{\partial \sigma'})^T (\frac{\partial F}{\partial \sigma'})]^{1/2} \tag{4.5}$$

The loading flow direction vector $\mathbf{n}_{gl}$ is specified by the unit vector normal to plastic potential $G(\sigma')$

$$\mathbf{n}_{gl}^T = \frac{\partial G}{\partial \sigma'} / [(\frac{\partial G}{\partial \sigma'})^T (\frac{\partial G}{\partial \sigma'})]^{1/2} \tag{4.6}$$

Imposing the consistency condition $dF=0$ during plastic deformation, results in

$$H_l = - \frac{\partial F}{\partial q_n} (\frac{\partial q_n}{\partial \varepsilon^P})^T \mathbf{n}_{gl} / [(\frac{\partial F}{\partial \sigma'})^T (\frac{\partial F}{\partial \sigma'})]^{1/2} \tag{4.7}$$

The unloading is always assumed to be elastic in classical plasticity:

$$H_u = \infty \quad , \quad \mathbf{D}_u = \mathbf{D}^e \tag{4.8}$$

In bounding surface theory, the bounding surface is identified as the yield surface if loading takes place at the bounding surface. However, if the actual stress point is within the bounding surface, $\mathbf{n}$, $\mathbf{n}_{gl/u}$ and $H_{l/u}$ are defined by a suitable interpolation rule from the values of its 'image' on the bounding surface. The definition of image point and interpolation rule could be very flexible according to generalized plasticity.

The proposed model is based on the generalized plasticity-bounding surface formulation (Zienkiewicz and Mroz, 1984 and Dafalias, 1975). It is also a simplified version of the two-surface elasto-plastic model introduced by Poorooshasb and

Pietruszczak (1986). A brief description of this two-surface model is given below. It invokes two families of surfaces (Figure 4.1). The first family is called the bounding surface which is assumed to be created by an active loading process imposed upon virgin material. The bounding surface expands along with the accumulation of plastic distortion which serves as the measure of the loading history until the stress point tends to move inside it (stress reversal) or a limit state (failure) is reached. It is of an isotropic plastic distortion strain hardening type. The second family is called the yield surface which defines a pure elastic domain and is involved in all stress reversal programs. Upon stress reversal, the yield surface moves within and indeed is guided by the bounding surface. As long as the stress point reaches the bounding surface and tends to move outside, it will behave again as a virgin material. It should be emphasized that during the stress reversal programs the bounding surface may expand or contract depending on the mode of accumulation of plastic distortion. The non-associated flow rule is used. A global plastic potential is incorporated in the model to define the direction of plastic strain increment for the virgin loading process while a local plastic potential is for the stress reversal program (Figure 4.2). Nevertheless, the local plastic potential is related to the global plastic potential in a reflecting manner as shown in Figure 4.5 for the triaxial configuration.

In the light of the generalized plasticity formulation, it is not necessary to use a yield surface and plastic potential, if one can specify D^e, n, $n_{gl/u}$ and $H_{l/u}$ in some way. This idea is quite clear and useful in modelling soil behaviour under complicated loading conditions.

45
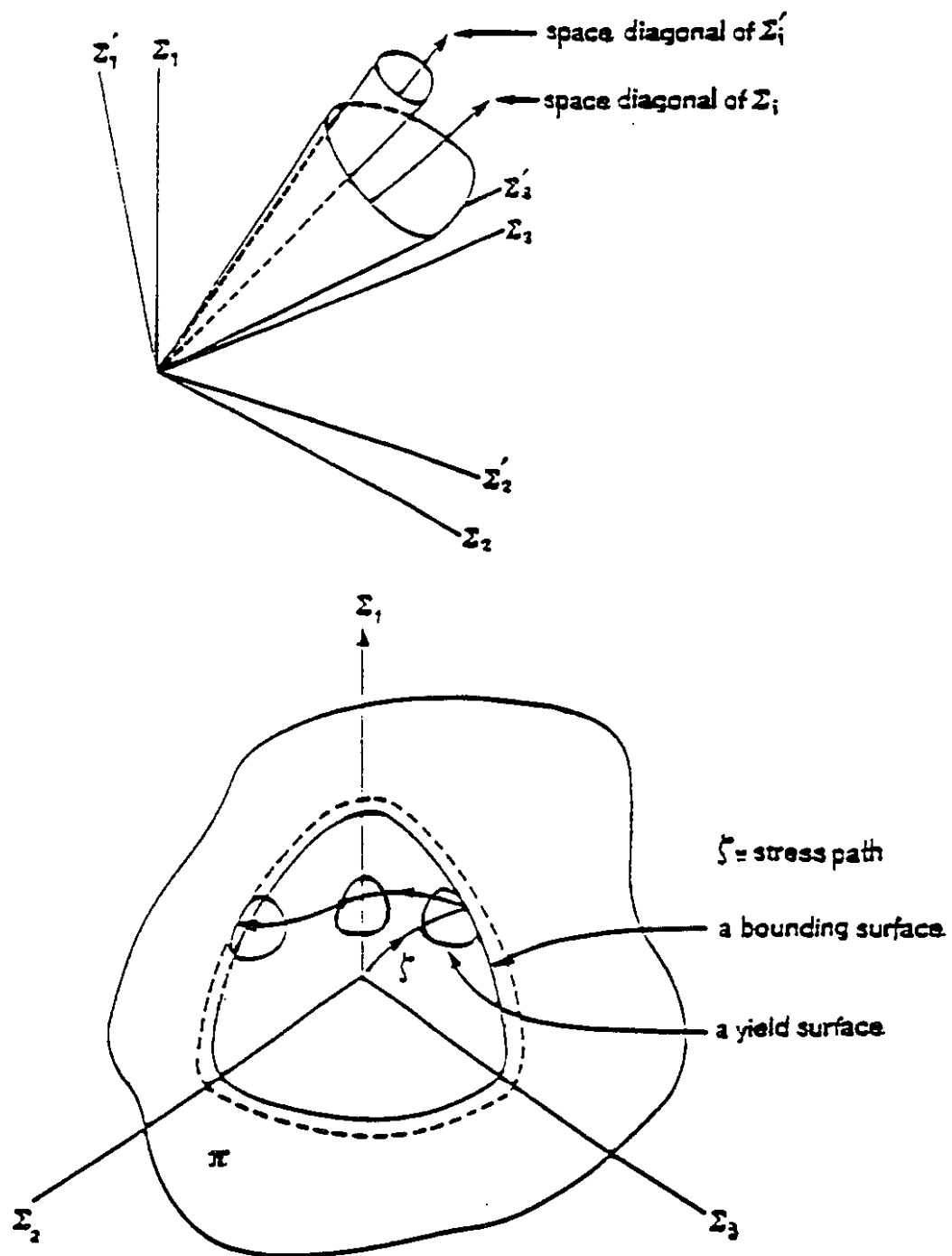
Figure 4.1 Bounding surface and yield surface of the two-surface model

(Poorooshasb and Pietruszczak, 1986)

46
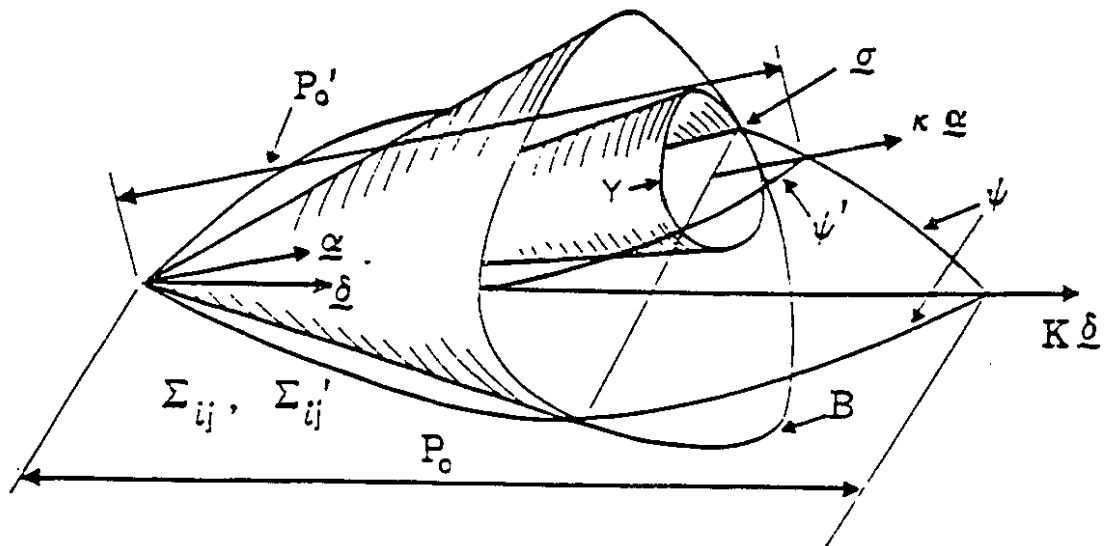
Figture 4.2 Global and local plastic potentials of the two-surface model

(Poorooshasb and Pietruszczak, 1986)

4.3 DERIVATION OF THE PROPOSED MODEL

4.3.1 Modelling in the triaxial configuration

In the triaxial configuration ($\sigma'_2 = \sigma'_3$), the usual stress and strain measurements

p', q and $d\varepsilon_v$, $d\varepsilon_s$ are given in terms of the principal effective stress and strain

$$p' = (\sigma'_1 + 2 \sigma'_3) / 3 , \qquad q = \sigma'_1 - \sigma'_3 \qquad\qquad (4.9)$$

$$d\varepsilon_v = d\varepsilon_1 + 2 d\varepsilon_3 , \qquad d\varepsilon_s = 2(d\varepsilon_1 - d\varepsilon_3) / 3$$

The increment of work dW would equal to

$$dW = p' d\varepsilon_v + q d\varepsilon_s = \sigma'_1 d\varepsilon_1 + 2\sigma'_3 d\varepsilon_3$$

p' and q are related to the effective stress invariants by

$$p' = I_1 / 3 \qquad , \qquad\qquad q = (3 J_2)^{1/2} \qquad\qquad (4.10)$$

where I_1 is the first invariant of the effective stress tensor and J_2 is the second invariant of the stress deviation tensor.

The yield loci are almost straight lines radiating outwards from the origin according to several test results (see Figure 4.3, Tatsuoka and Ishihara , 1974). So it is reasonable to choose the bounding / yield surface as follows

$$F = F (p', q, e^*) = q - \eta(e^*) p' = 0 \qquad\qquad (4.11)$$

$$\eta(e^*) = \eta_f [1 - \exp(- e^* / A)] \qquad\qquad (4.12)$$

$$e^* = \int | d\varepsilon^P_s |$$

where $d\varepsilon^P_s$ is the plastic deviatoric strain increment, A is the plastic hardening parameter

and η_f can be related to the angle of internal frection , ϕ_f , by the Mohr-Coulomb relation

$$\eta_f = (6 \sin \phi_f) / (3 - \sin \phi_f) \qquad \text{when } \sigma'_1 > \sigma'_3 \text{ (compression)}$$

$$\eta_f = (6 \sin \phi_f) / (3 + \sin \phi_f) \qquad \text{when } \sigma'_1 < \sigma'_3 \text{ (extension)}$$

$$R = \eta_f \text{ (compression) } / \eta_f \text{ (extension) } = (3 + \sin \phi_f) / (3 - \sin \phi_f) \qquad (4.13)$$
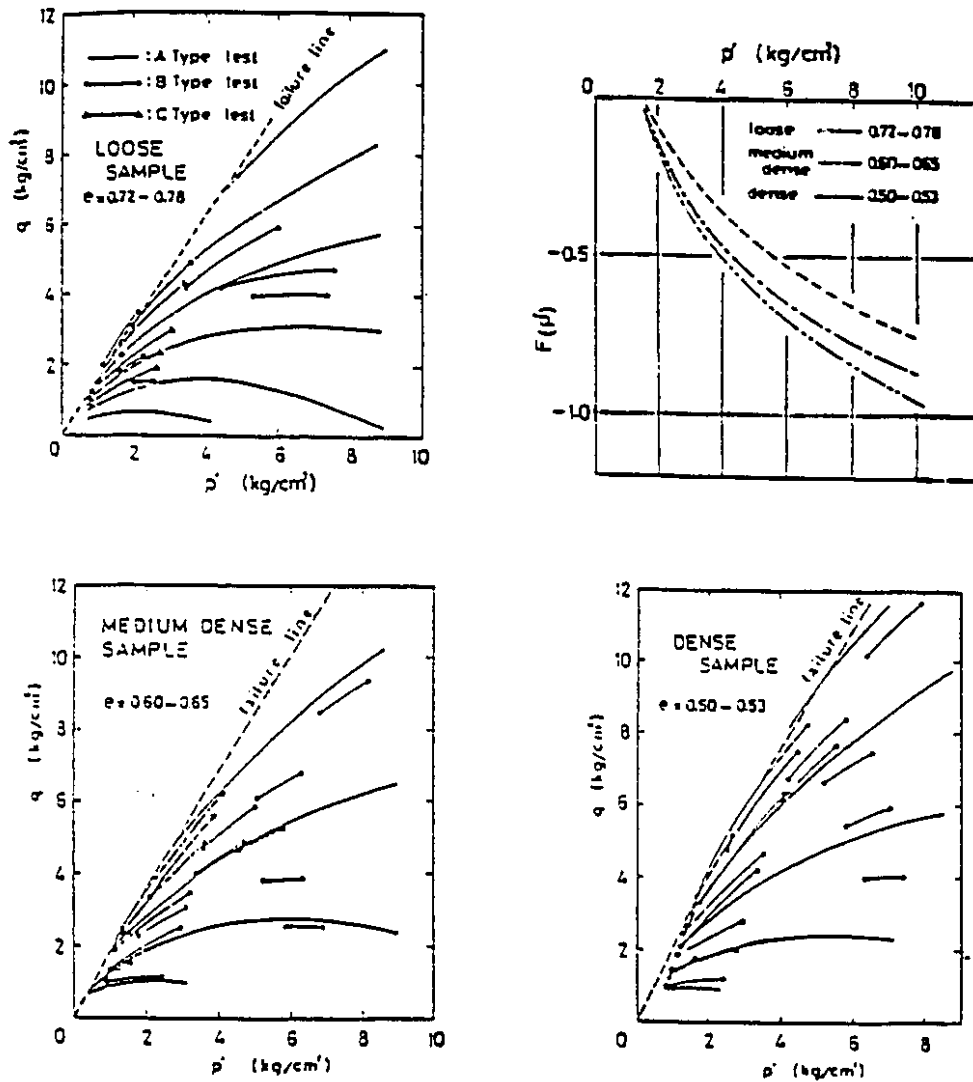
Figure 4.3 Yield surface for sand with different densities

(after Tatsuoka and Ishihara 1974)

49

The plastic potential G could be written as

$$G = G (p',q) = 0 \qquad \text{or} \qquad q = q(p') \qquad (4.14)$$

The plastic volumetric and deviatoric strain increments would be

$$d\varepsilon^P_v = d\lambda \left(\partial G / \partial p' \right), \qquad d\varepsilon^P_s = d\lambda \left(\partial G / \partial q \right)$$

Therefore the dilatancy d, defined as the ratio of the plastic strain increments, could be expressed by

$$d = d\varepsilon^P_v / d\varepsilon^P_s = \left(\partial G / \partial p' \right) / \left(\partial G / \partial q \right) = - dq / dp' \qquad (4.15)$$

On the basis of the experimental work of Stroud (1971) on sand it is possible to assume that the dilatancy depends only on the state of stress and not on the stress increment. A plot of the experimental data of Frossard (1983) is shown in Figure 4.4.
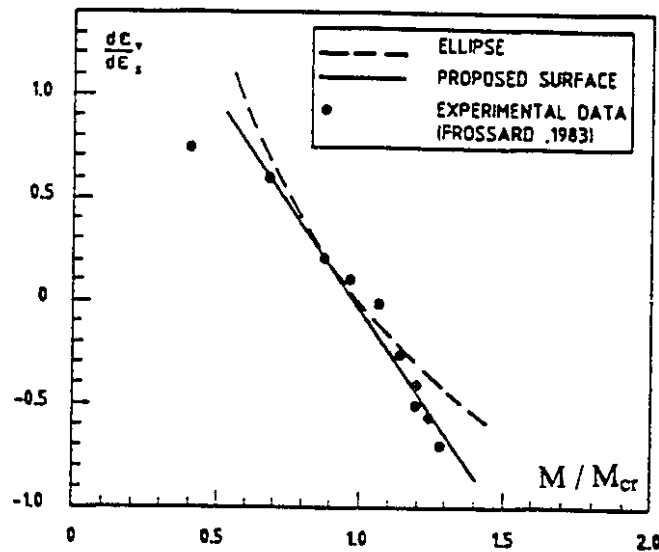
Figure 4.4   Experimental and predicted values for dilatancy

50

Nova (1982) suggested a linear stress-dilatancy relationship

$$M = M_{cr} - \mu d \qquad (4.16)$$

where M_{cr} and μ are positive material constants while M is the stress ratio

$$M = q / p' \qquad (4.17)$$

so that $\qquad d = - dq / dp' = - (M - M_{cr}) / \mu \qquad (4.18)$

If $\mu = 1$ then integration of equation (4.18) leads to

$$G = q + M_{cr} \, p' \ln (p' / p'_0) = 0 \qquad (4.14)$$

In the above equation p_0' is a size parameter at which q=0. It has no influence on defining

the plastic flow vector $\mathbf{n}_g$.

It is easy to show that equation (4.14) may be written, alternatively, as

$$G = p' \exp (M / M_{cr}) - p'_0 = 0$$

which falls into the general form of plastic potential suggested by Poorooshasb et al.(1966).

The line $M=q/p'=M_{cr}$ on which no plastic volumetric strain occurs is synonymous with the

'critical state line' (CSL), which has been also termed 'the characteristic state line' by

Habib and Luong (1978) or 'the phase transformation line' by Ishihara, et al. (1975). Its

slope is given by M_{cr} which can be related to the residual angle of friction, ϕ_{cr}, by the Mohr-

Coulomb relations as

$$M_{cr} = (6 \sin \phi_{cr}) / (3 - \sin \phi_{cr}) \quad \text{when} \ \sigma'_1 > \sigma'_3 \ \text{(compression)}$$

$$M_{cr} = (6 \sin \phi_{cr}) / (3 + \sin \phi_{cr}) \quad \text{when} \ \sigma'_1 < \sigma'_3 \ \text{(extension)} \qquad (4.19)$$

For virgin loading, the bounding surface F in (4.11) and the plastic potential G in

(4.14) are used to determine $\mathbf{n}$ and $\mathbf{n}_{gl}$ by (4.5) and (4.6) respectively. While H_1 could be

obtained from (4.7) with $q_n = \eta(e^*)$,

51

$$H_l = \frac{q}{A} \left(\frac{\eta_f}{M} - 1\right) \left|\frac{\partial G}{\partial q}\right| / \left[\left(\frac{\partial F}{\partial \sigma'}\right)^T \left(\frac{\partial F}{\partial \sigma'}\right) \right]^{1/2} \tag{4.20}$$

If unloading (stress reversal) occurs, it is assumed $H_u = \infty$ at this moment.

For the stress reversal process, the stress point lies inside the bounding surface. However, it will be on a surface F_c with a certain value of e^{*}_c.

$$F_c (p', q, e^{*}_c) = 0 \tag{4.21}$$

which is used to define n_c according to (4.4). One can now distinguish loading and unloading in terms of this n_c.

The vector n_{gl} is specified by G_c which passes through the actual stress point. However, instead of a small yield surface and a local reflecting plastic potential used in the two-surface model, n_{gu} is directly related to n_{gl} as shown in Figure 4.5 and Figure 4.6,

$$n_{gu} (n^{v}_{gu}, n^{s}_{gu}) = (n^{v}_{gl}, n^{s}_{gl}) \qquad \text{if } M > M_{cr}$$

$$n_{gu} (n^{v}_{gu}, n^{s}_{gu}) = (-n^{v}_{gl}, n^{s}_{gl}) \qquad \text{if } M < M_{cr} \tag{4.22}$$

where the superscripts v and s refer to the components along the p' and q axis respectively.

It is evident that this definition of n_{gu} will produce almost the same results as those by the two-surface model since the pure elastic domain is very small for many soils. However it simplifies the model considerably.

The 'image' point on the bounding surface is defined by a simple 'deviatoric radial' rule Figure 4.6. The image point is the intersection of the bounding surface and the straight line which is perpendicular to the p' axis and passes through the actual stress point. The image point and the actual point are located on the same side for loading and on the opposite sides for unloading, i.e.

52

$$\delta = \underline{ac} \qquad\qquad \text{if loading}$$

$$\delta = \underline{ad} \qquad\qquad \text{if unloading} \qquad (4.23)$$

$$\delta_0 = \underline{ac} + \underline{ad} \qquad\qquad \text{(see Figure 4.6)}$$

Finally, we need $H_{l/u}$ which could be defined by the interpolation rule:

$$\frac{1}{H_{l/u}} = \frac{1}{H_B} \left(1 - \frac{\delta}{\delta_0} \right)^\gamma \qquad\qquad (4.24)$$

where γ is a material parameter and H_B is the plastic moduli at the image point.

It may be noted that although H_l and H_u are expressed similarly in equation (4.24), they are different. The reason is that H_B and δ have different values in the two cases: the image points are not the same for loading and unloading.

Another point worthy of mention is as follows. The results of drained cyclic test (Fig.4.11 and Figure 4.12) show the cyclic load - densification phenomena. A remarkable fact is that volumetric plastic strain developed during unloading is always of a contractive nature, which makes the material exhibit an overall densifying character. This unloading - contraction feature is ensured by the definition of n and n_{gu} in the proposed model. However, volumetric compression occurs at a progressively decreasing rate as the sand densifies. This is obtained by changing the interpolation index γ along with the densification process.

$$\gamma = \gamma_0 \qquad\qquad \text{if } \varepsilon_v \leq B \qquad (4.25)$$

$$\gamma = \gamma_0 \, \varepsilon_v \, / B \qquad\qquad \text{if } \varepsilon_v > B$$

where γ_0 and B are positive constants.

4.3.2. Material parameters of the model

In order to identify the model, elastic parameters are required to determine $\mathbf{D^e}$. In this study ν, Possion's ratio is taken as constant and K, the bulk modulus is assumed to depend on the mean effective stress in such a manner that;

$$K = K_Z + \sqrt{3} \, \sigma'_m / \kappa \qquad (4.26)$$

where K_z and κ are constants.

In total, eight material constants, K_z, κ, ν, ϕ_f, ϕ_{cr}, A, B, γ_0 are used in the model. All the above parameters except for B and γ_0 can be determined from the results of a conventional triaxial compression test. The parameter γ_0 can be evaluated from the results of an undrained cyclic test by a process of trial and error. Finally B can be determined from the results of a drained cyclic test.
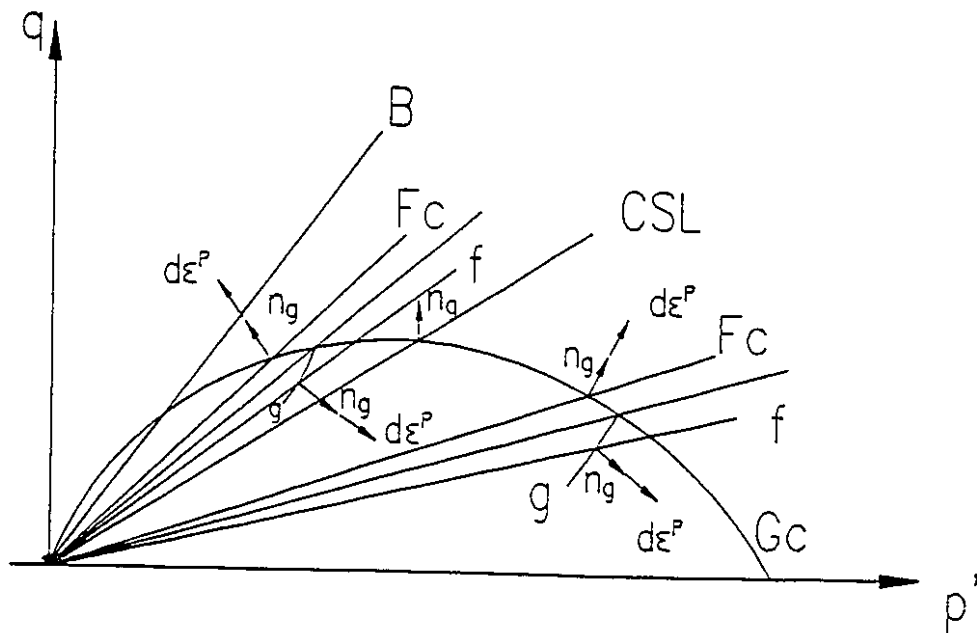
Figure 4.5   Two-surface model with reflecting plastic potential
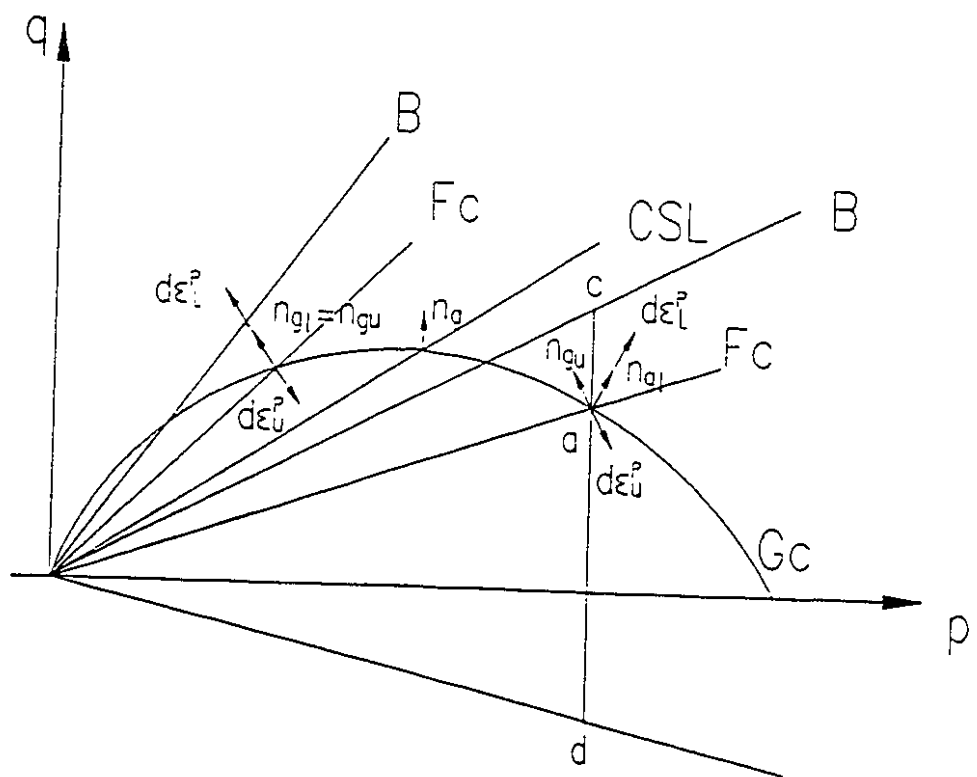
Figure 4.6   Simple model in triaxial plane

55

4.4 FORMULATION IN GENERAL EFFECTIVE STRESS SPACE

So far, only the triaxial configuration has been considered. To be employed in a computer program for the solution of boundary value problems, the model must be generalized to describe every possible stress path in the effective stress space. Following Drucker and Prager (1952) it is possible to generalize the formulations from a triaxial field to the full principal stress space.

In the triaxial configuration, the bounding surface and the plastic potential are

$$F = q - \eta(e^*) \, p' \qquad (4.11)$$

$$\eta(e^*) = \eta_f \, [\, 1 - \exp(-e^*/A) \,] \qquad (4.12)$$

$$\eta_f \text{ (compression)} = 6 \sin \phi_f / (3 - \sin \phi_f) \qquad (4.13)$$

$$G = q + M_{cr} \, p' \ln (p' / p'_0) = 0 \qquad (4.14)$$

$$M_{cr} \text{ (compression)} = 6 \sin \phi_{cr} / (3 - \sin \phi_{cr}) \qquad (4.19)$$

or expressed by the principal stress I_1 and J_2,

$$F = (3 \, J_2)^{1/2} - \eta(e^*) \, I_1 / 3 \qquad (4.11)'$$

$$G = (3 \, J_2)^{1/2} + M_{cr} \, (I_1 / 3) \ln (I_1 / I_1^{\,0}) \qquad (4.14)'$$

It is convenient to use the set (r, θ, Z) which have the true values in the π plane and diagonal of the principal stress space as shown in Figure 4.7,

$$r = (2 \, J_2)^{1/2}$$

$$\theta = \sin^{-1} (-3 \sqrt{3} \, J_3 / (2 \, J_2^{3/2})) / 3 , \quad -\pi/6 \le \theta \le \pi/6$$

$$Z = I_1 / \sqrt{3} \qquad (4.27)$$

Where I_1 is the first invariant of the effective stress tensor σ'_{ij} while J_2 and J_3 are the second and the third invariants of the stress deviation tensor s_{ij}.

$$I_1 = \sigma'_{kk}$$

$$J_2 = s_{ij} \, s_{ij} / 2$$

$$J_3 = s_{ij} \, s_{jk} \, s_{ki} / 3 \qquad\qquad (4.28)$$

$$s_{ij} = \sigma'_{ij} - \sigma'_{kk} \, \delta_{ij} / 3$$
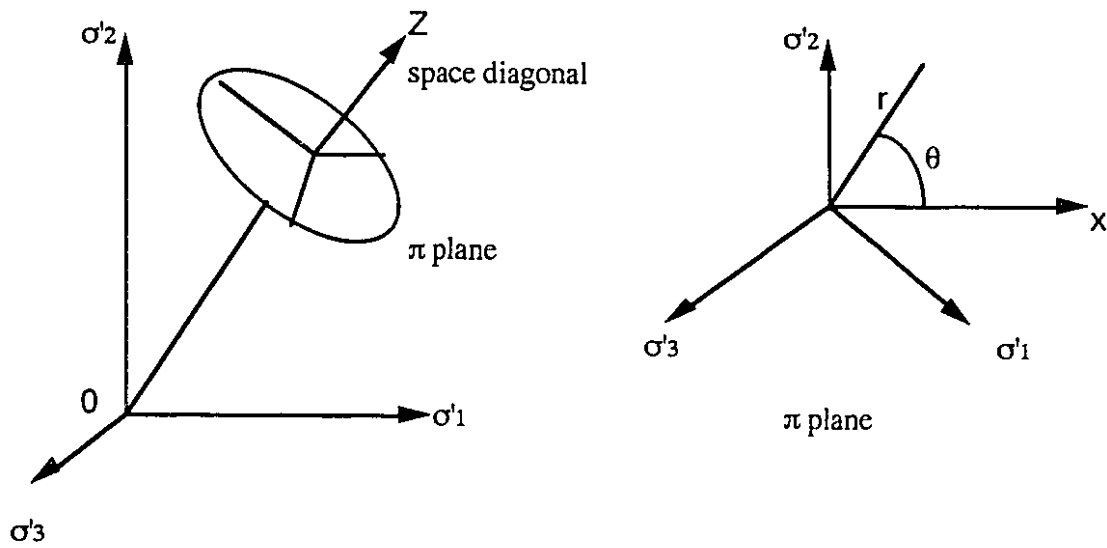
Figure 4.7 The expression of r, θ, Z in the principal stress space.

Firstly, F and G can be transformed by the set (r, θ, Z) with $\theta = -\pi / 6$ for triaxial compression and eliminating a constant coefficient $(2/3)^{1/2}$

$$F = r - (\sqrt{2}/3) \, \eta(e^*) \, Z = 0 \qquad\qquad (4.11)''$$

$$G = r + (\sqrt{2}/3) \, M_{cr} \, Z \ln (Z / Z_0) = 0 \qquad\qquad (4.14)''$$

Secondly, the equation of the bounding surface could be generalized to the whole stress space with all the features in the triaxial formulation retained,

$$F = r - \eta(e^*) \, g(\theta) \, Z = 0 \qquad\qquad (4.29)$$

where e^* is a measure of the total plastic distortion given by the expression

$$e^* = \int de^* \, ,$$

$$de^* = (de^P_{ij} \, de^P_{ij})^{1/2} \, ,$$

$$de^P_{ij} = d\varepsilon^P_{ij} - d\varepsilon^P_{kk} \, \delta_{ij} / 3$$

Here de^P_{ij} is the incremental plastic deviatoric strain. The function $\eta(e^*)$ recording the loading history is given by the relation

$$\eta(e^*) = \eta_f \, [\, 1 - \exp (- e^* / A)] \, ,$$

$$\eta_f = 2\sqrt{2} \sin \phi_f / (3 - \sin \phi_f) \qquad\qquad (4.30)$$

by which the size of the bounding surface is determined. The bounding surface approaches the failure envelope when e^* increases continuously. However, it is better to have a very small value η_0 when e^* equals zero to avoid certain difficulties in dealing with the purely hydrostatic pressure state of stress.

The function $g(\theta)$ is used to describe the cross section shape of the bounding surface on the π plane. It should be convex and symmetric with respect to three axes for

58

isotropic materials. The ellipse formulation first proposed by William and Wande (1975) is adopted to quantify the function $g(\theta)$. It is symmetric and will be convex if

$$1 \leq g_{max} / g_{min} \leq 2$$

In the present case

$$g(-\pi/6) = g_{max} = 1 \qquad\qquad \text{for triaxial compression}$$

$$g(\pi/6) = g_{min} = (3 - \sin \phi_f) / (3 + \sin \phi_f) \qquad \text{for triaxial extension}$$

are chosen to be consistent with the Mohr-Coulomb failure criterion.

$$R = g_{max} / g_{min} = (3 + \sin \phi_f) / (3 - \sin \phi_f) \qquad\qquad (4.31)$$

Therefore, the convexity is always ensured . Function $g(\theta)$ could be expressed by θ_1 as shown in Figure 4.8.

$$\theta_1 = \theta - \pi / 6 \qquad -\pi/6 \leq \theta \leq \pi/6 \quad, \qquad -\pi/3 \leq \theta_1 \leq 0$$

$$g(\theta) = g(\theta_1 + \pi / 6) = (C_1 \cos \theta_1 + C_5) / (C_4 + C_2) \qquad\qquad (4.32)$$

where

$$C_1 = 2(R^2 - 1)$$

$$C_2 = (2 - R)^2$$

$$C_3 = 5 - 4R$$

$$C_4 = 2 C_1 \cos^2 \theta_1$$

$$C_5 = (C_2(C_4 + C_3))^{1/2}$$

It is easy to calculate its derivative

$$g'(\theta) = g'(\theta_1) = [2\sin 2\theta_1 (C_1 \cos \theta_1 + C_5) - (\sin \theta_1 + (C_2 / C_5) \sin 2\theta_1)(C_4 + C_2)] C_1 / (C_4 + C_2)$$

Some values used in next section are listed below:

$$g'(-\pi/6) = 0, \quad g''(-\pi/6) = -3C_1 / (2C_2) = -3(R^2 - 1) / (2 - R)^2 < \infty$$

$$g'(\pi/6) = 0, \quad g''(\pi/6) = C_1 / (R^2(2R-1)) = 2(R^2-1) / (R^2(2R-1)) < \infty \qquad (4.33)$$

The shape of bounding surface is similar to that in the two-surface model (Poorooshasb and Pietruszczak,1986) which is a cone having straight meridians and a non-circular cross section with its apex at the origin and its axis along the diagonal of the stress space, as shown in Figure 4.1 .

Thirdly, the plastic potential could be generalized in the same way

$$G = r + M_{cr} \, g(\theta) \, Z \ln (Z / Z_0) = 0 \qquad (4.34)$$

$$M_{cr} = 2\sqrt{2} \, \sin \phi_{cr} / (3 - \sin \phi_{cr})$$
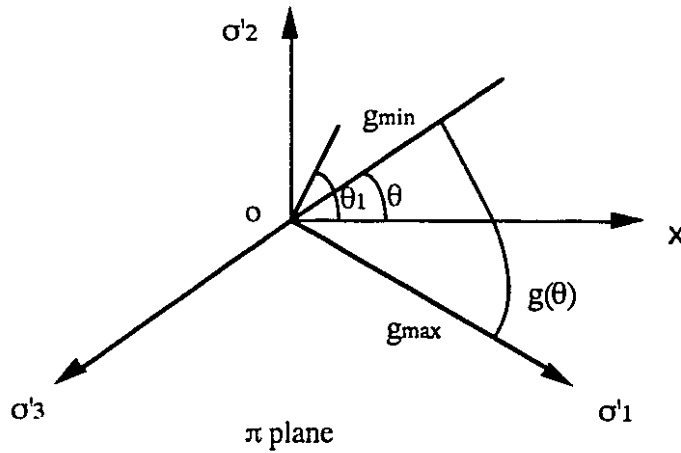
Figure 4.8   Elliptic trace of the function $g(\theta)$

60

In summary, the constitutive equations are determined by $\mathbf{D}^e$, $\mathbf{n}$, $\mathbf{n}_{gl/u}$, $H_{l/u}$

If $\mathbf{n}^T d\sigma' > 0$ loading   ,   use $\mathbf{n}_{gl}$ and H_l ,

If $\mathbf{n}^T d\sigma' < 0$ unloading   ,   use $\mathbf{n}_{gu}$ and H_u.

$$d\varepsilon = d\varepsilon^e + d\varepsilon^p = (\mathbf{D}_{l/u})^{-1} d\sigma' \tag{4.1}'$$

$$(\mathbf{D}_{l/u})^{-1} = (\mathbf{D}^e)^{-1} + \mathbf{n}_{gl/u} \, \mathbf{n}^T / H_{l/u} \tag{4.2),(4.3}$$

$$d\sigma' = (\mathbf{D}_{l/u}) d\varepsilon \tag{4.1}$$

$$\mathbf{D}_{l/u} = \mathbf{D}^e - \frac{\mathbf{D}^e \, \mathbf{n}_{g\,l/u} \, \mathbf{n}^T \, \mathbf{D}^e}{H_{l/u} + \mathbf{n}^T \mathbf{D}^e \, \mathbf{n}_{g\,l/u}} \tag{4.4}$$

For virgin loading process $F(\sigma', e^*) = 0$

$$\mathbf{n}^T = \frac{\partial F}{\partial \sigma'} / [\, (\frac{\partial F}{\partial \sigma'})^T (\frac{\partial F}{\partial \sigma'}) \,]^{1/2} \tag{4.5}$$

If $\mathbf{n}^T d\sigma' > 0$,   virgin loading

$$\mathbf{n}_{gl}^T = \frac{\partial G}{\partial \sigma'} / [\, (\frac{\partial G}{\partial \sigma'})^T (\frac{\partial G}{\partial \sigma'}) \,]^{1/2} \tag{4.6}$$

$$H_l = \frac{r}{A} (\frac{\eta_f}{\eta} - 1) \, [\, (\mathrm{dev}\,\frac{\partial G}{\partial \sigma'})^T (\mathrm{dev}\,\frac{\partial G}{\partial \sigma'}) \,]^{1/2} / [\, (\frac{\partial F}{\partial \sigma'})^T (\frac{\partial F}{\partial \sigma'}) \,]^{1/2} \, [\, (\frac{\partial G}{\partial \sigma'})^T (\frac{\partial G}{\partial \sigma'}) \,]^{1/2}$$

$$\tag{4.35}$$

with

$$\eta = r / (g(\theta) \, Z) \tag{4.36}$$

If $\mathbf{n}^T d\sigma' < 0$, pure elastic response

$$H_u = \infty \quad , \qquad \mathbf{D}_u = \mathbf{D}^e \tag{4.8}$$

61

For stress reversal process, $F(\sigma', e^*) < 0$. The condition $F_c(\sigma', e^*_c) = 0$ leads to

$$\mathbf{n}_c^T = \frac{\partial F_c}{\partial \sigma'} / \left[\left(\frac{\partial F_c}{\partial \sigma'} \right)^T \left(\frac{\partial F_c}{\partial \sigma'} \right) \right]^{1/2}$$

(4.5)'

If $\mathbf{n}_c^T d\sigma' > 0$, the process is loading; $\mathbf{n}_c^T d\sigma' = 0$, pure elastic response and

$\mathbf{n}_c^T d\sigma' < 0$, unloading. The loading flow vector $\mathbf{n}_{gl}$ is given by

$$\mathbf{n}_{gl}^T = \frac{\partial G_c}{\partial \sigma'} / \left[\left(\frac{\partial G_c}{\partial \sigma'} \right)^T \left(\frac{\partial G_c}{\partial \sigma'} \right) \right]^{1/2}$$

(4.6)

The unloading flow vector $\mathbf{n}_{gu}$ is related to $\mathbf{n}_{gl}$ in the same manner as indicated in (4.22)

$$\mathbf{n}_{gu} (n^v_{gu}, n^s_{gu}) = (n^v_{gl}, n^s_{gl}) \qquad \text{if } \eta > M_{cr} / g(\theta)$$

$$\mathbf{n}_{gu} (n^v_{gu}, n^s_{gu}) = (-n^v_{gl}, n^s_{gl}) \qquad \text{if } \eta < M_{cr} / g(\theta) \qquad (4.22)$$

where superscript s refers to the deviatoric component in the π plane and v stands for the

hydrostatic component along the diagonal of the space. $H_{l/u}$ is obtained according to the

definition of the image point (4.23) (see Figure 4.6)

$$\delta = \underline{ac} \qquad \qquad \text{if loading}$$

$$\delta = \underline{ad} \qquad \qquad \text{if unloading} \qquad (4.23)$$

$$\delta_0 = \underline{ac} + \underline{ad} \qquad \qquad \text{(see Figure 4.6)}$$

and the interpolation rule (4.24) in which H_B is the plastic moduli at the image point

$$\frac{1}{H_{l/u}} = \frac{1}{H_B} \left(1 - \frac{\delta}{\delta_0} \right)^\gamma$$

(4.24)

$$\gamma = \gamma_0 \qquad \qquad \text{if } \varepsilon_v \leq B$$

$$\gamma = \gamma_0 \, \varepsilon_v / B \qquad \qquad \text{if } \varepsilon_v > B \qquad (4.25)$$

4.5 NUMERICAL IMPLEMENTATION

4.5.1 Stress controlled drained path

The stress controlled drained path requires the determination of the strain increment for a given effective stress increment with the initial state known. The algorithm is straightforward. However, for implementation of the model into a numerical code, all the quantities have to be expressed in terms of stress variables r, θ and Z_1. This is given as follows:

$$I_1 = \sigma'_{kk}$$

$$J_2 = s_{ij}\, s_{ij} \, / \, 2$$

$$J_3 = s_{ij}\, s_{jk}\, s_{ki} \, / \, 3 \qquad\qquad (4.28)$$

$$s_{ij} = \sigma'_{ij} - \sigma'_{kk}\, \delta_{ij} \, / \, 3$$

$$t_{ij} = s_{ik}\, s_{kj} - s_{lk}\, s_{kl}\, \delta_{ij} \, / \, 3$$

$$\partial I_1 \, / \, \partial \sigma' = \mathbf{m}^T$$

$$\partial J_2 \, / \, \partial \sigma' = \mathbf{s}^T$$

$$\partial J_3 \, / \, \partial \sigma' = \mathbf{t}^T$$

where

$$\mathbf{m}^T = [\, 1, \, 1, \, 0, \, 1, \, 0, \, 0 \,]$$

$$(\sigma')^T = [\, \sigma_x, \, \sigma_y, \, 2\tau_{xy}, \, \sigma_z, \, 2\tau_{xz}, \, 2\tau_{yz} \,]$$

$$\mathbf{s}^T = [\, s_x, \, s_y, \, 2\tau_{xy}, \, s_z, \, 2\tau_{xz}, \, 2\tau_{yz} \,]$$

$$\mathbf{t}^{T} = [\ (s_y s_z, -\tau^2_{yz} + J_2 / 3\ ),\ (s_z s_x, -\tau^2_{zx} + J_2 / 3\ ),\ 2(\tau_{xz}\tau_{yz}, -s_z\tau_{xy}\ ),$$

$$(s_x s_y, -\tau^2_{yz} + J_2 / 3\ ),\ 2(\tau_{yx}\tau_{zx}, -s_x\tau_{yz}\ ),\ 2(\tau_{xy}\tau_{zy}, -s_y\tau_{xz}\ )\ ]$$

$$r = (2\,J_2)^{1/2}$$

$$\theta = \sin^{-1}(\ -3\sqrt{3}\,J_3\,/\,(\,2\,J_2^{3/2}))\,/\,3\ ,\quad -\pi/6 \le \theta \le \pi/6$$

$$Z = I_1 / \sqrt{3} \tag{4.27}$$

$$\partial r\,/\,\partial\sigma' = (\ \partial r\,/\,\partial J_2\ )(\partial J_2\,/\,\partial\sigma') = \mathbf{s}^{T}\,/\,r$$

$$\frac{\partial\theta}{\partial\sigma'} = -\frac{\sqrt{3}}{2\cos 3\theta}\frac{1}{J_2^{3/2}}\frac{\partial J_3}{\partial\sigma'} - \frac{\tan 3\theta}{2\,J_2}\frac{\partial J_2}{\partial\sigma'} = \frac{-\sqrt{6}}{r^3\cos 3\theta}\,\mathbf{t}^{T} + \frac{-\tan 3\theta}{r^2}\,\mathbf{s}^{T}$$

$$\partial Z\,/\,\partial\sigma' = (\ \partial Z\,/\,\partial I_1\ )(\partial I_1\,/\,\partial\sigma') = \mathbf{m}^{T}\,/\,\sqrt{3}$$

Thus

$$\mathbf{a}^{T} = \partial F\,/\,\partial\sigma' = (\partial F\,/\,\partial Z)(\partial Z\,/\,\partial\sigma') + (\partial F\,/\,\partial r)(\partial r\,/\,\partial\sigma') + (\partial F\,/\,\partial\theta)(\partial\theta\,/\,\partial\sigma')$$

$$= \frac{1}{\sqrt{3}}\frac{\partial F}{\partial Z}\,\mathbf{m}^{T} + (\ \frac{1}{r}\frac{\partial F}{\partial r} - \frac{\tan 3\theta}{r^2}\frac{\partial F}{\partial\theta}\ )\,\mathbf{s}^{T} + \frac{-\sqrt{6}}{r^3\cos 3\theta}\frac{\partial F}{\partial\theta}\,\mathbf{t}^{T}$$

$$= c_{11}\,\mathbf{m}^{T} + c_{12}\,\mathbf{s}^{T} + c_{13}\,\mathbf{t}^{T} \tag{4.37}$$

For bounding surface

$$F = r - \eta(e^*)\,g(\theta)\,Z = 0 \tag{4.29}$$

$$c_{11} = -r\,/\,(\sqrt{3}\,Z\,)$$

$$c_{12} = (1 + \tan 3\theta\,(g'(\theta)\,/\,g(\theta)\,)\,)\,/\,r \tag{4.38}$$

$$c_{13} = \sqrt{6}\,g'(\theta)\,/\,(\,g(\theta)\,r^2\cos 3\theta\,)$$

$\mathbf{b}^T = \partial G / \partial \sigma' = (\partial G / \partial Z)(\partial Z / \partial \sigma') + (\partial G / \partial r)(\partial r / \partial \sigma') + (\partial G / \partial \theta)(\partial \theta / \partial \sigma')$

$$= \frac{1}{\sqrt{3}} \frac{\partial G}{\partial Z} \mathbf{m}^T + (\frac{1}{r} \frac{\partial G}{\partial r} - \frac{\tan 3\theta}{r^2} \frac{\partial G}{\partial \theta}) \mathbf{s}^T + \frac{-\sqrt{6}}{r^3 \cos 3\theta} \frac{\partial G}{\partial \theta} \mathbf{t}^T$$

$$= c_{14} \mathbf{m}^T + c_{15} \mathbf{s}^T + c_{16} \mathbf{t}^T \qquad (4.39)$$

For plastic potential

$$G = r + M_{cr} g(\theta) Z \ln (Z / Z_0) = 0 \qquad (4.34)$$

$$c_{14} = - (r / Z - M_{cr} g(\theta)) / \sqrt{3}$$

$$c_{15} = c_{12} \qquad (4.40)$$

$$c_{16} = c_{13}$$

$$| \mathbf{a} | = (\mathbf{a}^T \mathbf{a})^{1/2} \qquad\qquad \mathbf{n} = \mathbf{a} / | \mathbf{a} |$$

$$| \mathbf{b} | = (\mathbf{b}^T \mathbf{b})^{1/2} \qquad\qquad \mathbf{n}_g = \mathbf{b} / | \mathbf{b} |$$

$$\mathbf{v}^T = c_{14} \mathbf{m}^T$$

$$\mathbf{d}^T = \text{dev} (\partial G / \partial \sigma') = \text{dev } \mathbf{b}^T = c_{15} \mathbf{s}^T + c_{16} \mathbf{t}^T \qquad | \mathbf{d} | = (\mathbf{d}^T \mathbf{d})^{1/2}$$

$$H_l = (r / A)(\eta_f / \eta - 1) | \mathbf{d} | | \mathbf{a} | | \mathbf{b} | \qquad (4.35)$$

It is worth mentioning that

(1) $Z = 0$ means that the effective stress becomes zero, i.e. the soil sample liquefies. c_{11} and c_{14} in (4.38) and (4.40) would also become singular. The model could drive the material to reach this state under certain conditions but cannot proceed further.

(2) $Z \neq 0$ but $r = 0$, i.e. isotropic compression state. θ is undetermined and singularity would be encountered in calculating c_{12} and c_{13}. This may be avoided by setting a small value of r when it approaches zero.

(3) When $\theta = \pm\pi / 6$, an indeterminate form 0/0 is involved in c_{12} and c_{13}. This problem is solved by L'Hopital's rule with the value of $g''(0)$ in (4.33)

$$\lim_{\theta \to -\pi/6} \frac{g'(\theta)}{\cos 3\theta} = \lim_{\theta \to -\pi/6} \frac{g''(\theta)}{-3 \sin 3\theta} = -\frac{(R^2 - 1)}{(2 - R)^2}$$

$$\lim_{\theta \to \pi/6} \frac{g'(\theta)}{\cos 3\theta} = \lim_{\theta \to \pi/6} \frac{g''(\theta)}{-3 \sin 3\theta} = -\frac{-2(R^2 - 1)}{(3R^2(2R-1))}$$

for $\theta = -\pi/6$, $c_{12} = c_{15} = (1 + (R^2-1) / (2 - R)^2) / r$

$c_{13} = c_{16} = -\sqrt{6} (R^2 - 1) / ((2 - R)^2 r^2)$ (4.31)

for $\theta = \pi/6$, $c_{12} = c_{15} = (1 - 2(R^2-1) / (3R (2R - 1)) / r$

$c_{13} = c_{16} = -2\sqrt{6} (R^2 - 1) / (3R (2R - 1) r^2)$ (4.32)

4.5.2 Stress controlled undrained path

For incompressible fluid and solid phases, the undrained condition would imply the internal constraint $d\varepsilon_{kk} = 0$, which by means of equations (4.2), (4.3), (4.5) and (4.6) yields

$$d\varepsilon_{kk} = d\varepsilon^e_{kk} + d\varepsilon^p_{kk} = C^e_{kkij}d\sigma'_{ij} + \frac{1}{K_p} \frac{\partial G}{\partial \sigma'_{kk}} \frac{\partial F}{\partial \sigma'_{ij}} d\sigma'_{ij} = 0$$ (4.33)

where $K_p = H_{l/u} |a| |b|$.

The undrained effective stress path has to satisfy this differential equation. Thus the effective stress is no longer independently controlled . The constitutive relation should be

66

expressed in terms of the total strain and stress increments

$$d\sigma'_{ij} = ds_{ij} + d\sigma'_{mm}\delta_{ij} / 3 \qquad (4.44)$$

$$d\varepsilon^c_{kk} = C^c_{kkij} d\sigma'_{ij} = C^c_{kkij} ds_{ij} + C^c_{kkii} d\sigma'_{mm} / 3 = d\sigma'_{mm} / (3K) \qquad (4.45)$$

where K is the elastic bulk modulus

$$C^c_{kkii} = 1 / K \quad \text{and} \quad C^c_{kkij} ds_{ij} = 0 \qquad (4.46)$$

On the other hand, undrained conditions demand that

$$d\varepsilon^c_{kk} = -d\varepsilon^p_{kk} = -d\lambda(\partial G / \partial\sigma'_{kk}) \qquad (4.47)$$

Therefore, it is given by (4.45) and (4.47)

$$d\sigma'_{kk} = -3 K d\lambda(\partial G / \partial\sigma'_{kk}) \qquad (4.48)$$

and

$$dp = (d\sigma_{kk} - d\sigma'_{kk}) / 3 = d\sigma_{kk} /3 + K d\lambda(\partial G / \partial\sigma'_{kk}) \qquad (4.49)$$

Substituting this value of dp into the expression of dλ, results in the expression:

$$d\lambda = (\partial F / \partial\sigma'_{ij})(d\sigma_{ij} - dp\delta_{ij}) / K_p$$

$$= (\partial F / \partial\sigma'_{ij}) (d\sigma_{ij} - d\sigma_{kk} \delta_{ij} / 3 - K\delta_{ij} d\lambda (\partial G / \partial\sigma'_{kk})) / K_p$$

which can be solved to obtain dλ using equation (4.46)

$$(K_p + K)(\partial F/\partial\sigma'_{mm})(\partial G / \partial\sigma'_{kk}) d\lambda = (\partial F / \partial\sigma'_{ij}) d\sigma_{ij} - (\partial F / \partial\sigma'_{nn}) d\sigma_{kk} / 3$$

$$= (\partial F / \partial\sigma'_{ij}) d\sigma_{ij} - K(\partial F / \partial\sigma'_{nn}) C^c_{mmij} (\delta_{ij} d\sigma_{kk}/3 + ds_{ij})$$

$$d\lambda = \frac{\dfrac{\partial F}{\partial\sigma'_{ij}} - K (\dfrac{\partial F}{\partial\sigma'_{nn}})C^c_{mmij}}{K_p + K(\dfrac{\partial F}{\partial\sigma'_{mm}}) (\dfrac{\partial G}{\partial\sigma'_{kk}})} d\sigma_{ij}$$

$$(4.50)$$

Actually ds_{ij} can be used instead of $d\sigma_{ij}$,

$$d\sigma_{ij} = ds_{ij} + d\sigma_{kk}\, \delta_{ij}\, /3 \qquad\qquad (4.51)$$

Substituting (4.51) into (4.50) and using (4.46)

$$d\lambda = \frac{\dfrac{\partial F}{\partial \sigma'_{ij}}}{K_p + K(\dfrac{\partial F}{\partial \sigma'_{mm}})\,(\dfrac{\partial G}{\partial \sigma'_{kk}})}\, ds_{ij} \qquad\qquad (4.52)$$

For a given total stress increment $d\sigma_{ij}$, it is easy to calculate ds_{ij} and $d\sigma_{kk}$ from

(4.51). Then $d\lambda$ is determined by (4.52). Afterwards, $d\sigma'_{kk}$, dp, $d\sigma'_{ij}$ and $d\varepsilon^P_{ij}$ could be

obtained from (4.48), (4.49), (4.44) and (4.47).

4.5.3 Strain controlled path

The strain controlled path requires the determination of effective stress increment

for a given strain increment and the initial state. In any numerical scheme employed for the

analysis of elastoplastic problems it eventually becomes necessary to integrate the

constitutive equations governing material behavior. The state variables are computed for a

given deformation history in the displacement type finite element method. The precision of

integration in the local level of the constitutive equation has a direct impact on the overall

accuracy of the analysis.

The importance of the integration algorithm for the strain controlled path has

motivated a number of studies, such as Hughes (1984), Ortiz and Popov (1985), Simo

and Taylor (1985, 1986), Owen, Marques and Cesae (1986), Crisfield (1987).

A wide range of elastoplastic materials can be characterized by means of a set of

constitutive relations of the general form

$$\varepsilon = \varepsilon^e + \varepsilon^P \qquad\qquad (4.53a)$$

$$\sigma' = \mathbf{D}^e \, \varepsilon^e \qquad\qquad (4.53b)$$

$$d\varepsilon^P = d\lambda \, b(\sigma', q) \qquad , \qquad b^T = \partial G \, / \, \partial\sigma' \qquad\qquad (4.53c)$$

$$dq = d\lambda \, h\,(\sigma', q) \qquad , \qquad d\lambda \geq 0 \qquad\qquad (4.53d)$$

where q signifies some suitable set of internal variables. Equation (4.53d) is the hardening law which governs the evolution of plastic internal variables. $d\lambda$ is a plastic parameter to be determined analytically by means of the differential plastic consistency condition

$$dF = (\partial F \, / \, \partial\sigma') \, d\sigma' + (\partial F \, / \, \partial q) \, dq = a^T \, d\sigma' + c^T \, dq = 0 \qquad\qquad (4.54)$$

Here $F(\sigma', q)$ signifies the bounding / yield function,

$$a^T = \partial F \, / \, \partial\sigma' \quad , \qquad c^T = \partial F \, / \, \partial q$$

However, the basic problem now is to update the state variables (σ', q) in a numerical way. That is, assuming that

$$\sigma'_n, \, \varepsilon_n, \, \varepsilon^P_n, \, q_n \qquad \text{are known with} \qquad F_n \leq 0,$$

and

$$\varepsilon_{n+1} \qquad \text{or} \qquad d\varepsilon_n = \varepsilon_{n+1} - \varepsilon_n \qquad\qquad \text{is given}$$

determine

$$\sigma'_{n+1} \qquad \text{or} \qquad d\sigma' = \sigma'_{n+1} - \sigma'_n$$

$$\varepsilon^P_{n+1} \qquad \text{or} \qquad d\varepsilon^P = \varepsilon^P_{n+1} - \varepsilon^P_n \qquad\qquad (4.55)$$

$$q_{n+1} \qquad \text{or} \qquad dq = q_{n+1} - q_n$$

in a manner consistent with the elastoplastic constitutive equations (4.53) subjected to the constraint

$$F_{n+1} \leq 0 \tag{4.56}$$

Many different schemes have been proposed for integrating the elastoplastic constitutive equations. Ortiz and Popov (1985) have shown that most of these methods can be considered as particular cases of the generalized trapezoidal rule or alternatively, the midpoint rule.

Generalized trapezoidal rule.

$$\sigma'_{n+1} = \mathbf{D}^c \left(\varepsilon_{n+1} - \varepsilon^P_{n+1} \right) \tag{4.57a}$$

$$\varepsilon^P_{n+1} = \varepsilon^P_n + d\lambda[(1 - \alpha) \mathbf{b}_n + \alpha \mathbf{b}_{n+1}] \tag{4.57b}$$

$$\mathbf{q}_{n+1} = \mathbf{q}_n + d\lambda[(1 - \alpha) \mathbf{h}_n + \alpha \mathbf{h}_{n+1}] \tag{4.57c}$$

$$F_{n+1}(\sigma'_{n+1}, \mathbf{q}_{n+1}) = 0 \tag{4.57d}$$

with

$$\mathbf{b}_n = \mathbf{b}(\sigma'_n, \mathbf{q}_n) \qquad , \qquad \mathbf{b}_{n+1} = \mathbf{b}(\sigma'_{n+1}, \mathbf{q}_{n+1})$$

$$\mathbf{h}_n = \mathbf{h}(\sigma'_n, \mathbf{q}_n) \qquad , \qquad \mathbf{h}_{n+1} = \mathbf{h}(\sigma'_{n+1}, \mathbf{q}_{n+1}) \tag{4.58}$$

Here $d\lambda$ may be regarded as an incremental plastic parameter to be determined with the aid of (4.57d), which may be called the incremental plastic consistency condition. The algorithmic parameter α ranges from 0 to 1.

A revealing geometric interpretation of algorithm (4.57) can be given by substituting (4.57b) in to (4.57a) and using (4.53)

70

$$\sigma'_{n+1} = \mathbf{D}^e \{ \varepsilon_{n+1} - \varepsilon_n + \varepsilon_n - \varepsilon^p_n - d\lambda[(1 - \alpha)\mathbf{b}_n + \alpha \mathbf{b}_{n+1}] \}$$

$$= \sigma'_n + \mathbf{D}^e (\varepsilon_{n+1} - \varepsilon_n) - d\lambda \mathbf{D}^e[(1 - \alpha) \mathbf{b}_n + \alpha \mathbf{b}_{n+1}]$$

which one may write as

$$\sigma'_{n+1} = \sigma^*_{n+1} - d\lambda \mathbf{D}^e [(1 - \alpha)\mathbf{b}_n + \alpha \mathbf{b}_{n+1}] \tag{4.59}$$

where

$$\sigma^*_{n+1} = \sigma'_n + \mathbf{D}^e (\varepsilon_{n+1} - \varepsilon_n) = \sigma'_n + d\sigma^* \tag{4.60}$$

or equivalently as

$$d\sigma' = d\sigma^* - d\lambda \mathbf{D}^e [(1 - \alpha)\mathbf{b}_n + \alpha \mathbf{b}_{n+1}] \tag{4.61}$$

The update process splits into an elastic predictor of trial state and a plastic corrector of return mapping that restores incremental plastic consistency. It is graphically shown in Figure 4.9, which illustrates how stresses are updated in two steps. The first one takes σ'_n into an elastic predictor σ^*_{n+1} by $d\sigma^*$, obtained from the elastic stress-strain relation. The elastic predictor is subsequently mapped onto a suitably updated yield surface. Such return mapping can be in turn divided into two substeps. First, the stresses are projected along the initial plastic flow direction $\mathbf{b}_n$. The stresses so obtained are then projected onto the yield surface along the final plastic flow direction $\mathbf{b}_{n+1}$. The definition of the return mapping with the adjustable parameter α determines the relative weight given to the initial and final plastic flow directions $\mathbf{b}_n$ and $\mathbf{b}_{n+1}$, respectively. For $\alpha > 0$, the algorithm is implicit which requires a set of nonlinear algebraic equations (4.57) and (4.58) to be solved for the unknown σ'_{n+1}, ε^p_{n+1}, $\mathbf{q}_{n+1}$ and $d\lambda$. Hence iterations are usually involved at a sample point level. For $\alpha = 1/2$, the algorithm coincides with the mean-normal procedure

proposed by Rice and Tracy (1971). For $\alpha = 1$, the closest point projection algorithm

(Simo and Taylor, 1986) is obtained. This integrated the plastic corrector by an implicit

backward-Euler difference scheme and solved the consistency equation (4.57d) by a
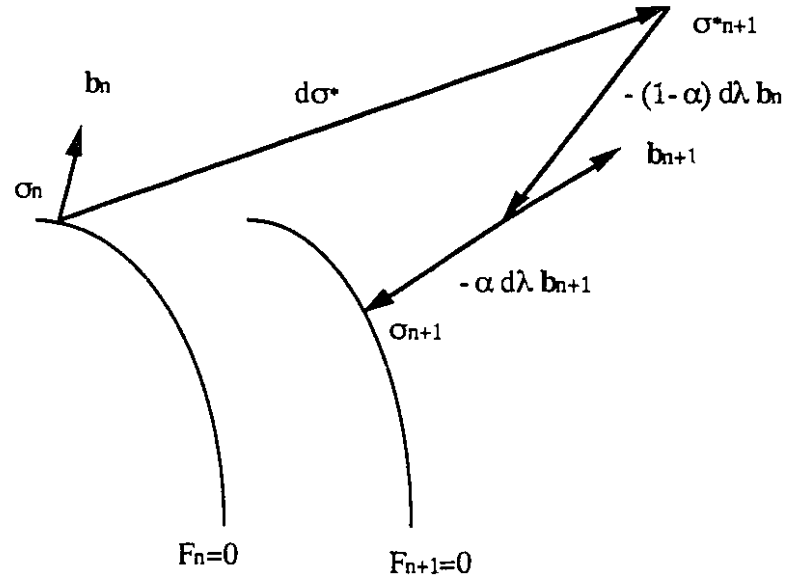
Newton type of iterative procedure.

Figure 4.9 Geometric interpretation of the generalized trapezoidal rule.

For $\alpha = 0$, the algorithm is an explicit integration or forward-Euler difference

scheme. The main advantages of the forward-Euler scheme are its relative simplicity and

the avoidance of equation solving and iterations, involving only function evaluations. The

simple forward-Euler scheme has probably remained the most popular despite certain

disadvantages. For effective use, it must be coupled with a sub-incremental scheme as

shown in Figure 4.10. Even if sub-increments are used, some form of "artificial return to

the yield surface" may also be required. In this study, an artificial deviatoric radial return

combined with the sub-increment forward-Euler scheme is adopted in the numerical implementation of the constitutive model.
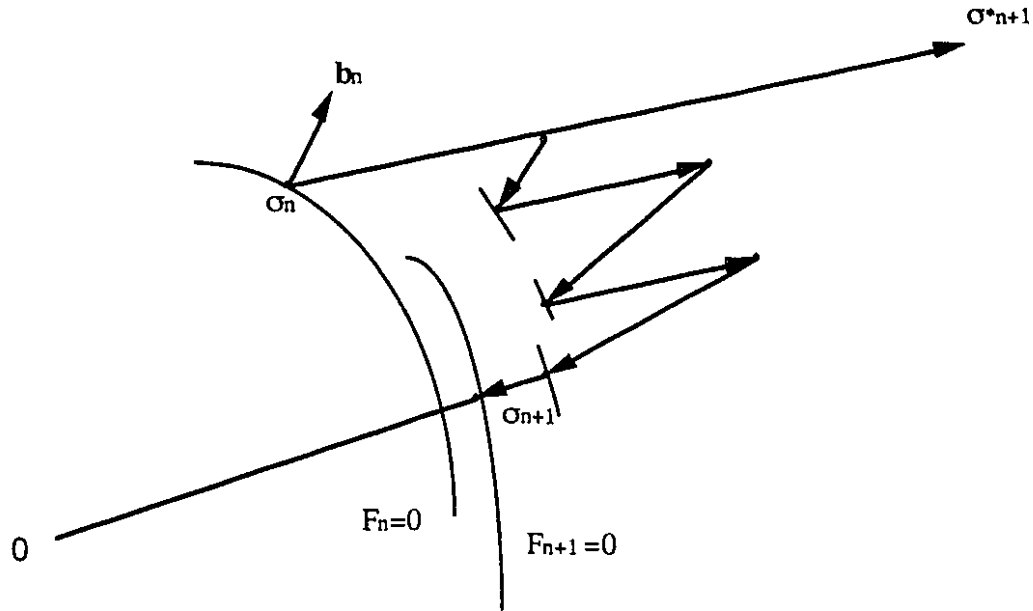

Figure 4.10 Forward - Euler scheme with sub-increment and artificial return.

4.6 MODEL TEST RESULTS

The proposed simple constitutive model for sands in the general effective stress space was implemented into a computer program MDTEST. The program can be utilized to simulate three types of loading processes: stress controlled drained path, stress controlled undrained path and strain controlled path.

A number of numerical model tests has been done to simulate the loose and dense sand behavior under monotonic and cyclic, drained and undrained conditions. The values of material parameters used in these tests are listed in Table 1.

Figure 4.11 (a) and Figure 4.12 (a) present the results of cyclic drained tests

(Tatsuoka and Ishihara, 1974; Habib and Luong, 1978). The plastic volumetric strain develops throughout the test, causing the soil to contract. This densification plays an important role in sand behavior. A remarkable fact is that volumetric plastic strain developed during unloading is always of a contractive nature. Another feature is that volumetric compression is occurring at a progressively decreasing rate as the sand densifies. The model predicted behavior as shown in Figure 4.11 (b), and in Figure 4.12 (b) reproduces the cyclic load-densification phenomena fairly well.

Figure 4.13 shows the influence of relative density on undrained behavior. The numerical simulations agree well with the triaxial compression tests performed by Castro (1969). The strength of loose sand after reaching a peak, drops continuously to almost zero and complete liquefaction is achieved. For dense sand, negative pore pressure occurs while mean effective stress increases after passing the phase transformation line.

Figure 4.14 presents the results of a two-way stress controlled (constant stress amplitude) cyclic undrained test (Ishihara et al., 1975). During the test, the pore pressure progressively builds up causing the effective stress paths to migrate towards the origin. Initially, the pore pressures are generated successively in both compression and extension domains. After a number of cycles, a phenomenon called cyclic mobility occurs in which, during the loading phase, negative pore pressure develops (due to dilatancy of the material) followed by a subsequent build-up during unloading phase. In the present case cyclic mobility does not prevent the sample from attaining complete liquefaction. The numerical simulation indicates fairly close agreement with experimental data.

Figure 4.15 and 4.16 show the effects of large preshearing on cyclic behavior (tests conducted by Ishihara and Okada, 1982). In Figure 4.15, the sample was subjected to the same de, .toric stress on the triaxial compression and extension sides, respectively. During subsequent reloading the pore water pressure buids up to values as high as 97 percent of the initial confining pressure. In Figure 4.16, the sample was subjected to a

74

large preshear toward the triaxial compression side. Upon unloading a pore water pressure of almost 85 percent of the initial confining stress was produced. A further small amplitude cycle was needed to bring the specimen to the state of complete liquefaction. The numerical results from both Figures 4.15 and 4.16 are quite encouraging and indicate the same trends as those observed experimentally.

Figure 4.17 shows the results of a strain controlled undrained test (Ishihara et al. 1975) in which a constant strain amplitude varying between 0.05 and 0.71 percent was applied. Progressive reduction in stress amplitude accompanies the generation of pore pressure. After a number of cycles the sample liquifies. Numerical prediction seem satisfactory though fewer cycles are required to produce liquefaction.

As emphasized before, the main features of the model developed in this chapter are its relative simplicity and capability of simulating several fundamental aspects of sand behavior. It has been implemented into computer programs PCPSTAD and PCPTRAV for standing wave and travelling wave induced response analyses of seafloor deposits which are described in Chapter 8.
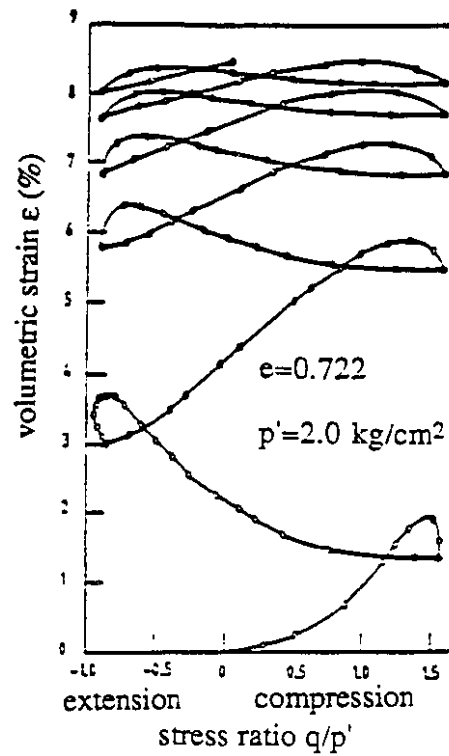
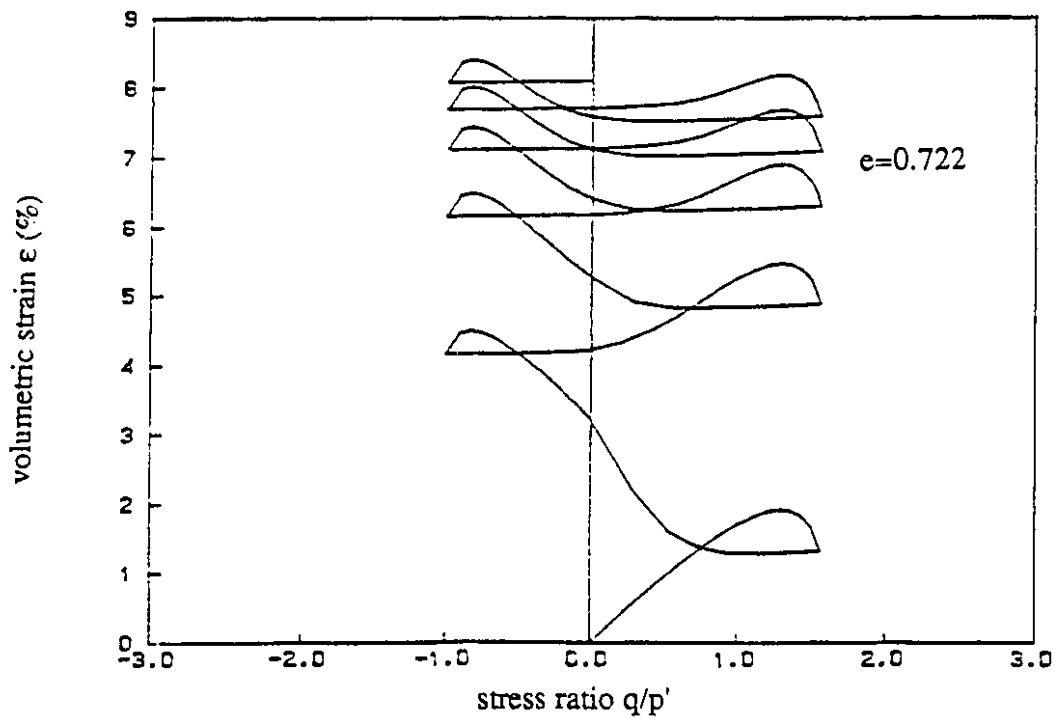Figure 4.11 (a) Drained test on Fuji river sand (after Tatsuoka and Ishihara 1974)

Figure 4.11(b) Cyclic drained triaxial test ($\sigma_r = 200$ kPa)
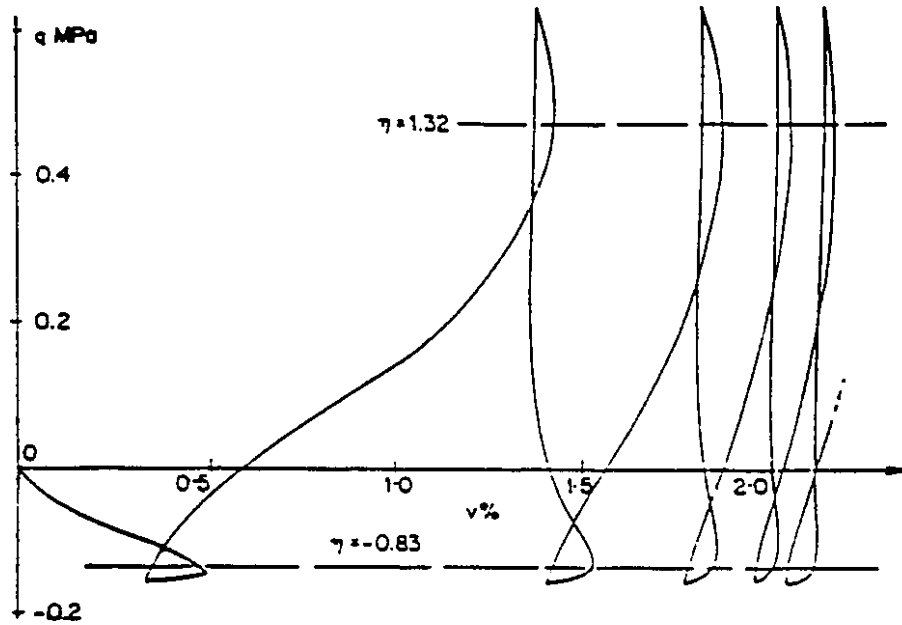
76

Figure 4.12 (a) Cyclic triaxial drained test on medium dense

Fontainebleau sand (after Habib. and Luong, 1978).

Initial $D_r = 62\%$, confining pressure $\sigma_r = 200$ kPa .
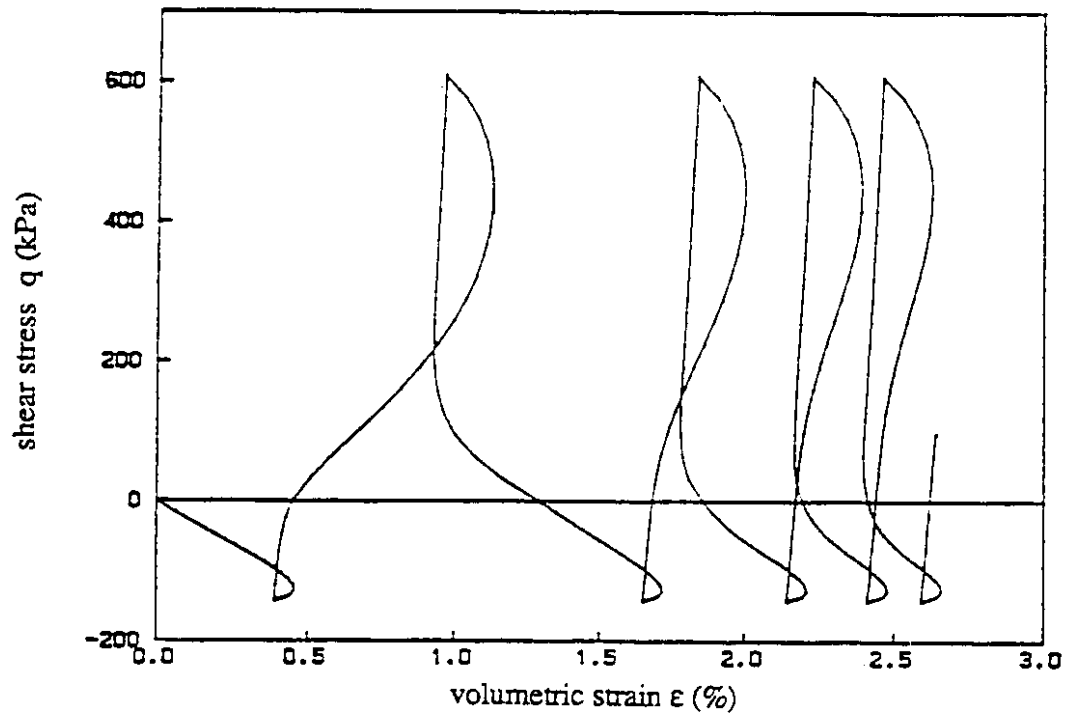
Figure 4.12 (b) Cyclic triaxial drained test ($\sigma = 200$ kPa)
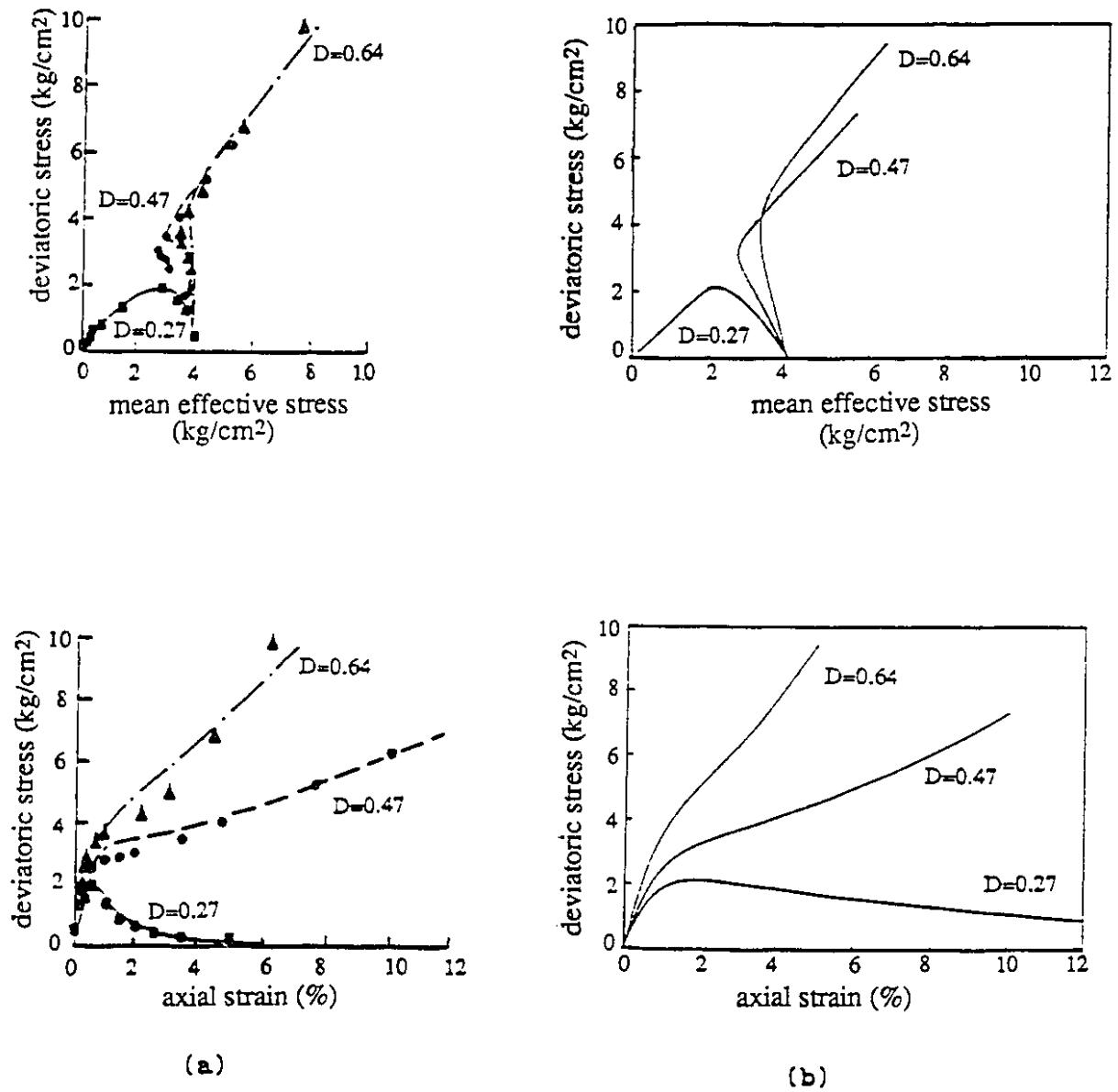
Figure 4.13 (a) Influence of relative density on undrained

behavior of Banding sand (after Castro, 1969)

(b) Undrained compression test
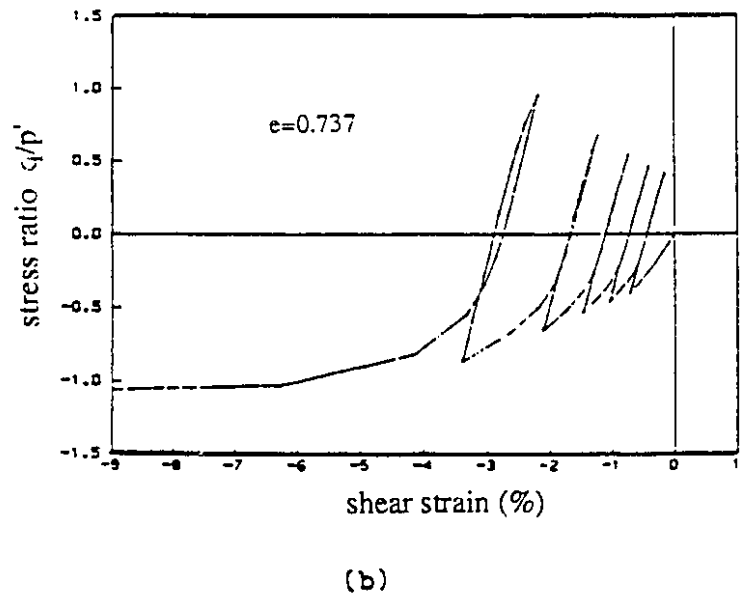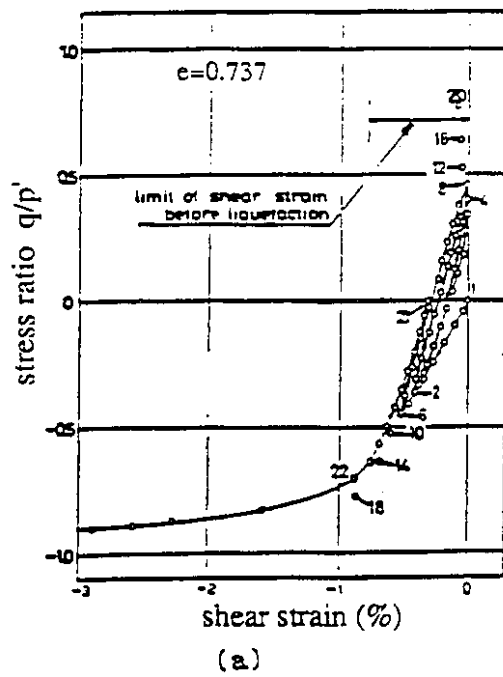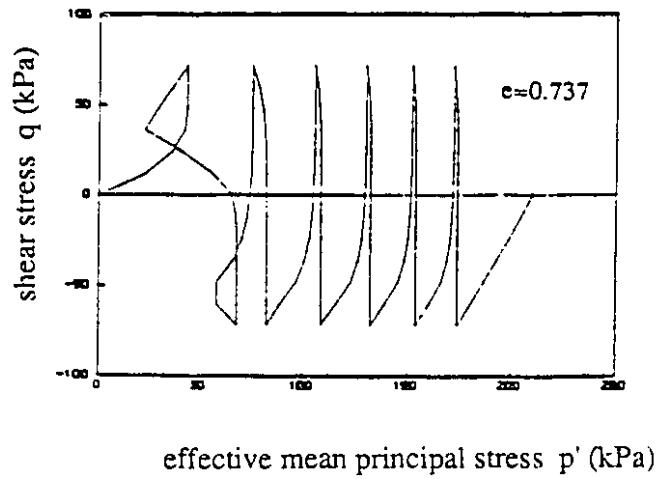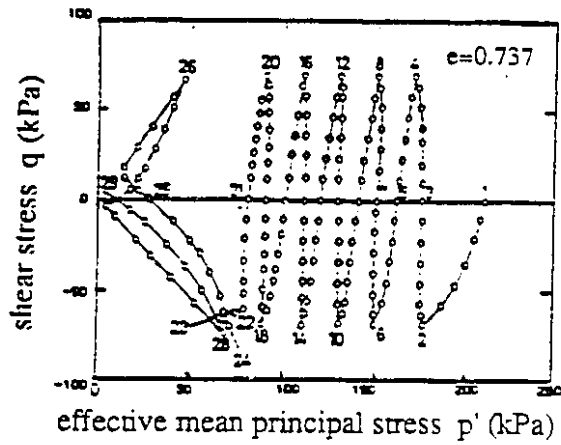
Figure 4.14 (a) Stress controlled cyclic undrained test (after Ishihara, 1975)

(b) Cyclic undrained triaxial test ($\sigma = 210$ kPa)

79
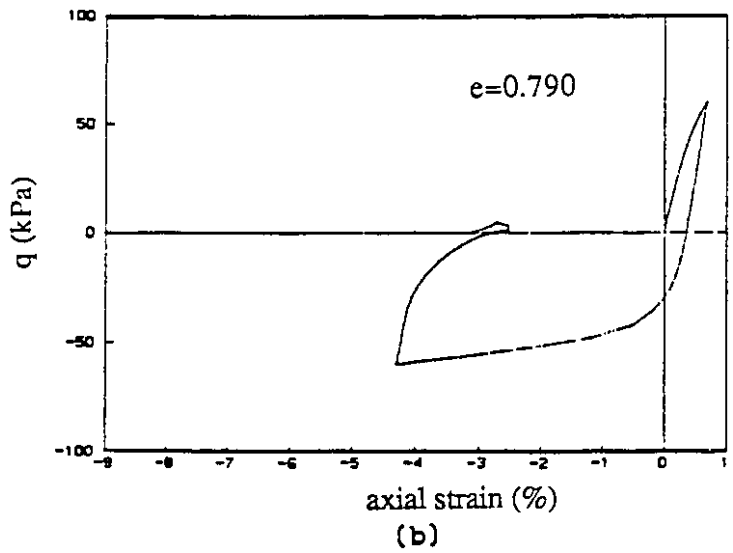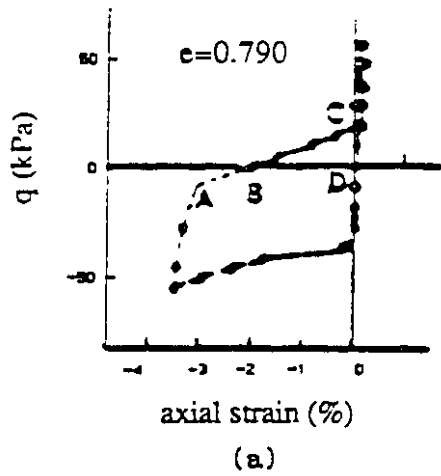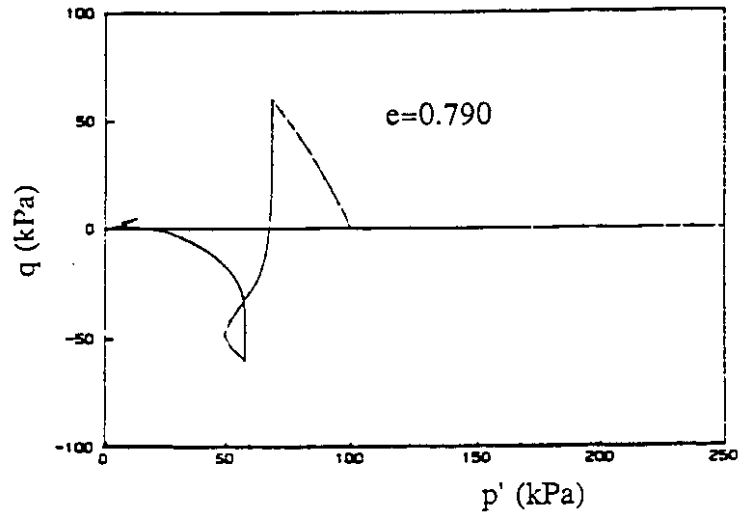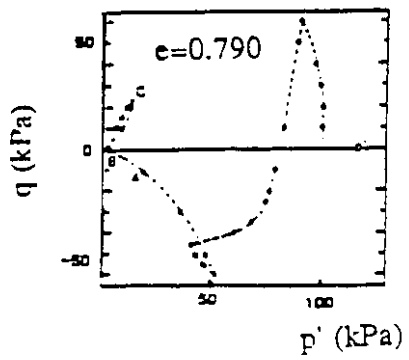
Figure 4.15 (a) Two way stress reversal test results (after Ishihara, 1982)

(b) Two way stress reversal undrained test ($\sigma_r = 100$ kPa)
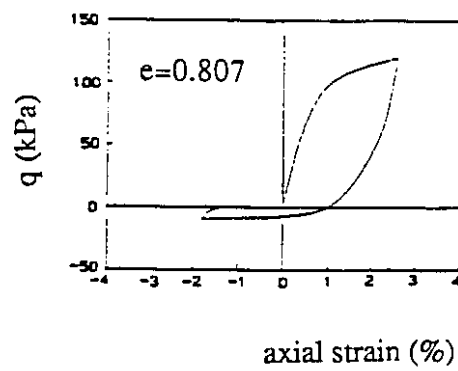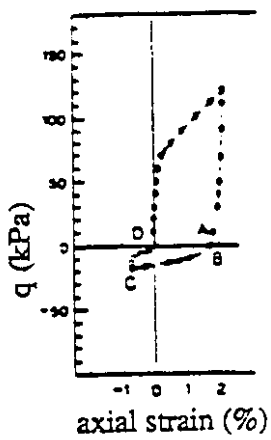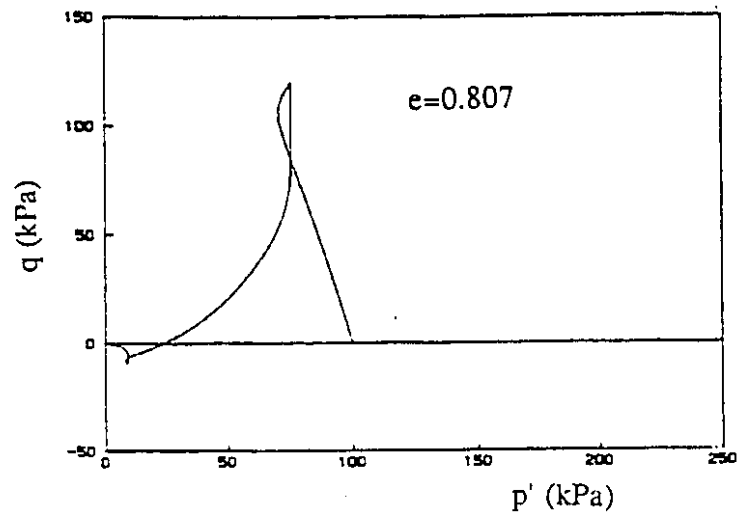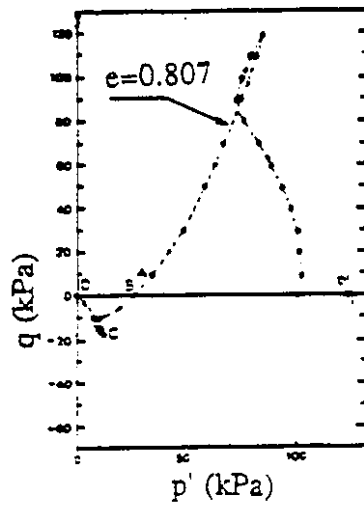
Figure 4.16 (a)   Two way stress reversal test result (after Ishihara, 1982)

(b)   Two way stress reversal undrained test (σ_r =100 kPa)
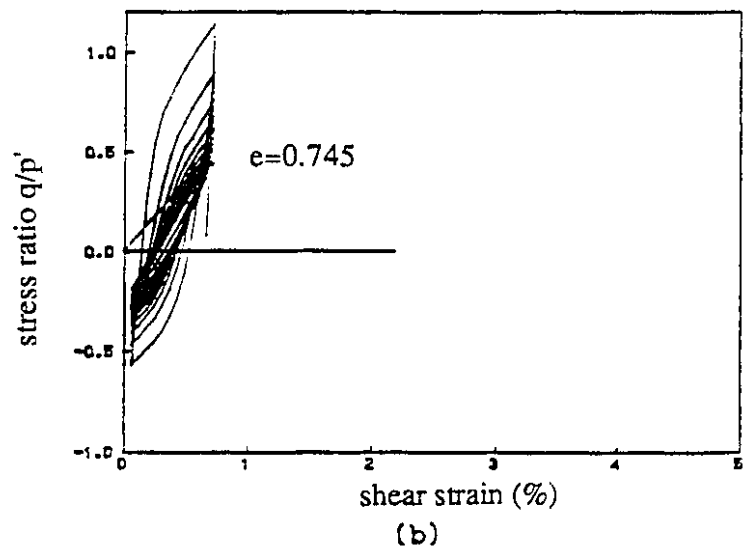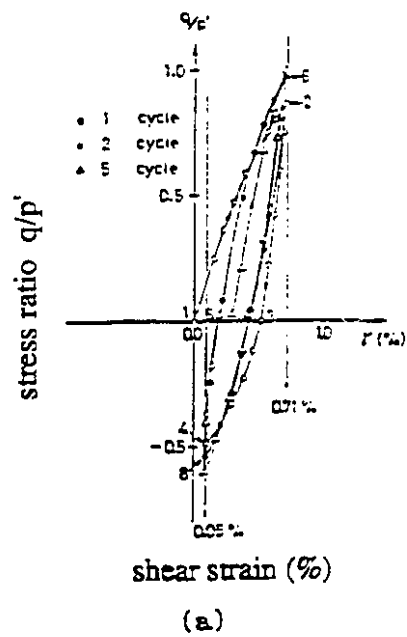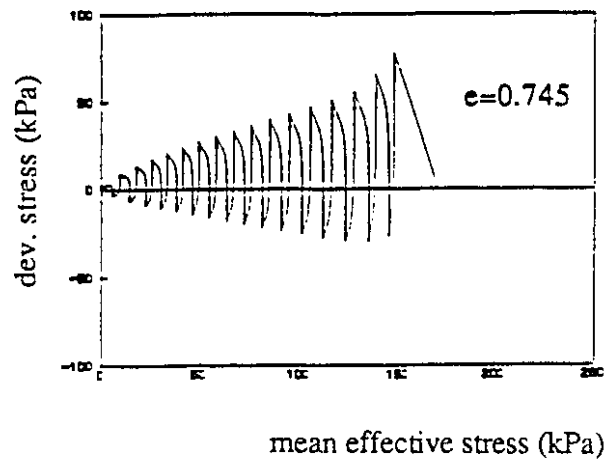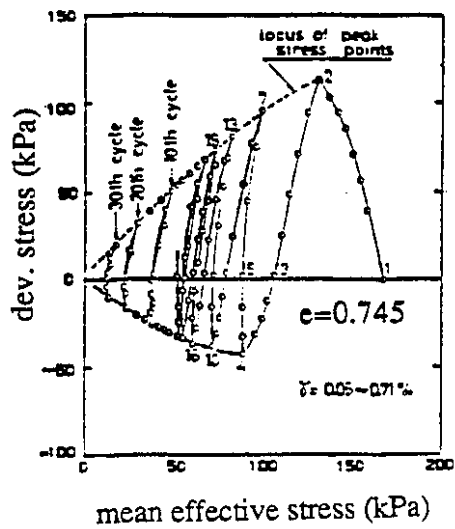
Figure 4.17 (a) Strain controlled undrained test results (after Ishihara, 1975)

(b) Strain controlled cyclic undrained test

Table 4.1 Material Parameters for Numerical Model Tests

TYPE	D	D	UD			UD	UD	UD	UD
	C	C	M			C	C	C	C
FIG. NO.	11	12	13			14	15	16	17
e_0	0.722	——	——	——	——	0.737	0.790	0.807	0.745
D_r	——	0.62	0.27	0.47	0.64	——	——	——	——
K_z	20000	20000	2000	2000	2000	2000	2000	2000	2000
κ	0.002	0.002	0.025	0.025	0.025	0.025	0.025	0.025	0.025
ν	0.3	0.3	0.25	0.25	0.25	0.15	0.15	0.15	0.15
η_0	0.004	0.004	0.004	0.004	0.004	0.004	0.004	0.004	0.004
ϕ_f	40	40	27	32	36.5	40.3	39.0	38.6	40
ϕ_{cr}	32	31	27	29	29	36.6	36.6	36.6	36.5
A	0.030	0.013	0.0074	0.0070	0.0050	0.008	0.0062	0.0035	0.0062
B	0.025	0.01	——	——	——	——	——	——	——
γ_0	3.0	3.5	——	——	——	7.0	5.0	5.0	5.0

5

FINITE ELEMENT METHOD

FOR NONLINEAR CONSOLIDATION

5.1 INTRODUCTION

One of the most popular numerical techniques which engineers and scientists everywhere are using is the finite element method. With the help of high-speed digital computers, the finite element method has greatly enlarged the range of engineering problems amenable to numerical analysis.

The method of finite elements originated in the aircraft industry as an effective means for analyzing complex airframe structures. It began as an extension of matrix methods of structural analysis, but now it is recognized as a powerful and versatile tool which permits a computer solution for previously intractable problems.

An appealing feature of the finite element method is that it is not restricted to solid mechanics.   Actually, it is applicable to almost all continua and field problems. Hence it is not surprising that the method is receiving much attention today in engineering, physics, and mathematics.

The solution of a continuum problem by the finite element method always follows an orderly step-by-step process. To summarize in general terms how the finite element method works these steps will be briefly listed in the following:

1. Discretize the continuum. The first step is to divide the continuum or solution region into elements. A variety of element shapes may be used. Although the number and the type of elements to be used in a given problem are matters of engineering judgment, the analyst can rely on the experience of others for guidelines.

2. Select interpolation functions. The next step is to assign nodes to each element and then choose the type of interpolation function to represent the variation of the field variable over the element. The field variable may be a scalar, a vector, or a higher-order tensor. Often, although not always, polynomials are selected as interpolation functions for the field variable because they are easy to integrate and differentiate. The degree of the polynomial chosen depends on the number of nodes assigned the element, the nature and number of unknowns at each node, and certain continuity requirements imposed at the nodes and along the element boundaries. The magnitude of the field variable as well as the magnitude of its derivatives may be the unknowns at the nodes.

3. Find the element properties. Once the finite element model has ben established (that is, once the elements and their interpolation functions have been selected), one is ready to determine the matrix equations expressing the properties of the individual elements. For this task one may use one of four approaches: the direct stiffness method, the variational principle method, the weighted residual method, or the energy balance method. The variational approach is often the most convenient and the weighted residual approach is

now in fashion, but for any application the approach used depends entirely on the nature of the problem.

4. Assemble the element properties to obtain the system equations. To find the properties of the overall system modeled by the network of elements, all the element properties must be assembled. In other words, one must combine the matrix equations expressing the behavior of the elements and form the matrix equations expressing the behavior of the entire solution region or system. The matrix equations for the system have the same form as the equations for an individual element except that they contain many more terms because they include all nodes.

The basis for the assembly procedure stems from the fact that at a node, where elements are interconnected, the value of the field variable is the same for each element sharing that node. Assembly of the element equations is a routine matter in finite element analysis and is usually done by digital computer.

5. Solve the system equations. The assembly process of the preceding step gives a set of simultaneous equations that we can solve to obtain the unknown nodal values of the field variable. If the equations are linear, a number of standard solution techniques can be used; if the equations are nonlinear, their solution is more difficult to obtain. Several alternative schemes for solving nonlinear problems are available.

To close this section it must be pointed out that the application of the finite element method can be divided into three categories, depending on the nature of the problem to be solved. The first category includes all the problems known as equilibrium problems or time-independent problems. The majority of applications of the finite element method fall into this category.

The second category is composed of the so-called eigenvalue problems in solid and fluid mechanics. These are steady-state problems whose solution often requires the determination of natural frequencies and modes of vibration of solids and fluids. Examples of eigenvalue problems involving both solid and fluid mechanics appear in civil engineering when the interaction of lakes and dams is considered, and aerospace engineering when the sloshing of liquid fuels in flexible tanks is involved. Another class of eigenvalue problems includes the stability of structures and the stability of laminar flows.

The third category includes the multitude of time-dependent or propagation problems of continuum mechanics. This category is composed of the problems in which the time dimension is added to the problems of the first two categories. The nonlinear consolidation with which this study is concerned falls into this third category.

In the following sections the above steps are taken in sequence as it pertains to the present study.

5.2 FINITE ELEMENT SPATIAL DISCRETIZATION

It is possible to identify four approaches (the direct stiffness method, the variational principle method, the weighted residual method and the energy balance method) for deriving finite element equations. Clearly it is largely a matter of taste how one sets up the finite element equations. The weighted residual method, is now in fashion and the energy balance method such as the principle of virtual work can be flexibly used to treat both linear and nonlinear problems and its physical meaning is easier to understand. These two methods are used to derive finite element equations for the nonlinear consolidation problems.

The system of governing differential equations in matrix form is given as follows (see Equation (2.31).)

Effective stress	$d\sigma = d\sigma' + \mathbf{m}\,dp$	(5.1a)
Strain - displacement	$d\varepsilon = \mathbf{L}\,d\mathbf{u}$	(5.1b)
Constitutive equation	$d\sigma' = \mathbf{D}_t\,d\varepsilon$	(5.1c)
Equilibrium equation	$\mathbf{L}^T d\sigma + \rho\,d\mathbf{b} = 0$	(5.1d)
Continuity equation	$\nabla^T ((\mathbf{k}/\gamma_w)(\nabla p - \rho_w \mathbf{b})) + \mathbf{m}^T \dot{\varepsilon} = \dot{p}\,n/K_w$	(5.1e)

where the subscript w indicates that the pore is filled by water.

If $\mathbf{b} = \mathbf{g}$ i.e. only the gravity force $\rho_w \mathbf{g}$ is considered as the body force. The excess pore water pressure can be used instead of the pore water pressure. The whole equation (5.1) will remain the same except (5.1e) which is transformed to

$$\nabla^T ((\mathbf{k}/\gamma_w)\nabla p) + \mathbf{m}^T \dot{\varepsilon} = \dot{p}\,n/K_w \qquad (5.1e)'$$

where p stands for the excess pore pressure.

Together with the appropriate initial conditions

$\mathbf{u} = \mathbf{u}_0$	at	$t = 0$
$p = p_0$	at	$t = 0$

and boundary conditions

$d\mathbf{u} = d\mathbf{u}_\Gamma$	on Γ_u	
$dt^T = \mathbf{n}^T d\sigma$	on Γ_σ	(5.2)
$dp = dp_\Gamma$	on Γ_p	
$h = h_\Gamma = -\mathbf{n}^T [(\mathbf{k}/\gamma_w)\nabla p]$	on Γ_h	

88

where **n** is the outward unit normal vector on the boundary surfaces, equations (5.1) specify the problem completely.

5.2.1 The Principle of Virtual Work and Virtual Power

Following standard finite element discretization procedures, the displacement **u** and pore water pressure p are described in terms of nodal parameters $\underline{u}$ and $\underline{p}$ respectively,

$$\mathbf{u} = \mathbf{N}_1 \, \underline{u} \tag{5.3}$$

$$p = \mathbf{N}_2 \, \underline{p} \tag{5.4}$$

where $\mathbf{N}_1$ and $\mathbf{N}_2$ are suitable shape functions.

For overall equilibrium, instead of starting from the differential equation (5.1d) one may directly use the incremental form of the principle of virtual work which states

$$\int_\Omega \delta\varepsilon^T \, d\sigma \, d\Omega - \int_\Omega \delta\mathbf{u}^T \rho \, db \, d\Omega - \int_{\Gamma\sigma} \delta\mathbf{u}^T \, dt \, d\Gamma = 0 \tag{5.5}$$

in which the incremental displacement, strain, effective stress, pore pressure, gradient of excess pore pressure and total stress could be expressed by the shape functions and increments of the nodal parameters in (5.3) and (5.4)

$$d\mathbf{u} = \mathbf{N}_1 \, d\underline{u}$$

$$d\varepsilon = \mathbf{L} \, \mathbf{N}_1 \, d\underline{u} = \mathbf{B} \, d\underline{u}, \qquad \mathbf{B} = \mathbf{LN}_1$$

$$d\sigma' = \mathbf{D}_t \, (\mathbf{B} \, d\underline{u})$$

$$dp = \mathbf{N}_2 \, dp$$

$$\nabla p = (\nabla \mathbf{N}_2) \, \underline{p}$$

$$d\sigma = d\sigma' + \mathbf{m} \, dp = \mathbf{D}_t \mathbf{B} \, d\underline{u} + \mathbf{m} \, \mathbf{N}_2 d\underline{p} \tag{5.6}$$

The virtual displacement, strain and excess pore water pressure are also expressed in terms of the shape functions and nodal virtual displacement and virtual excess pore water pressure

$$\delta u = N_1 \ \delta \underline{u}$$

$$\delta \varepsilon = B \ \delta \underline{u} \qquad\qquad (5.7)$$

Substituting (5.6) and (5.7) into (5.5)

$$\int_\Omega (B \ \delta \underline{u})^T \ (\ D_t B \ d\underline{u} + m \ N_2 d\underline{p}) \ d\Omega - \int_\Omega (N_1 \ \delta \underline{u})^T \rho \ db \ d\Omega - \int_{\Gamma\sigma}(N_1 \ \delta \underline{u})^T dt \ d\Gamma = 0$$

$$\delta \underline{u}^T \ [\ (\int_\Omega B^T D_t B d\Omega) d\underline{u} + (\int_\Omega B^T \ m \ N_2 d\Omega \ ) d\underline{p} - (\int_\Omega N_1^T db \ d\Omega + \int_{\Gamma\sigma} N_1^T dt \ d\Gamma)] = 0$$

Since the nodal virtual displacements are arbitrary, the above equation could be converted to

$$K \ d\underline{u} + Q \ d\underline{p} = df_1 \qquad\qquad (5.8)$$

where

$$K = \int_\Omega B^T D_t B d\Omega \ , \qquad\qquad B = LN_1$$

$$Q = \int_\Omega B^T \ m \ N_2 \ d\Omega \qquad\qquad (5.9)$$

$$df_1 = \int_\Omega N_1^T \rho db \ d\Omega + \int_{\Gamma\sigma} N_1^T \ dt \ d\Gamma$$

in which K is the usual form of the tangent stiffness matrix encountered in the uncoupled solid problem (D_t is elastoplastic tangential modulus of the solid phase). B is the standard strain matrix. Q is the coupling term and df_1 is the change in the external force due to boundary and body forces.

90

In the following it is shown that performing the same kind of operation on the continuity equation yields another 'virtual principle'. The first step is to multiply the differential continuity equation (5.1e)' by virtual pore pressure.

It is noted that the filter velocity obeys Darcy's law (2.30)

$$\dot{w} = -(k/\gamma_w)\nabla p \qquad (2.30)'$$

in which p is the excess pore pressure. Thus the continuity equation (5.1e)' is replaced by

$$\int_\Omega \delta p\{\nabla^T(-\dot{w}) + m^T\dot{\varepsilon} - \dot{p}\,n/K_w\}d\Omega = 0$$

Then integrating by parts for the first term, yields

$$\int_\Omega [\nabla^T(\delta p)]\dot{w}d\Omega - \int_\Gamma (\delta p)n^T\dot{w}d\Gamma + \int_\Omega (\delta p)m^T\dot{\varepsilon}\,d\Omega - \int_\Omega (\delta p)\dot{p}\,n/K_w\,d\Omega = 0$$

$$(5.10)$$

which could be regarded as ' the principle of virtual power '. This forms the starting point for deriving the finite element equation corresponding to the continuity. In the same way, one can write

$$\nabla p = (\nabla N_2)\underline{p} \qquad (5.11)$$

$$\dot{p} = N_2\underline{\dot{p}}$$

$$\dot{\varepsilon} = B\underline{\dot{u}}$$

$$\dot{w} = -(k/\gamma_w)\nabla N_2\,\underline{p}$$

and

$$\delta p = N_2\,\delta\underline{p} = (\delta\underline{p})^T N_2^T \qquad (5.12)$$

$$\nabla^T(\delta p) = [\nabla(N_2\,\delta\underline{p}]^T = (\delta\underline{p})^T(\nabla N_2)^T$$

91

Substituting (5.11) and (5.12) into (5.10)

$$(\delta \underline{p})^T \{- [\int_\Omega (\nabla N_2)^T (k/\gamma_w) \nabla N_2 \, d\Omega] \underline{p} + [\int_\Gamma N_2^T n^T (k/\gamma_w) \nabla p \, d\Gamma]$$

$$+ [\int_\Omega N_2^T m^T B d\Omega] \dot{\underline{u}} - [\int_\Omega N_2^T (n/K_w) N_2 d\Omega] \dot{\underline{p}} \} = 0$$

Since the nodal virtual excess pore water pressures are arbitrary, the above equation is converted to

$$Q^T \dot{\underline{u}} + S \dot{\underline{p}} + H \underline{p} = \dot{f}_2 \qquad (5.13)$$

where

$$H = - \int_\Omega (\nabla N_2)^T (k/\gamma_w) \nabla N_2 \, d\Omega$$

$$S = - \int_\Omega N_2^T (n/K_w) N_2 d\Omega$$

$$Q^T = \int_\Omega N_2^T m^T B d\Omega \qquad (5.14)$$

$$\dot{f}_2 = - \int_\Gamma N_2^T n^T (k/\gamma_w) \nabla p \, d\Gamma$$

and H and S are the conductivity and capacity matrices corresponding to an uncoupled

seepage problem. $\dot{f}_2$ indicates the outflow rate across Γ_h and n is the outward unit normal

vector of Γ_h.

5.2.2 The weighted residual method

The weighted residual methods obtain approximate solutions to systems of differential equations by arranging for the error in the solution to be distributed in some manner throughout the continuum. In fact, it is done by setting the integral of the weighted residue of the differential equation over the domain of the element to be equal to zero. The use of different weight functions will produce different results. The Galerkin-type discretization procedure actually is one kind of weighted residual method with the shape

function being its weight. For the equilibrium equation, Galerkin method will yield exactly the same finite element equation as that derived from the principle of virtual work. The essential boundary conditions (the prescribed displacement boundary) are not considered at the element level; instead they are included in the assembly process. However, the natural boundary conditions (the prescribed force boundary) emerge automatically in the formulation of the element equation.

The integral of the equilibrium equation (5.1d) multiplied by the interpolation function N_1^T over the element domain is set to zero

$$\int_\Omega N_1^T (L^T d\sigma + \rho db)d\Omega = 0$$

Integration by parts for the first term yields

$$- \int_\Omega (LN_1)^T d\sigma \, d\Omega + \int_\Gamma (nN_1)^T d\sigma \, d\Gamma + \int_\Omega N_1^T \rho db \, d\Omega = 0$$

Substituting (5.6) into above equation results in

$$- (\int_\Omega (B^T D_t Bd\Omega)d\underline{u} - (\int_\Omega B^T mN_2 d\Omega)d\underline{p} + \int_\Gamma N_1^T n^T d\sigma d\Gamma + \int_\Omega N_1^T \rho dbd\Omega = 0$$

which is the same as (5.8) and (5.9) derived from the principle of virtual work.

$$K \, d\underline{u} + Q \, d\underline{p} = df_1 \tag{5.8}$$

where

$$K = \int_\Omega B^T D_t Bd\Omega \ , \qquad B = LN_1$$

$$Q = \int_\Omega B^T \, m \, N_2 d\Omega \tag{5.9}$$

$$df_1 = \int_\Omega N_1^T \rho \, db \, d\Omega + \int_{\Gamma_\sigma} N_1^T dt \, d\Gamma$$

93

The integral of the continuity equation (5.1e) multiplied by the interpolation function N_2^T over the element domain is set to zero

$$\int_\Omega N_2^T \left[\nabla^T((k / \gamma_w)\nabla p) + m^T \dot{\varepsilon} - \dot{p}n / K_w \right] d\Omega = 0$$

Integration by parts for the first term gives

$$- \int_\Omega (\nabla N_2)^T (k/\gamma_w)\nabla p d\Omega + \int_\Gamma (nN_2)^T (k/\gamma_w)\nabla p d\Gamma + \int_\Omega N_2^T m^T \dot{\varepsilon}\, d\Omega - \int_\Omega N_2^T \dot{p}n/K_w d\Omega = 0$$

Substituting (5.11) into above equation results in

$$- \left(\int_\Omega (\nabla N_2)^T (k/\gamma_w)\nabla N_2 d\Omega\right)\underline{p} + \int_\Gamma N_2^T\, n^T (k/\gamma_w)\nabla p d\Gamma + \left(\int_\Omega N_2^T m^T B\, d\Omega\right)\underline{\dot{u}}$$

$$- \left(\int_\Omega N_2^T (n / K_w)N_2 d\Omega\right)\underline{\dot{p}} = 0$$

which is exactly the same as (5.13), (5.14) derived from the principle of virtual power.

$$Q^T\underline{\dot{u}} + S\underline{\dot{p}} + Hp = \dot{f}_2 \tag{5.13}$$

where

$$H = - \int_\Omega (\nabla N_2)^T (k / \gamma_w)\nabla N_2\, d\Omega$$

$$S = - \int_\Omega N_2^T (n / K_w)N_2 d\Omega$$

$$Q^T = \int_\Omega N_2^T m^T B d\Omega \tag{5.14}$$

$$\dot{f}_2 = - \int_\Gamma N_2^T n^T (k / \gamma_w)\nabla p\, d\Gamma$$

The coupled finite element equations (5.8) and (5.13) for the nonlinear, transient consolidation problems could be expressed in a compact form which appears to be symmetric provided K is symmetric.

$$\begin{bmatrix} K & Q \\ Q^T & S \end{bmatrix} \frac{d}{dt}\begin{Bmatrix} \underline{u} \\ \underline{p} \end{Bmatrix} + \begin{bmatrix} 0 & 0 \\ 0 & H \end{bmatrix}\begin{Bmatrix} \underline{u} \\ \underline{p} \end{Bmatrix} = \frac{d}{dt}\begin{Bmatrix} f_1 \\ f_2 \end{Bmatrix} \tag{5.15}$$

5.3   SOLUTION SCHEME FOR COUPLED SYSTEMS

It is convenient to introduce a classification of coupled problems into two distinct categories (Zienkiewicz, 1984), each amenable in general to similar treatment.

Class I. This contains problems in which the various domains overlap (totally or partially). Here the coupling occurs via the differential equations normally referring to different physical phenomena.

Class II. This contains problems in which coupling occurs only on domain interfaces and clearly this coupling will occur only through the boundary conditions imposed.

In many physical problems coupling may occur only in time-dependent (transient) forms and disappear when steady state conditions are reached, for example, a fully drained problem is uncoupled while pore water flows in steady state.

The transient consolidation problem falls into the category of Class I, which requires an integrated treatment of coupled soil skeleton displacement field and pore pressure field. The finite element spatial discretization of the system of coupled partial differential equations results the first-order system of temporal ordinary differential equations (5.15). The numerical solution of the coupled system of the form (5.15) can be carried out by three different approaches: field elimination, partitioned solution and simultaneous solution procedure.

5.3.1   Field elimination procedure

In the field elimination procedure, either the pore pressure or the soil displacement is eliminated from the coupled equations. The resulting equations may become a system of second-order ordinary differential equation.

For example, if the pore pressure is eliminated the resulting reduced equations in general become

$$G_0\ddot{u} + G_1\dot{u} + G_2u = r\ (K,Q,S,H,f) \tag{5.16}$$

where G_0, G_1 and G_2 are complicated matrices, and r consists of contributions of both external forces and fluid flow boundary conditions. This may be integrated by a suitable direct time integration method. If necessary, the reduced pore pressure can be obtained by back-substituting the displacement into the original differential equation.

Equation (5.16) leads to the consequence that the elimination scheme raises the order of the differential equations. Moreover, the sparseness of the stiffness matrix is in general lost. This can impose a major computational burden in the solution process.

5.3.2 Partitioned solution procedure (staggered method)

In the partitioned (or the staggered) solution procedure the solution of each field is obtained by adopting parallel, sequential, or hybrid execution of each field analysis module. The integration terms are treated as external forcing quantities, which have to be extrapolated judiciously in order to satisfy both stability and accuracy requirements for a given problem (Park, 1980; Park and Felippa, 1980). Hence the sparseness of the original system is preserved and many well established single field analysis programs can be applied to the coupled field problems which are decoupled now by the staggered method.

In an attempt to analyze the wave induced susceptibility of a seabed deposit Poorooshasb, Ishihara and Yang (1987) proposed a staggered procedure combining physical assumption with the numerical analysis to solve the coupled field problem. A distinct feature of the procedure is the load-time curve replaced approximately by a number of step functions as shown in Figure 5.1. This is reasonable if very small time steps are employed.

96
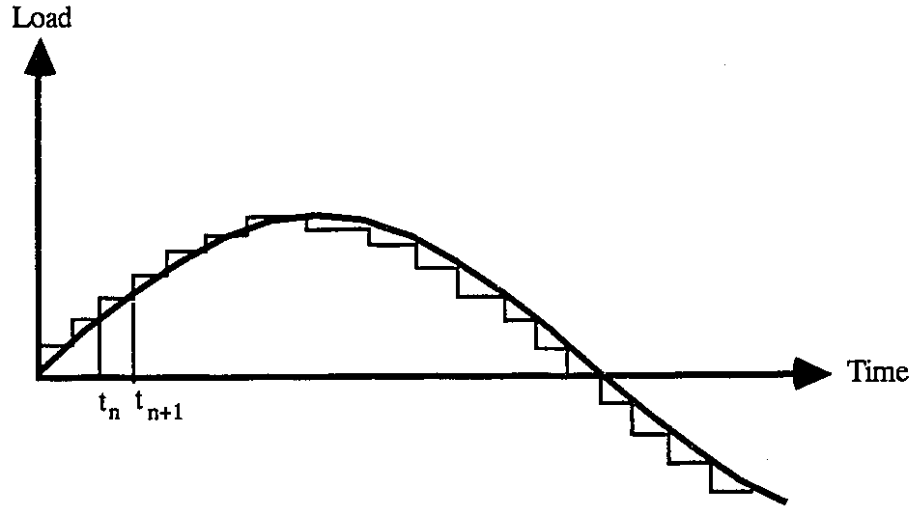
Figure 5.1   Step function representation of the load-time curve.

Hence each time step $t_n \rightarrow t_{n+1}$ is subdivided into two parts. The load increment is

applied at the very beginning $t_n \rightarrow t_n^+$. There is no time to drain. Thus, the continuity

equation (5.1e)' is reduced to

$$dp = (K_w / n)\ \mathbf{m}^T\ d\varepsilon \qquad\qquad (2.32)'$$

Substituting this into the equilibrium equation (5.1d) yields

$$\mathbf{L}^T [\ \mathbf{D}_t + \mathbf{m}^T (K_w / n)\ \mathbf{m}\ ]\ d\varepsilon + \rho\ d\mathbf{b} = 0$$

which is identical to a single field system with a modified stiffness matrix $\underline{\mathbf{K}}$ calculated

from a redefined total stress tangent modulus $\underline{\mathbf{D}}_t$,

$$\underline{\mathbf{K}}\ d\underline{\mathbf{u}} = d\underline{\mathbf{f}}_1 \qquad\qquad (5.17)$$

where

$$\underline{\mathbf{K}} = \int_\Omega \mathbf{B}^T\ \underline{\mathbf{D}}_t\ \mathbf{B}\ d\Omega$$

$$\underline{\mathbf{D}}_t = \mathbf{D}_t + \mathbf{m}^T (K_w / n)\ \mathbf{m}$$

97

The pore pressure field could be evaluated in terms of equation (2.32)' after solving equation (5.17) for the soil skeleton displacement field by a nonlinear finite element program of stress analysis.

In the second part $t_n^+ \rightarrow t_{n+1}$, the load keeps constant. Assuming $d\sigma = 0$, it follows from equations (5.1a) and (5.1c) that

$$d\sigma = d\sigma' + m^T dp = D_t \, d\varepsilon + m^T dp = 0$$

$$m^T \dot{\varepsilon} = - m \, (\, D_t \,)^{-1} \, m^T \, \dot{p} \qquad (5.18)$$

Substituting into equation (5.1e)', the transient seepage equation turns out a diffusion equation equivalent to a single fluid phase with a modified diffusion coefficient C.

$$\Delta p = \nabla^2 p = C \, \partial p \, / \, \partial t \qquad (5.19)$$

where

$$C = (n \, / \, K_w + m \, (D_t)^{-1} \, m^T \,) \, \gamma_w \, / \, k \qquad (5.20)$$

in which the constant permeability $k = k \, \delta_{ij}$ is assumed.

It is simple to solve the diffusion type of equation (5.19) by a finite difference program. The non-equilibrium nodal forces due to the pore pressure dissipation is added to the load increment of the next time step for the first part of the total stress analysis.

The numerical results appeared to be satisfactory. As shown in Figure 5.2 and 5.3, two graphs marked E2G1 and E8G3 represent the evolution of the pore pressure and the effective stress at two points (Gauss point 1 of element 2 and Gauss point 3 of element 8) respectively. It is seen that the pore pressure gradually developed, while the mean effective stress and the vertical effective stress decrease as the number of wave cycles increases. After about seven cycles the mean effective stress and the vertical effective stress appear to be approaching zero. This indicates that a state of liquefaction is being developed.
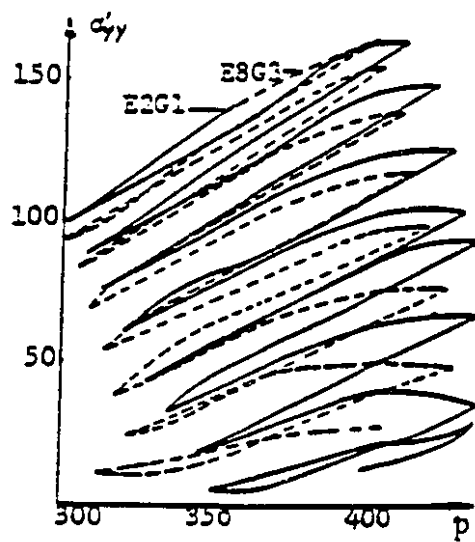
Figure 5.2   Vertical effective stress versus pore water pressure (kPa)
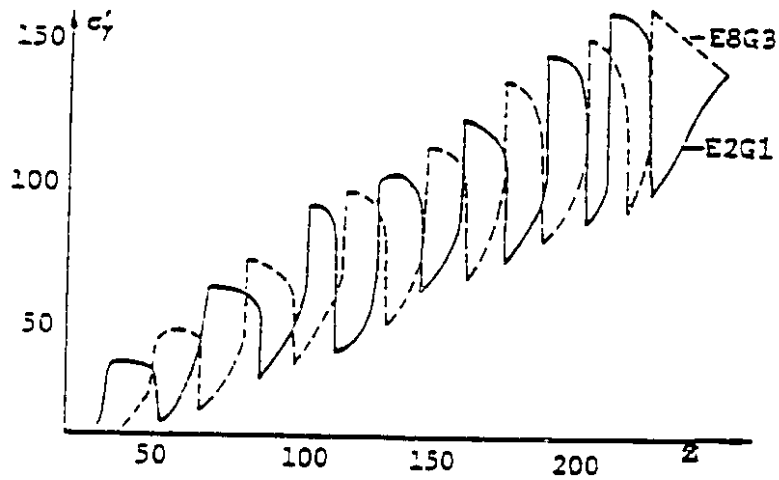
(after Poorooshasb, Ishihara and Yang, 1987)

Figure 5.3   Vertical effective stress versus mean effective stress (kPa)

(after Poorooshasb, Ishihara and Yang, 1987)

99

5.3.3 Simultaneous solution procedure (direct integration)

The simultaneous solution procedure may be carried out by direct time integration of the coupled system of equations (5.15), or (5.9) and (5.13)

$$\begin{bmatrix} K & Q \\ Q^T & S \end{bmatrix} \frac{d}{dt} \begin{Bmatrix} \underline{u} \\ \underline{p} \end{Bmatrix} + \begin{bmatrix} 0 & 0 \\ 0 & H \end{bmatrix} \begin{Bmatrix} \underline{u} \\ \underline{p} \end{Bmatrix} = \frac{d}{dt} \begin{Bmatrix} f_1 \\ f_2 \end{Bmatrix} \qquad (5.15)$$

Since (5.9) is already in the incremental form, it is only necessary to integrate (5.13).

In order to discretize in time domain, the single-step integration (two point formula) defined below is used

$$\int_{t_n}^{t_{n+1}} a(t)dt = [\, \theta\, a_{n+1} + (1-\theta)\, a_n \,]\, \Delta t \qquad (5.21)$$

where a_n and a_{n+1} are the values of the variable $a(t)$ at times t_n and t_{n+1} respectively.

The time step is $\Delta t = t_{n+1} - t_n$ and θ indicates the type of interpolation:

$\theta = 0$, forward interpolation (fully explicit), $\theta = 1/2$, linear interpolation (Crank-Nicolson), and $\theta = 1$, backward interpolation (fully implicit).

Integrating equation (5.13) from t_n to t_{n+1}

$$\int_{t_n}^{t_{n+1}} Q^T \underline{\dot{u}}dt + \int_{t_n}^{t_{n+1}} S\underline{\dot{p}}\, dt + \int_{t_n}^{t_{n+1}} H\underline{p}\, dt = \int_{t_n}^{t_{n+1}} f_2\, dt$$

and using formulation (5.21)

$$Q^T (\underline{u}_{n+1} - \underline{u}_n) + S (\underline{p}_{n+1} - \underline{p}_n) + H (\, \theta\, \underline{p}_{n+1} + (1-\theta)\, \underline{p}_n\,)\, \Delta t$$

$$= (\, \theta\, \dot{f}_{2,n+1} + (1-\theta)\, \dot{f}_{2,n}\,)\, \Delta t \qquad (5.13)'$$

Equation (5.9) could be written as

$$K (\underline{u}_{n+1} - u) + Q (\underline{p}_{n+1} - \underline{p}_n) = f_{1,n+1} - f_{1,n} \qquad (5.9)'$$

Combining (5.9)' with (5.13)', a recurrence relation is obtained

$$
\begin{bmatrix} K & Q \\ Q^T & S + \theta\,\Delta t\,H \end{bmatrix}
\begin{Bmatrix} \underline{u}_{n+1} \\ \underline{p}_{n+1} \end{Bmatrix} =
$$

$$
\begin{bmatrix} K & Q \\ Q^T & S-(1-\theta)\,\Delta t\,H \end{bmatrix}
\begin{Bmatrix} \underline{u}_n \\ \underline{p}_n \end{Bmatrix} +
\begin{Bmatrix} f_{1,n+1}-f_{1,n} \\ (\theta^{n+1}\dot{f}_{2,n+1} +(1-\theta)\,\dot{f}_{2,n})\Delta t \end{Bmatrix}
\qquad (5.22)
$$

An alternative form could be given as

$$
\begin{bmatrix} K & Q \\ Q^T & S + \theta\,\Delta t\,H \end{bmatrix}
\begin{Bmatrix} d\underline{u} \\ d\underline{p} \end{Bmatrix} =
$$

$$
\begin{bmatrix} 0 & 0 \\ 0 & -\Delta t\,H \end{bmatrix}
\begin{Bmatrix} \underline{u}_n \\ \underline{p}_n \end{Bmatrix} +
\begin{Bmatrix} df_1 \\ (\theta^{n+1}\dot{f}_{2,n+1} + (1-\theta)\dot{f}_{2,n})\Delta t \end{Bmatrix}
\qquad (5.22)'
$$

In several investigations the condition of stability and accuracy of the consolidation algorithm have been examined (Sandhu and Wilson, 1969; Sandhu, Liu and Singh, 1977; Booker and Small, 1975 and 1977). It has shown that if θ is chosen between 1/2 and 1 the process is unconditionally stable and that for $\theta < 1/2$, the process is stable if

$$
\Delta t \le 1 / (1/2 - \theta)\, S_N
\qquad (5.23)
$$

101

where S_N is the greatest eigenvalue. In this study $\theta = 1/2$ was chosen, i.e. Crank-Nicolson method which is unconditionally stable.

An accuracy condition of numerical solution of one-dimensional consolidation has been given by Vermeer and Verruijt (1981) as a lower bound for the time step in terms of the coefficient of consolidation C_v and element size for a homogeneous mesh Δh is:

$$\Delta t \geq ((\Delta h)^2 / \theta \, C_v) / 6 \qquad\qquad (5.24)$$

The minimum time step criterion can be used for two-dimensional consolidation as an approximate value and for choosing an adequate finite element mesh.

5.4   SOME RELATIVE TECHNIQUES

5.4.1   Composite element

Clearly it will be logistically desirable to use the same finite element domain for each of the variables encountered but it is not necessary to use the same order of approximation or the same number of nodes (Sandhu and Wilson, 1969). Indeed good accuracy will usually be obtained by using an interpolation function for p which is one order lower than that used for **u**. A composite element consisting of an eight-node isoparametric quadrilateral is used for **u** combined with the four-corner node element to compute p. Thus the displacement field **u** varies quadrilaterally over the element while the variation of p, the excess pore water pressure, is only linear. It must be noted, however, that since the strain is the gradient of the displacement, the variation of the strain (and hence the variation of the stress field) over the element is linear and therefore of the same nature as the pore water pressure p.

102

5.4.2 Fictitious freedom and element stiffness matrix

In equation (5.25), the unknowns are arranged with all the displacement increments followed by the pore water pressure increments. This is convenient for derivation of the expressions, but is not efficient due to its very large band width or frontal width, which leads to great waste of core storage space. In practice all the unknowns associated with the nodal points are arranged sequentially and the rows and columns of the stiffness matrix are rearranged accordingly.

Since some nodes (corner nodes) have three degrees of freedom, two for u and one for p, but the mid-side nodes have only two degrees of freedom (for u), an effective bookkeeping must be developed to record the degrees of freedom for each node. In the present study the following simple scheme which proved to be quite effective was adopted.

All nodes were assumed to have three degrees of freedom. For the mid-side nodes, however, all the elements of the columns and rows associated with the third freedom are set to zero, except the pivot point where a non-zero number is assigned. Thus, the pore water pressure term is always evaluated as zero at these fictitious freedoms and make no contribution to the system. The scheme is illustrated in Figure 5.4 for node No. 2 of the element shown.

If the prescribed flow boundaries are impervious i.e. $f_2 = 0$, the recurrence equation (5.22)' is reduced to

$$
\begin{bmatrix} K & Q \\ Q^T & S + \theta \, \Delta t \, H \end{bmatrix} \begin{Bmatrix} d\underline{u} \\ d\underline{p} \end{Bmatrix} = \begin{Bmatrix} df_1 \\ -\Delta t \, H\underline{p}_n \end{Bmatrix} \tag{5.25}
$$

$$
\begin{bmatrix}
& & & & & 0 & & & & \\
& & & & & 0 & & & & \\
& & & & & 0 & & & & \\
& & & & & 0 & & & & \\
& & & & & 0 & & & & \\
0 & 0 & 0 & 0 & 0 & 1 & 0 & 0 & 0 \cdots & 0 \\
& & & & & 0 & & & & \\
& & & & & 0 & & & & \\
& & & & & 0 & & & & \\
& & & & & \vdots & & & & \\
& & & & & 0 & & & &
\end{bmatrix}
\left\{
\begin{array}{c}
du_{x1} \\
du_{y1} \\
dp_1 \\
du_{x2} \\
du_{y2} \\
dp_2 \\
du_{x3} \\
du_{y3} \\
dp_3 \\
\vdots
\end{array}
\right\}
=
\left\{
\begin{array}{c}
df_{x1} \\
df_{y1} \\
-dtH_{1j}p_j \\
df_{x2} \\
df_{y2} \\
0 \\
df_{x3} \\
df_{y3} \\
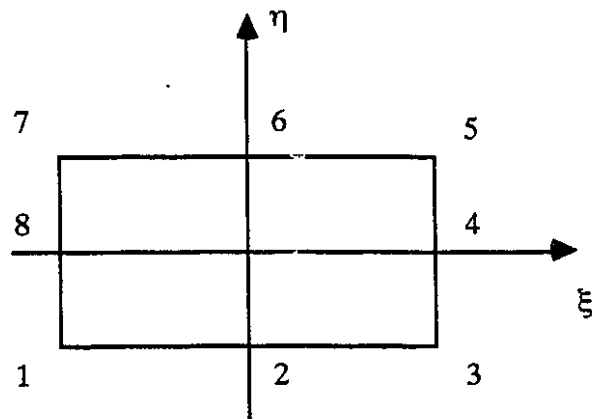-dtH_{3j}p_j \\
\vdots
\end{array}
\right\}
$$

Figure 5.4 Rearranged element stiffness matrix.

5.4.3 Non-symmetric frontal solver

The linear simultaneous stiffness equations are solved by using the frontal solution method. In essence this is just Gaussian elimination , but programmed in such a way as to minimize operation on zero terms and to use minimum computer memory for the stiffness matrix.

The frontal technique (Irons, 1970) starts from the observation that in Gaussian elimination one can start eliminating variables before the global matrix is fully assembled. The main feature of the frontal solution technique is that it assembles the equations and eliminates the variables at the same time. The globe stiffness is never fully formed.

Since the non-associative flow rule is adopted in the material constitutive model, the resulting stiffness matrix is non-symmetrical, and since Iron's frontal solver is only for symmetric matrices, it is necessary to modify the procedure to account for the non-symmetry. A non-symmetric frontal solver subroutine is developed in this study.

5.4.4 Incremental iteration algorithm for nonlinear analysis

In general, non-linearity of a system may be due to geometric non-linearity, material non-linearity, or both. Cater (1977) and Cater et al. (1977) examined the importance of non-linear geometric effects in geotechnical analysis. His general conclusion was that the 'linear' assumption of small strains and small displacements is usually satisfactory in the solution of geotechnical problems.

Thus, in most geotechnical analyses, non-linearity arising from material behavior is of more importance than non-linearity from geometrical effects. The small-displacement, small-strain approach is used in this study.

A non-linear finite element analysis is most effectively performed using an incremental formulation by which the variables are updated incrementally corresponding to successive time steps in order to trace out the complete solution path. An accurate solution

can be expected if the time steps are made sufficiently small but such a solution may prove to be prohibitively expensive. For efficiency, larger time steps are employed using iteration processes that ensure a sufficiently accurate solution. In the present study the modified Newton-Raphson iteration scheme is adopted. The tangent stiffness matrix is only updated at the initiation or updated at the second iteration of each time step.

5.4.5 Equilibrium check

The effective stress and elastoplastic matrix D_t are calculated at the Gaussian integration points of each element. The reduced integration technique is used, i.e. the order of 2 x 2 Gaussian numerical integration in evaluation of the composite element integration.

The program incorporates an equilibrium check to ensure that equilibrium is satisfied at the end of each increment. In this equilibrium check the stress in the elements currently in the mesh are integrated over the volume to calculate the equivalent nodal force and these are then compared with the external loadings. The difference is then expressed as a percentage of the applied load and called the error in the equilibrium or the out-of-balance force. This form of equilibrium check is essential in any analysis using iterative methods. A convergence tolerance of the non-equilibrium nodal force based on trial and error or previous experiences is specified. After convergence the residue forces are added to the load increment of the next time step.

5.4.6 Stop-restart facility

Non-linear finite element analysis tends to be a time-consuming business (for both the computer and program user). Getting the appropriate size of the load increments usually involves re-running the program several times and examining the computer output. In order that the user does not have to continually rerun the analysis from the beginning each time, a stop-restart facility is provided.

106

6

WAVE-INDUCED PRESSURE AT THE SEA BOTTOM

6.1   INTRODUCTION

Water waves propagating on the ocean may be considered to consist of an infinite number of wave trains having a constant amplitude and wave length. Passage of such an array of surface waves, creates harmonic pressure waves on the sea-floor increasing the pressure under the crest and reducing it under the trough.

The height of waves in the ocean is generally very small as compared to the length of the waves. The basic equation of water waves solved on this assumption leads to the well-known theory of small amplitude wave (Horikawa, 1978).

6.2   LINEAR WAVE THEORY

6.2.1   Governing Equations

A Cartesian coordinate system (x,y,z) is defined with x measured in the direction of wave propagation, z upward from the still water level and y orthogonal to x and z. It is assumed that the waves are two-dimensional in the x-z plane, progressive in the positive x direction and propagate over a smooth horizontal bed in water of constant undisturbed depth d. It is further assumed that the wave maintains a permanent form, i.e. there is no

underlying current and the free surface is uncontaminated. The fluid (water) is taken to be incompressible and inviscid and the flow to be irrotational. Figure 6.1 indicates the general form of a wave train conforming to these assumptions. Here the wave height H is the vertical distance from trough to crest, the wave length L is the distance between successive crests, the wave period T is the time interval between successive crests passing a particular point and the wave speed or celerity c is the speed of the wave travelling through the fluid ($c = L / T$). It is often convenient to work with the wave angular frequency $\omega = 2\pi / T$ and wave number $N = 2\pi / L$ (and thus $c = \omega / N$ also).
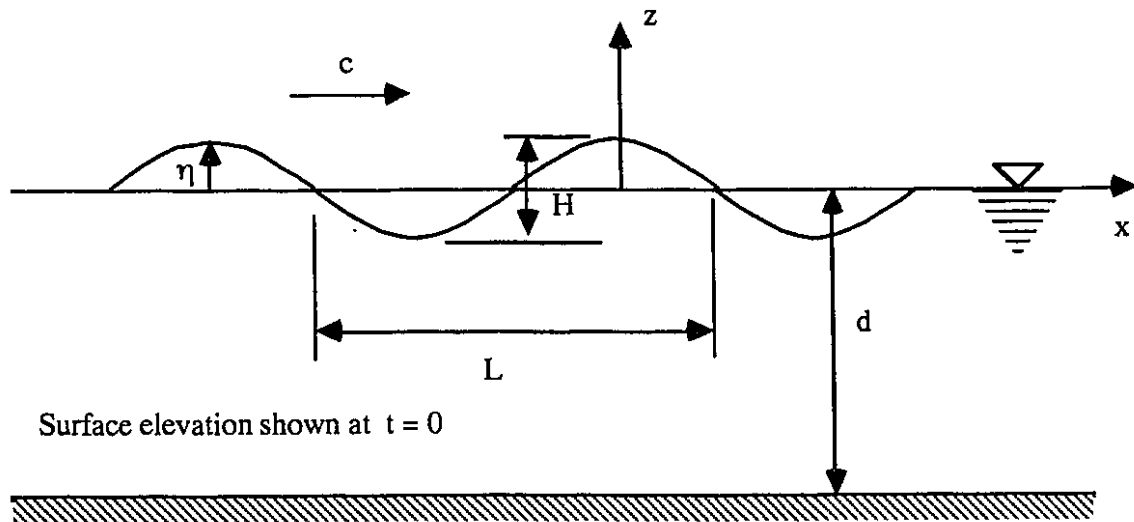

Figure 6.1 Definition sketch for a progressive wave.

Any particular wave train is generally specified by the quantities H, L and d or by H, T and d. The objective of any wave theory is to determine c (and therefore T or L as

appropriate) and a description of the water particle motions throughout the flow. Dimensionless parameters are frequently used to characterize a wave train. The wave height is often expressed in terms of H/gT^2, the wave steepness H/L or the relative height H/d. And the water depth is often expressed in terms of the depth parameter d/gT^2 or Nd or the relative depth d/L. For steeper waves in shallow water the Ursell number $U = HL^2/d^3$ is often used. Thus a design wave specified by H, T and d may conveniently be characterized, for example, by the parameters H/gT^2 and d/gT^2.

It is required to determine the velocity potential ϕ pertaining to the fluid region. This satisfies the Laplace equation

$$\frac{\partial^2 \phi}{\partial x^2} + \frac{\partial^2 \phi}{\partial z^2} = 0$$

(6.1)

subjected to the boundary conditions

$$\frac{\partial \phi}{\partial z} = 0 \qquad \text{at } z = -d$$

(6.2)

$$\frac{\partial \eta}{\partial t} + \frac{\partial \phi}{\partial x}\frac{\partial \eta}{\partial x} - \frac{\partial \phi}{\partial z} = 0 \qquad \text{at } z = \eta$$

(6.3)

$$\frac{\partial \phi}{\partial t} + \frac{1}{2}\left[\left(\frac{\partial \phi}{\partial x}\right)^2 + \left(\frac{\partial \phi}{\partial z}\right)^2\right] + g\eta = f(t) \qquad \text{at } z = \eta$$

(6.4)

$$\phi\,(\,x,\,z,t\,) = \phi\,(\,x\text{-}ct,\,z\,)$$

(6.5)

where $\eta(x,t)$ is the free surface elevation measured above the still water level $z=0$.

The existence of the velocity potential ϕ and the validity of the Laplace equation follow from the assumptions of an irrotational flow and an incompressible fluid. Equation

109

(6.2) corresponds to the boundary condition at the seabed which imposes a zero vertical component on the fluid particle velocity at the seabed. Equations (6.3) and (6.4) represent the kinematic and dynamic free surface boundary conditions respectively. The former describes the condition that the fluid particle velocity normal to the free surface is equal to the velocity of the free surface itself in that direction, while the dynamic condition expressed in terms of the Bernoulli equation states that the pressure at the free surface is constant. This later requirement follows from the assumptions that the atmospheric pressure (immediately above the fluid) is constant and the free surface is uncontaminated (corresponding to a zero surface tension). Equation (6.5) describes the periodic nature of the wave train. In the absence of an underlying current the waves are progressive with a celerity c and are of permanent form: the dependence of variables of interest upon x and t may consequently be written in terms of dependence upon a single variable (x - ct).

6.2.2 Linear Wave Theory

Two serious difficulties arise in the attempt to obtain an exact solution for a two-dimensional wave train. The first is that the free-surface boundary conditions are nonlinear and the second is that these conditions are prescribed at the free surface $z=\eta$ which is initially unknown. The simplest and most fundamental approach is to seek a linear solution of the problem by taking the wave height H to be very much smaller than both the wave length L and the still water depth d, i.e. H << L, d. The wave theory which results from this additional assumption is referred to alternatively as small amplitude wave theory, linear wave theory, sinusoidal wave theory or Airy theory. The nonlinear terms in equations (6.3) and (6.4) are negligible in comparison with the remaining linear term. Furthermore, the free surface boundary conditions may now be applied directly at the still water level $z=0$.

Equations (6.3) and (6.4) reduce to

$$\frac{\partial \phi}{\partial z} - \frac{\partial \eta}{\partial t} = 0 \qquad \text{at } z = 0 \qquad (6.6)$$

$$\frac{\partial \phi}{\partial t} + g\eta = 0 \qquad \text{at } z = 0 \qquad (6.7)$$

which may be combined to give

$$\frac{\partial^2 \phi}{\partial t^2} + g\frac{\partial \phi}{\partial z} = 0 \qquad \text{at } z = 0 \qquad (6.8)$$

$$\eta = -\frac{1}{g}\left(\frac{\partial \phi}{\partial t}\right)_{z=0} \qquad (6.9)$$

Due to the periodic condition given by equation (6.5), the solution may be obtained by separation of variables in which ϕ is written in the form

$$\phi = Z(z)\, \Phi(x - ct) \qquad (6.10)$$

Substituting this expression for ϕ into the Laplace equation(6.1) and imposing upon the boundary conditions (6.2) and (6.9), the velocity potential is obtained

$$\phi = \frac{gH}{2Nc} \frac{\cosh[N(z+d)]}{\cosh(Nd)} \sin[N(x-ct)] \qquad (6.11)$$

in which time is defined to be zero when a wave crest crosses the plane, $x = 0$.

The remaining boundary condition (6.8) could be used to obtain the linear dispersion relation.

$$\omega^2 = gN \tanh(Nd) \qquad (6.12)$$

$$c^2 = (g/N)\tanh(Nd) \qquad (6.13)$$

111

Therefore, the velocity potential may be written alternatively in forms

$$\phi = \frac{gH}{2\omega} \frac{\cosh\,[N(z+d)]}{\cosh\,(Nd)} \sin\theta$$

$$= \frac{\pi H}{NT} \frac{\cosh\,[N(z+d)]}{\sinh\,(Nd)} \sin\theta \tag{6.14}$$

where $\theta = N(x\text{-}ct) = Nx\text{-}\omega t$ is the wave phase angle.

The velocity of water particles is given by the velocity potential ϕ,

$$\mathbf{v} = \nabla\,\phi \tag{6.15}$$

The pressure p is governed by the unsteady Bernoulli equation for irrotational motion

$$\frac{\partial\phi}{\partial t} + \frac{1}{2}\,v^2 + gz + \frac{p}{\rho_w} = f(t) \tag{6.16}$$

Frequently, $f(t)$ is absorbed into ϕ since this does not affect the physical quantities of interest. In accordance with the present linear approximation, the nonlinear velocity squared term could be omitted to yield

$$p = -\,\rho_w\,gz - \rho_w\,\partial\phi\,/\,\partial t \tag{6.16'}$$

Therefore,

$$p = -\rho_w gz + \rho_w g\,\frac{H}{2}\,\frac{\cosh[N(z+d)]}{\cosh(Nd)}\,\cos\theta \tag{6.17}$$

In the above the first term is hydrostatic pressure and the second term is the hydrodynamic pressure.

6.3 WAVE–INDUCED PRESSURE AT THE SEA BOTTOM

At sea bottom, z = - d, the water pressure could be directly obtained from (6.17)

$$p = \rho_w g d + \rho_w g \frac{H}{2} \frac{1}{\cosh(Nd)} \cos \theta \qquad (6.18)$$

The amplitude of pressure exerted on the sea bottom due to the travelling wave is given by

$$p_0 = \rho_w g \frac{H}{2} \frac{1}{\cosh(Nd)} \qquad (6.19)$$

This is obtained by using linear wave theory and assuming the seafloor to be rigid and impermeable. Mallard and Dalrymple (1977) analyzed the effect of a deformable seafloor on dynamic pressure amplitude. Their analysis predicts that pressures on a deformable impermeable seafloor are higher than those on a rigid base. The increases may be significant for very soft cohesive sediments (increases up to 15% are quoted), but may be ignored for most sands.

A distinction is made between ranges of Nd. The shallow and deep water ranges correspond to Nd<π/10 and Nd>π respectively. A complete range of water depths may be conveniently divided into shallow water, intermediate depth and deep water ranges as follows

	Nd	d/L	d/gT²
Shallow water wave	(0, π/10)	(0, 1/20)	(0, 0.0025)
Intermediate depth wave	(π/10,π)	(1/20, 1/2)	(0.0025, 0.08)
Deep water waves	(π,∞)	(1/2, ∞)	(0.08, ∞)

It is easy to show that these limits in terms of Nd, d/L and d/gT^2 are equivalent by using the dispersion relations (6.12) and (6.13) or another form,

$$L = (gT^2 / 2\pi) \tanh (Nd) \qquad (6.20)$$

For deep water waves (Nd > π), tanh (Nd) $\approx$ 1. The wave length in deep water is given from (6.20)

$$L_0 = gT^2 / 2\pi \qquad (6.21)$$

thus, the dispersion relation (6.20) can be written as

$$L = L_0 \tanh (Nd) \qquad (6.20)'$$

It is also assumed that no energy loss is involved during the wave propagation over the sloping bottom towards the shore, therefore Bernoulli's equation (6.16) in the following form holds.

$$\rho_w \frac{\partial \phi}{\partial t} = -\rho_w gz - p + F(t) \qquad (6.16)'$$

The energy flux, i.e. the time rate of change of energy per unit area normal to the flow direction is (6.16)' multiplied by the particle velocity (6.15)

$$\rho_w \frac{\partial \phi}{\partial t} \mathbf{v} = \rho_w \frac{\partial \phi}{\partial t} \nabla \phi \qquad (6.22)$$

The average energy flux per wave transmitted by the wave train through a cross section at x is obtained by integrating (6.22) over the wave period T and water depth d,

$$E = \frac{1}{T} \int_d^0 \int_0^T \rho_w \frac{\partial \phi}{\partial t} \frac{\partial \phi}{\partial x} dt \, dz \qquad (6.23)$$

Replacing ϕ by (6.14) and using (6.20)', (6.23) yields

$$E = \frac{\rho_w gH^2 L_0}{16T} \left[1 + \frac{2Nd}{\sinh(2Nd)} \right] \tanh (Nd) \qquad (6.24)$$

114

For deep water waves, $\tanh (Nd) \approx 1$ and $1 + 2Nd / \sinh (2Nd) \approx 1$

$$E = \frac{\rho_w g H_0^2 L_0}{16T} \qquad (6.25)$$

Thus, combining equations (6.24) and (6.25), one obtains

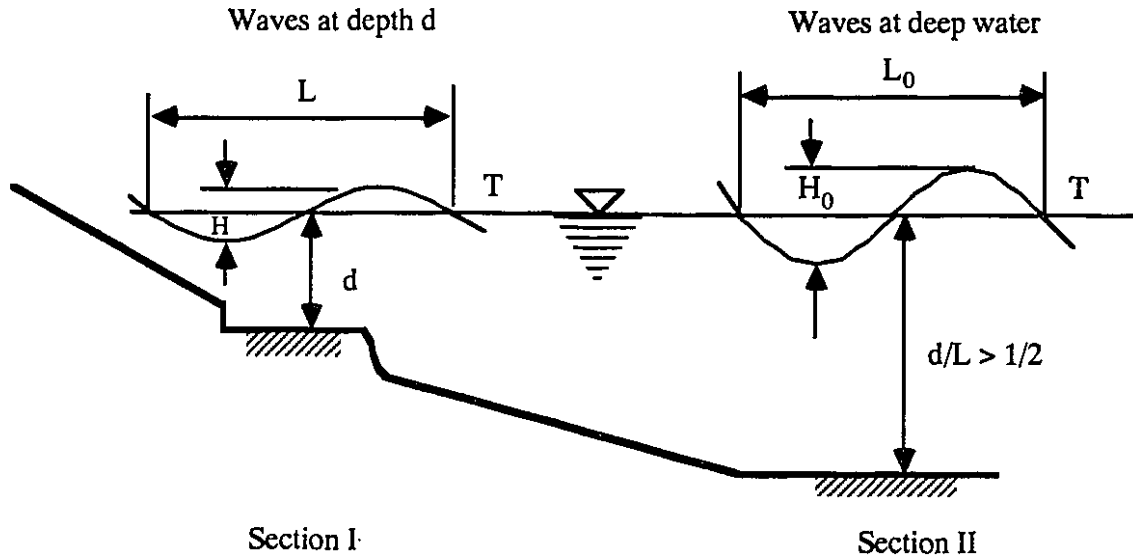$$H = H_0 [(1 + 2Nd / \sinh (2Nd)) \tanh (Nd)]^{-1/2} \qquad (6.26)$$

Figure 6.2 Deformation of wave profile during shoaling

A commonly used procedure to evaluate the amplitude pressure, p_0 , exerted on the sea bottom at a location of given water depth, d, is envisaging an overall profile of waves propagating from the deep water towards the shore, as illustrated in Figure 6.2, and determining the wave height, H, and length, L, from equations (6.20) and (6.26) on the basis of the key wave parameters, T, L_0 and H_0 specified at a location in deep water. The wave period, T, is assumed unchanged. The values of L and H determined in water depth, d, are then introduced in equation (6.19) to determine the amplitude of pressure, p_0 .

115

7

NUMERICAL METHOD FOR AN UNBOUNDED DOMAIN

7.1 INTRODUCTION

The analysis of unbounded continuum problems with discrete methods such as finite element and finite difference which must be terminated somewhere calls for the use of special boundary artifacts. These boundary conditions are particularly useful in studies of soil-structure interaction effects by the finite element method. The finite portion of the soil being modeled is customarily referred to as "the soil island" or "the soil box".

Finite element procedures were first used to evaluate wave-induced seafloor movements in 1971 (Dunham et al.). These procedures have received considerable use in practice and a number of refinements have been made in the models (Arnold, 1973; Kraft and Watkins, 1976; Wright and Dunham, 1972 and Wright, 1976). Soil beneath a particular wave is characterized by finite elements extending to the maximum depth of anticipated movement. Lateral boundaries of the region described by finite elements are assigned boundary conditions consistent with the assumption of an infinite train of uniform plane waves. Almost all the finite element analyses of wave-induced response of sea floor deposits employed elastic or some kind of nonlinear elastic stress-strain relationships to represent the soil properties. Nonlinear stress-strain curves were used with iterative processes to compute equivalent linear elastic modulus in each element consistent with the stresses (Seed et al. 1973). In such cases, without permanent deformation and residual stresses, the sea floor response will be simply a harmonic type due to the harmonic wave

pressure load. Therefore, the wave could be frozen in position and fixed, impermeable lateral boundaries are assigned due to the symmetric character. The wave induced changes of pressure at the sea bottom are applied as static loads to the upper surface of the finite element mesh and corresponding stress and displacement within the soil are calculated.

The proposed simple material model for sands is used in this study. In considering the time-dependent progressive nature of the wave loading and the path-dependent cumulative response of the sea floor, there is no symmetric lateral boundary at all. A simple lateral artificial boundary is proposed to deal with this unbounded domain problem.

7.2   CONSISTENT BOUNDARY

In certain cases, it is possible to formulate exact solutions, exact in the finite element sense, in which the behavior of the boundaries and their effects on the soil island are completely equivalent to that of an infinite succession of finite elements beyond the artificial edges of the model. In such cases, the boundaries are said to be consistent. Examples are the boundaries developed by Lysmer and Waas (1972) and Kausel (1974) in matching finite element solutions to analytical or semi-analytical solutions for the propagation of elastic waves in unbounded layered strata. More general consistent boundaries can also be developed using Green's functions in connection with the boundary integral method (Kausel and Peek 1982). Unfortunately, such exact boundaries not only couple all boundary points (i.e., they are non-local in space), but they are properly formulated only in the frequency domain (i.e., they are non-local in time). Hence, they cannot be used to study nonlinear problems using time-step integration techniques. This fact has led to the search for high quality approximation which are local in space and time, that is, approximations involve only points in the neighborhood of the boundary point under consideration within a small time-window.

117

7.3 LOCAL BOUNDARY

7.3.1 Truncation (Elementary Boundary)

Brutal truncation is widely practiced, widely accepted, easy to implement, inaccurate or expensive in static problems, and expensive or disastrous in any time dependent problem. It must employ large finite elements to model as large a medium as possible with a minimum number of degrees of freedom or employ a very large finite model. It can sometimes work fairly well, but it is usually better to improve the finite element model of the exterior. An elegant variation, which is highly accurate, was suggested by Smith (1974) for transient problems in which two solutions are carried out with free and clamped (Neumann and Dirichlet) boundary conditions. In the two cases, in and out of phase reflections occur. The addition of the two solutions cancels out of the reflection, so the effect of the boundary vanishes. Unfortunately, for every wave that hits the boundary, another two solutions are required, i.e. for n reflections there would be 2^n solutions. Research on this algorithm has therefore concentrated on improving the averaging algorithm (Zienkiewicz, Kelly, and Bettess, 1977; Cundall et al 1978).

7.3.2 Damper (Transmitting Boundary)

Dampers were first proposed by Zienkiewicz and Newton (1969) for fluid problems, and by Lysmer and Kuhlemeyer (1969) for elastic problems . Since then they have also been used in numerous periodic problems and a few transient ones. The idea is fairly simple; a damper can be designed to absorb an outgoing wave completely. The problem is that the form of the wave must be known a priori. It is usually assumed to be plane, although better results are often obtained if the wave is assumed to be cylindrical (Zienkiewicz, Kelly and Bettess, 1972). An extension of the damper concept has been proposed by Bayliss, Gunzberger and Turkel (1978). The dampers are normally referred to as absorbing, silent, anechoic, non reflecting, viscous or transmitting boundaries.

A very general set of transmitting boundaries was proposed by Lindman (1973, 1975), who used projection operators to obtain boundary conditions having a high degree of effectiveness for the scalar equation. Closely related to Lindman's contribution is the family of boundary conditions proposed a few years later by Engquist and Majda (1977) for the scalar wave equation and by Clayton and Engquest (1977) for the elastic wave equation. These so-called para-axial boundaries are formed with growing effectiveness and complexity.

7.4   INFINITE ELEMENT

As an alternative, special infinite elements are placed at the edges of the mathematical models which previously must remain finite in size.

Infinite elements were introduced independently by Ungless (1973), Anderson and Ungless (1977) who used a reciprocal type of decay and Bettess (1977) who used an exponential decay. The shape function for an element which extends to infinity should lead to finite integrations over the infinite element domain .

The infinite element method was originally applied to potential problems. Subsequently it was applied to periodic or harmonic problems, first by Zienkiewicz and Bettess (1976), Bettess and Zienkiewicz (1977) for surface waves problem in shallow water; then by Saini, Bettes and Zienkiewicz (1978) in dam reservoir interaction problems. It has been applied to elasto-static problems by Chow and Smith (1981), Beer and Meek (1981) and for electro-magnetic fields by Lynn (1981). Elastodynamic problems have also been analyzed by Chow and Smith (1981), Chow (1981) and Medina (1981).

It is important to note that these methods described above do not give a true indication of the behavior of the mathematical model towards infinity. Rather the effect of the far region on the domain of interest is modelled.

119

7.5 A SIMPLE ARTIFICIAL BOUNDARY

Many methods for unbounded field problems have been developed and implemented for analyses with varying degrees of success. It seems all the transmitting boundaries deal with linear problems such as elastic wave propagation. They may not be applicable to nonlinear analyses. Infinite elements can be used for non-linear problems which boundary integral methods fail to solve. However, there are some difficulties in treating the wave train induced pressure which extends to infinity as applied surface load. It appears that employing a large finite element solution domain remains to be the only available approach, but the cumulative response of the sea floor deposits with the cyclic nature of wave-loading makes it impractical.

A simple artificial boundary is suggested in terms of Taylor series expansion of unknown variables to solve unbounded domain problems. If $u(x,t)$ is the boundary value at time t, here the x axis is perpendicular to the lateral boundary, then the boundary value at time $t+dt$ can be estimated as

$$u(x, t+dt) = u((x-dx)+dx, t+dt)$$

$$= u(x-dx, t) + \frac{\partial u}{\partial x}\bigg|_{x-dx} dx + \frac{\partial u}{\partial t}\bigg|_{t} dt + O((dx)^2,(dt)^2) \qquad (7.1)$$

The first-order approximation is obtained by setting only the first term in (7.1)

$$u(x, t+dt) = u(x-dx, t) \qquad (7.2)$$

then

$$du(x, t) = u(x-dx, t) - u(x,t) \qquad (7.2)'$$

which means

120

$$\frac{\partial u}{\partial x} dx + \frac{\partial u}{\partial t} dt + O((dx)^2,(dt)^2) = 0$$

Let $dt \to 0$ and $dx = c\, dt$. One can reach

$$\frac{\partial u}{\partial x} + \frac{1}{c}\frac{\partial u}{\partial t} = 0 \qquad (7.3)$$

This is exactly the same as that given by the viscous boundary condition (boundary damper). One may also write

$$u(x-2dx, t-dt) = u((x-dx)-dx, t-dt)$$

$$= u(x-dx, t) - \frac{\partial u}{\partial x}\bigg|_{x-dx} dx - \frac{\partial u}{\partial t}\bigg|_{t} dt + O((dx)^2,(dt)^2)$$

$$(7.4)$$

The second-order approximation can be obtained by adding (7.1) and (7.4),

$$u(x, t+dt) = 2u(x-dx, t) - u(x-2dx, t-dt) \qquad (7.5)$$

then

$$du(x, t) = 2u(x-dx, t) - u(x-2dx, t-dt) - u(x, t) \qquad (7.5)'$$

Thus, the boundary values at current time could be predicted by extrapolation of the values of variables in the vicinity of the boundary at past time. The simple artificial boundary conditions (7.2) and (7.5) are easy to implement in the finite element program. Since dt and dx should be chosen as small values, the interior auxiliary point usually would not fall on nodal point. However, the values at these auxiliary points could be interpolated from values of the nodal points. The simple artificial boundary conditions derived above are similar to those proposed by Liao and Wong (1984) for linear wave propagation problems. However, the boundary conditions (7.2) and (7.5) derived from Taylor's series without any problem dependence could be used for nonlinear analysis.

The second-order approximation of the artificial boundary condition is used in nonlinear analysis of the travelling wave induced response of sea floor deposits.

8

WAVE INDUCED RESPONSE OF SEAFLOOR DEPOSITS

8.1 INTRODUCTION

The stability and deformation of the seafloor under the action of storm waves is an important consideration in the design of pipelines, anchors and offshore structures such as gravity and pile supported platforms. The interaction of ocean and seafloor is a very complex problem and all methods for assessing stability are based on extensive simplifying assumptions. Storm waves are almost invariably represented as a series of harmonic waves. These waves create dynamic pressure waves on the ocean floor, increasing the pressure under the crest and reducing it under the trough.

Many investigators have been attracted to the problem of assessing the transient stress field and the variation of pore water pressure. These investigators have made various simplified assumptions in order to study seafloor response. In various approaches, the seafloor has been treated as either a one-phase (total stress theory) or a two-phase (effective stress theory) medium by uncoupled or coupled schemes.

Henkel (1970) was one of the first to provide an analytical framework for stability analyses under wave loading. It followed the classical procedures of limit equilibrium slope stability analysis. He assumed the seafloor to be a one-phase medium and examined the limiting equilibrium condition along a circular failure plane. His contribution is historically

important because he demonstrates conclusively that the pressure changes on the seafloor induced by storm waves could be a significant factor affecting seafloor stability.

Putnam (1949) analyzed the flow induced in a rigid and non-deformable saturated porous bed by the pressure field. He assumed incompressible flow with an isotropic permeability, the validity of Darcy's law and hydraulic isotropy, and showed that under these conditions flow was governed by Laplace's equation. Sleath (1970) extended the Putnam analysis to include anisotropic permeability and Liu (1977) considered stratified permeability. These analyses neglect the mechanical properties of the sand. The coupling of the sand skeleton and pore water in resisting the waves is ignored. Consequently, it is called uncoupled analyses of pore water pressure response.

Taking the assumption of deformability of the soil skeleton and the interaction of the solid and fluid phases, different authors have carried out studies by applying the general theory of three dimensional consolidation (Biot, 1941). The elastic deformation of a porous medium was considered by Yamamoto (1978) for a saturated soil bed of both infinite and finite depth with isotropic permeability, by Yamamoto (1981) for a non-homogeneous soil and by Madsen (1978) for deposits of infinite depth with anisotropic permeability. There is a unique one-to-one relationship between the predicted response and the applied load at any time. Therefore, the design storm wave condition in the coupled effective stress analysis is specified in terms of a single wave with the largest amplitude.

A computer program was developed by Siddharthan and Finn (1979) for the analysis of transient pore water pressure and effective stress due to wave loading. It is also based on Biot's equations and extends the capacity for analysis to layered soils with hydraulic anisotropy and variable depth. The program evaluates the stability of the seafloor under the wave-induced effective stress system using the Mohr-Coulomb failure criterion. Gatmiri (1990) extended the linear analysis of the coupled effective stress and pore pressure to a submarine sediment with sloping surface. However, none of the above

mentioned response analysis accounts for the residual pore water pressure and permanent deformation.

The problems associated with seafloor instability were brought sharply into focus in 1969 when Hurricane 'Camille' struck areas around the Gulf of Mexico. 'Camille' demonstrated that ocean waves produce pressures on the seafloor that can trigger seafloor instability even though the bottom slope is very flat, less than 0.5% (Focht & Kraft 1977). Two structures were destroyed by massive seafloor movements during the storm. It was clear therefore that the lateral loads imposed on these structures by moving soil from unstable slopes could be substantial, and could even exceed the wave forces from the design storm.

The phenomenon of wave-induced liquefaction has been recognized in recent years. It may occur in sand or silt deposits, thereby exerting damaging influences on the engineering installations placed nearby such as the flotation of pipelines (Christian,1974), loss of anchor resistance, loss of significant lateral resistance of piles (Finn and Martin, 1979), and slope failures in soil structures such as the artificial islands used for oil and gas exploration in the Beaufort Sea (Finn et al., 1982). The term 'liquefaction' was originally associated with the loss in strength of the soil that causes flow slides. The definition of the term 'liquefaction' has been extended to a particular value of pore pressure (the value of the confined pressure, Seed and Lee, 1966) or a particular level of strain (5% double-amplitude strain, Ishihara, 1983). The common procedure to evaluate the resistance of soil to liquefaction is to test soil specimens by means of the cyclic triaxial test apparatus.

Lee an Focht (1975) studied the liquefaction potential under the Ekofisk tank in the North Sea. It was probably the first investigation of ocean wave-induced liquefaction utilizing the principles established for the solution of seismic liquefaction problems.

Several investigators have collaborated to shape analytical frameworks for the liquefaction analysis under wave loadings. Seed and Rahman (1978) developed a

124

methodology in which generation and contemporaneous dissipation of excess pore water pressures during strong wave loading can be evaluated. An uncoupled scheme was adopted. This was accomplished by solving the usual continuity equation of flow in conjunction with a pore water pressure generation model proposed by Seed et al. (1976). The effective stress was computed assuming elastic behavior. The residual pore water pressure is not uniquely related to the instantaneous values of wave-induced stresses, but depends on the intensity and duration of the storm and on the drainage characteristics of the seafloor. Under these circumstances, the design storm wave condition in Seed's liquefaction analysis is specified in terms of the wave height, number of waves and duration. Finn and Lee (1979) extended this approach for performing an effective stress stability analysis of the seabed deposits.

Siddharthan (1987) presented a paper in which the wave-induced response was split into the transient and residual components. The coupled transient response was obtained by solving Madsen's equations (1978) analytically with inertia terms introduced. An equivalent linear elastic approach (Seed et al., 1973) has been used, employing an iterative process to obtain shear modulus and damping. The residual response was obtained by solving the uncoupled equation (Seed and Rahman, 1977) for the residual pore water pressure based on finite element method. An empirical relation of the cyclic pore water pressure generation model (Seed et al., 1976) was used. The full response is the addition of the independently obtained solutions. For typical storm wave conditions that exist in the North Sea, it appears that the inclusion of damping, inertia and anisotropic permeability is not important relative to ocean sands.

In an attempt to analyze the liquefaction susceptibility of the seafloor deposits under wave action, Poorooshasb, Ishihara and Yang (1987) presented a paper in which the seabed was assumed to be a saturated porous medium simulated by a two-surface plastic model for the solid phase. Probably it was the first time that the wave-induced seabed

125

response was investigated by elasto-plastic effective stress analysis step by step following the wave loading history.

The build-up of pore water pressure and the accumulation of permanent deformations are produced by the model itself. Results from the coupled nonlinear analysis predict that liquefaction may indeed occur for certain loose deposits. A FEM and FDM hybrid computational procedure is used which provides an example of the staggered solution scheme combined with some simplifications to solve the coupled field problem. A simultaneous solution (direct integration) scheme is also used for analysis of the seabed deposit subjected to standing wave action by FEM (Poorooshasb, Yang and Clark, 1990) in which the two-surface plastic constitutive model is adopted.

The results shown in the next sections are the response analyses of seafloor deposits to standing waves and to travelling waves by FEM. The simple constitutive model proposed in this study has been incorporated into computer programs PCPSTAD and PCPTRAV for standing wave and travelling wave cases respectively.

8.2 RESPONSE OF SEAFLOOR DEPOSITS TO STANDING WAVE

When a traveling wave strikes a vertical flat barrier such as a sea wall, the wave is reflected and a standing wave results. In this section, an analysis of nonbreaking waves that are perfectly reflected at a vertical barrier is presented.

Perfect reflection can be represented mathematically by adding the expression for the free-surface displacement of a right-running wave and that for its mirror image, which is a left-running wave with the same profile but a phase velocity directed to the left . If the right-running wave is described by

126

$$\eta^+ = a \cos (Nx - \omega t) \qquad\qquad (8.1)$$

and its mirror image by

$$\eta^- = a \cos (Nx + \omega t) \qquad\qquad (8.2)$$

then the reflected wave is described by

$$\eta = \eta^+ + \eta^- = 2a \cos (Nx) \cos (\omega t) \qquad\qquad (8.3)$$

where the wave number $N = 2\pi/L$ and the angular frequency $\omega = 2\pi/T$. Equation (8.3) describes a standing wave with an amplitude twice that of the incident traveling wave.

According to the linear wave theory the water pressure exerted on the seabed due to standing waves would be of a sinusoidal nature. Thus it is sufficient, by the argument of symmetry, to consider only a half wave length $L/2$ as shown in Figure 8.1.

Plane strain is assumed. The initial and boundary conditions for the standing wave action problem are

$t = 0$ $\qquad$ $\sigma'_{yy} = (\gamma_s - \gamma_w) \, y \, , \qquad \sigma'_{xy} = 0 \, , \qquad \sigma'_{xx} = \sigma'_{zz} = K_0 \, \sigma'_{yy}$

$\qquad\qquad$ $p = 0 \qquad$ (excess pore water pressure) $\qquad (8.4)$

$y = 0$ $\qquad$ $d\sigma'_{yy} = 0, \qquad d\sigma'_{xy} = 0,$

$\qquad\qquad$ $p = p_0 \cos (Nx) \cos (\omega t)$

$\qquad\qquad$ $dp = p_0 \cos (Nx) \, [\, \cos \omega(t + dt) - \cos \omega t \,]$

$\qquad\qquad$ $p_0 = 0.5 \, \gamma_w \, H \, / \cosh (Nd)$

$y = h$ $\qquad$ $\partial p \, / \, \partial y = 0 \, , \, du_x = 0 \, , \, du_y = 0$

$x = 0$ $\qquad$ $\partial p \, / \, \partial x = 0 \, , \, du_x = 0$

$x = L/2$ $\qquad$ $\partial p \, / \, \partial x = 0 \, , \, du_x = 0 \qquad\qquad (8.5)$

where K_0 is the coefficient of earth pressure at rest, T is the wave period and H is the wave height.

In the particular example cited in this study the following geometrical and material parameters were employed (Figure 8.1)

L/2 =80m.	h = 40m.	d = 20m.
H/2 = 6.62m.	T = 100sec.	$K_0 = 0.5$
$\gamma_s = 19$ KN/m^3	$\gamma_w = 10$ KN / m^3	$n/K_w = 10^{-7}$ m^2 / KN
A = 0.0022	B = 0.05	$\gamma_0 = 5.0$
$\kappa = 0.008$	$v = 0.2$	$\eta_0 = 0.004$
$K_z = 4000$kPa	$\phi_f = 27^0$	$\phi_{cr} = 27^0$
$k = 10^{-3} \sim 10^{-1}$ cm/sec		

The material properties stated above correspond to data for loose Fuji river sand as tested by Ishihara and Tatsuoka (1975).

The finite element recurrence equation (5.25)

$$\begin{bmatrix} K & Q \\ Q^T & S + \theta \, \Delta t \, H \end{bmatrix} \begin{Bmatrix} d\underline{u} \\ d\underline{p} \end{Bmatrix} = \begin{Bmatrix} df_1 \\ -\Delta t \, H \, \underline{p}_n \end{Bmatrix} \qquad (5.25)$$

is accommodated in computer program PCPSTAD in conjunction with the initial and boundary conditions listed above for the standing wave case.

The finite element mesh used is given in Figure 8.2 which shows the nodal numbering system, element numbering system and the position of Gauss integration points within an element. $\theta=0.5$ is used in the recurrence equation (Crank-Nicolson method). The displacement is calculated at nodal points, however the effective stress and pore water

128

pressure are evaluated at the Gauss points. Hence the various curves are labeled by their Gauss point number, for example E2G1 means the results of the computations at Gauss point No.1 of element No.2.

The graphs shown in Figure 8.3 represent the variation of the pore water pressure with time. It may be noted that in the case of sands with relatively high permeability the variation in the pore water pressure essentially oscillates about a constant mean value. This is not, however, the case for the low permeability sand. The pore water pressure oscillates about a mean value which is increasing with time. This build up of the pore water pressure is detrimental to the integrity of the system.

Figure 8.4 shows the variation of the mean effective stress with time. When the permeability of the sand is high, the surface loading appears to have little effect on the variation of the mean effective stress, i.e. the water just enters and leaves the pores of the soil without affecting the stress regime to any extent. The situation is quite different for the low permeability sands. Take, for example, k=0.01 cm/sec. Curves indicate a general tendency for the mean effective stress to decrease in magnitude as the number of loading cycles increase. The decrease in effective stress for the case of k=0.001 cm/sec is more rapid. Here the mean effective stress at the Gauss points E2G2 and E2G1 approaches zero only after ten cycles of surface loading. This reduction of the mean effective stress is clearly an indication of the loss of strength of the system at these points and can lead to failure. The system behaves as a fluid with no intrinsic shear strength and the phenomenon is generally referred to as liquefaction. Massive movement of shallow sea bed soils due to the action of the surface waves and the collapse of the foundation of waterfront structures when subjected to storm waves is the direct result of liquefaction.

Figure 8.5 and 8.6 give what may be loosely termed as the stress paths followed by the sand element located at the Gauss points E8G3 and E8G4. They show the variation of the vertical effective stress with the pore water pressure and with the mean effective stress

129

as loading proceeds. The situation is as before. The water waves appear to have no effect on highly permeable sand, but for the low permeability sand, the decrease in the vertical effective stress is associated with the increase in pore water pressure and the decrease in the mean effective stress.

Finally in Figure 8.7 the settlement at nodal point No. 37 is plotted against time for the three cases. In the first case a small but finite amount of densification of the sand is experienced. This is, of course, expected since plastic deformation is always irreversible. In the third case, the initial soil densification is followed by a heave (upward movement which in the convention of geotechnics is shown by negative numbers) of the deposit. This is the liquefaction phenomenon referred to earlier.

It is a well known fact that the relative density of a sand plays a very important role in its liquefaction potential when subjected to dynamic loadings such as those imposed by a severe earthquake. What is not as well known is that such loose deposits may liquefy under cyclic loading even without dynamic (inertial) effect if the permeability of the sand is low enough. The example cited here clearly demonstrates this phenomenon.

The behavior of sand under standing wave action is different from that under fully drained or undrained conditions. When the permeability of the sand is relatively high, in excess of 0.01 cm/sec in the case studied here, the system is safe. On the other hand, if the same system has a low permeability (say less than 0.001 cm/sec) then instability due to liquefaction is likely to take place.
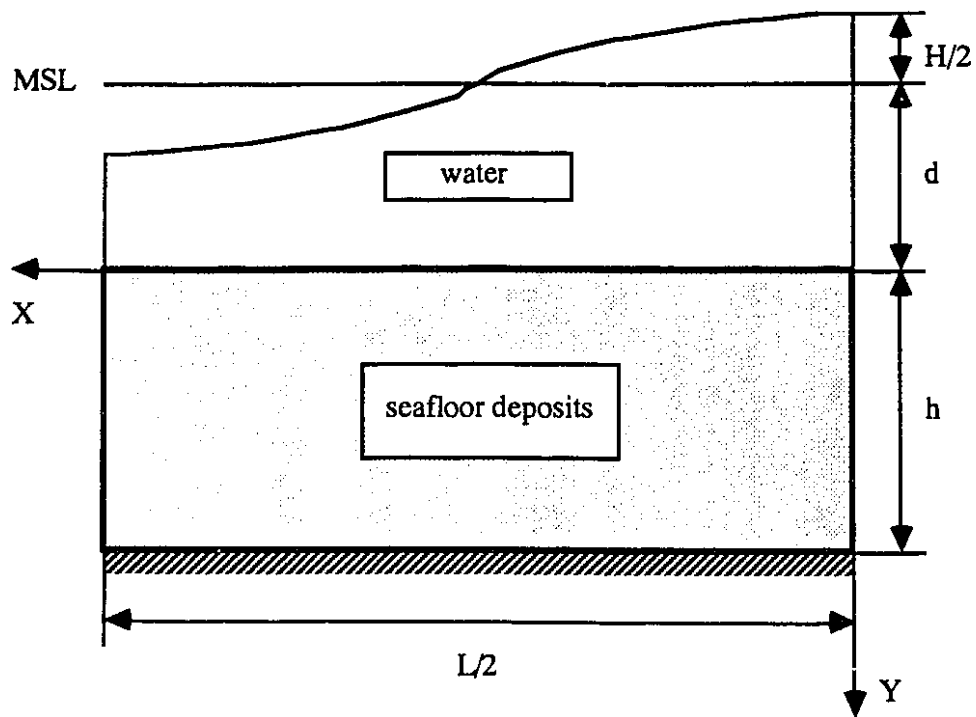
Figure 8.1 Seabed subjected to the action of standing wave
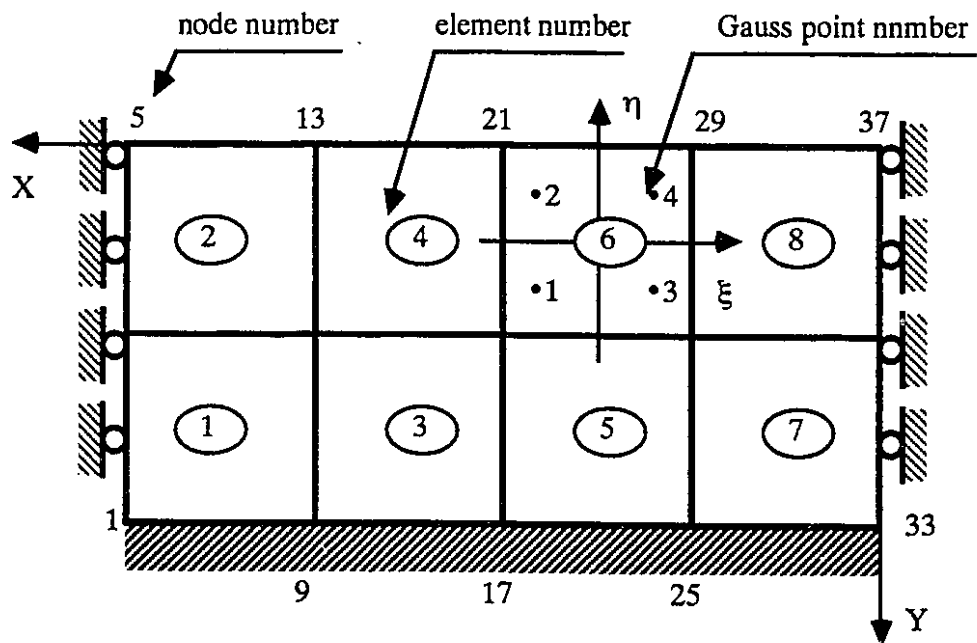
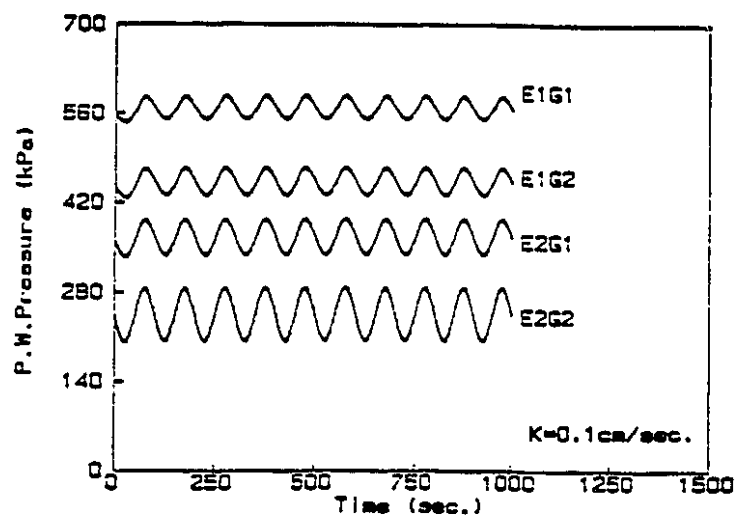Figure 8.2 The finite element mesh used for standing wave case.

131
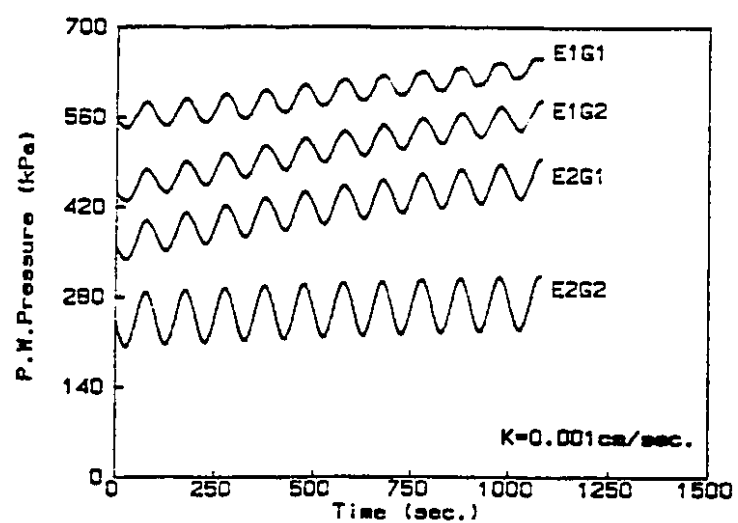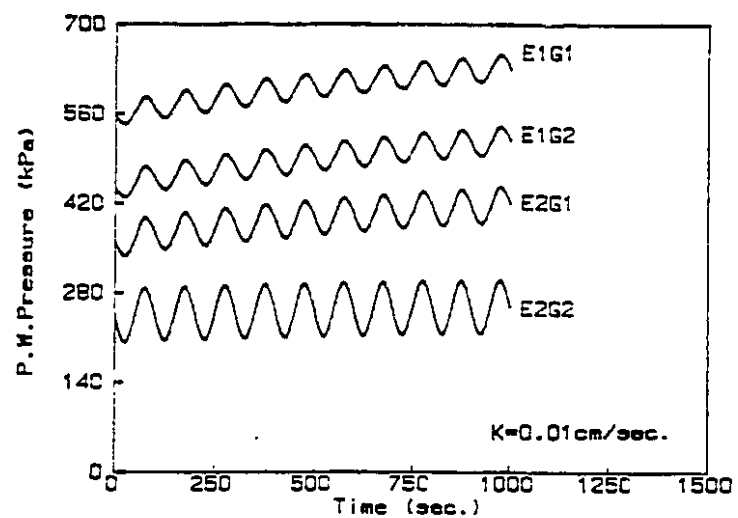
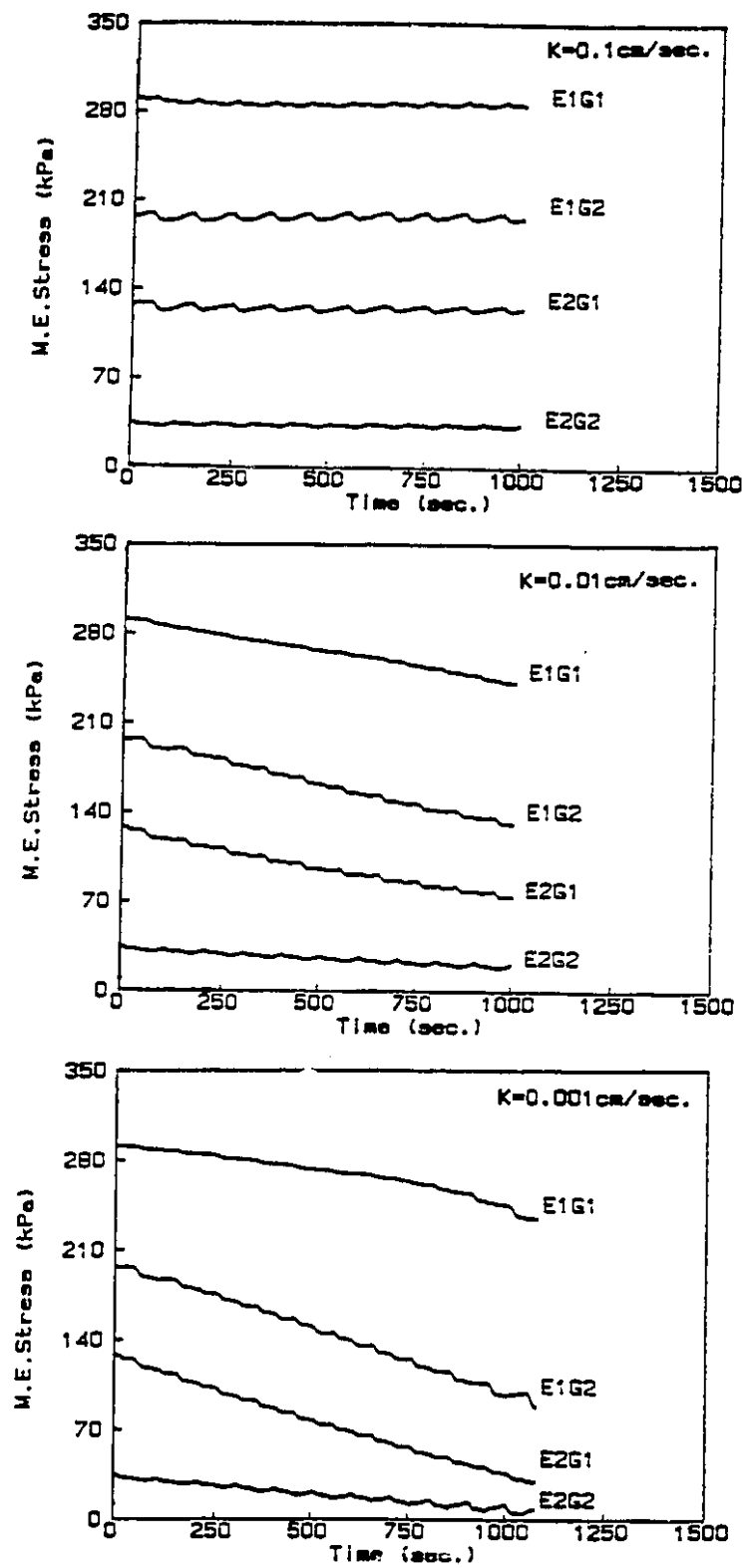Figure 8.3   P. W. Pressure vs Time for standing wave case

132

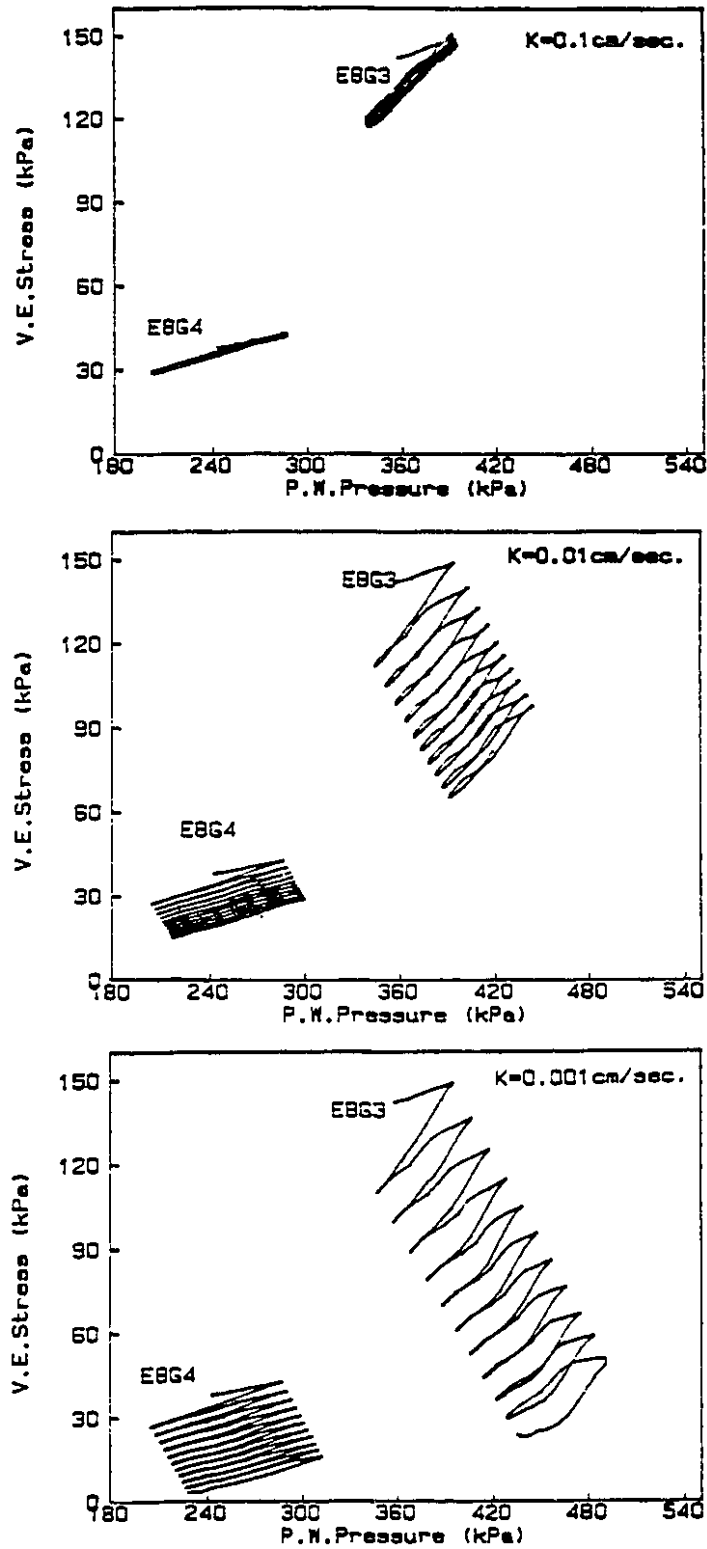Figure 8.4   M. E. Stress vs Time   for standing wave case

133

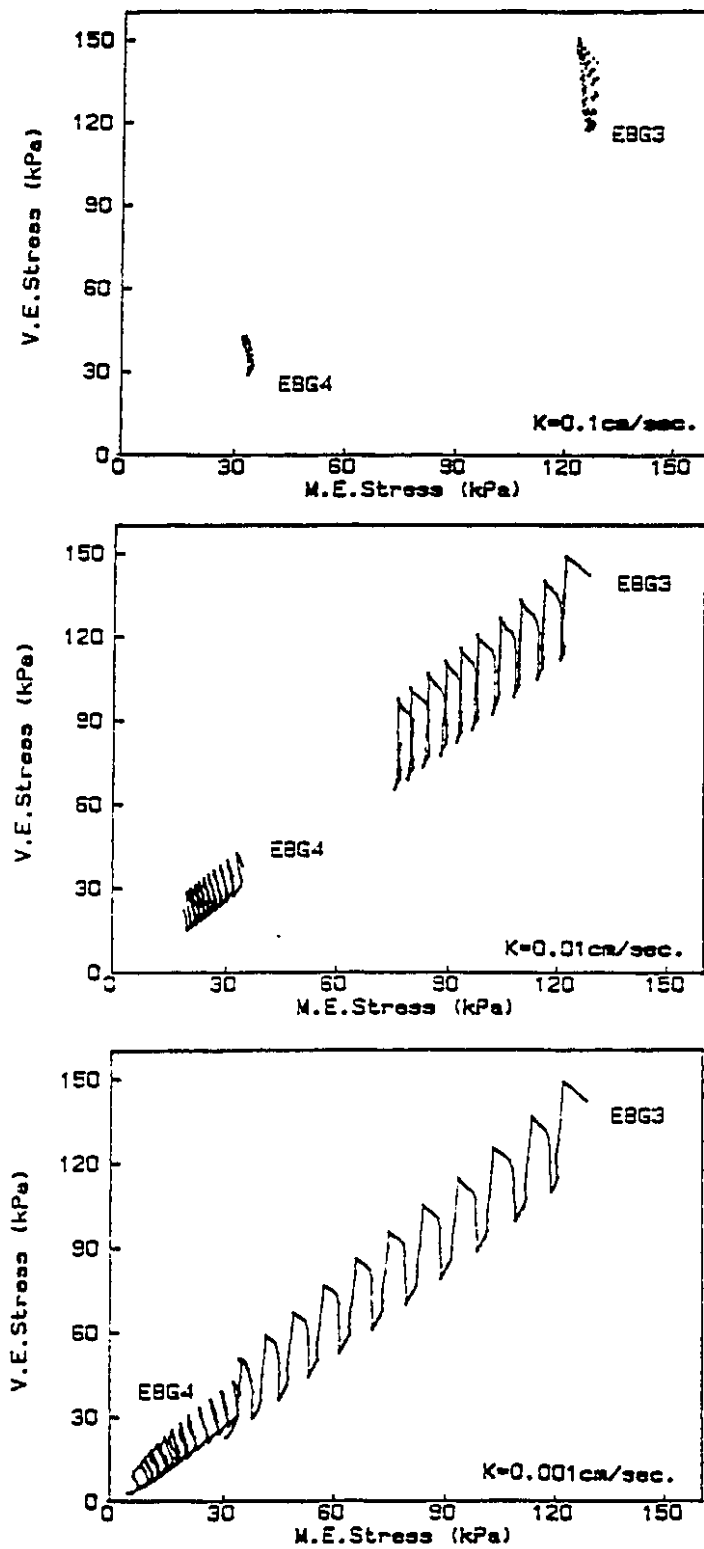Figure 8.5   V. E. Stress vs P. W. Pressure   for standing wave case

134

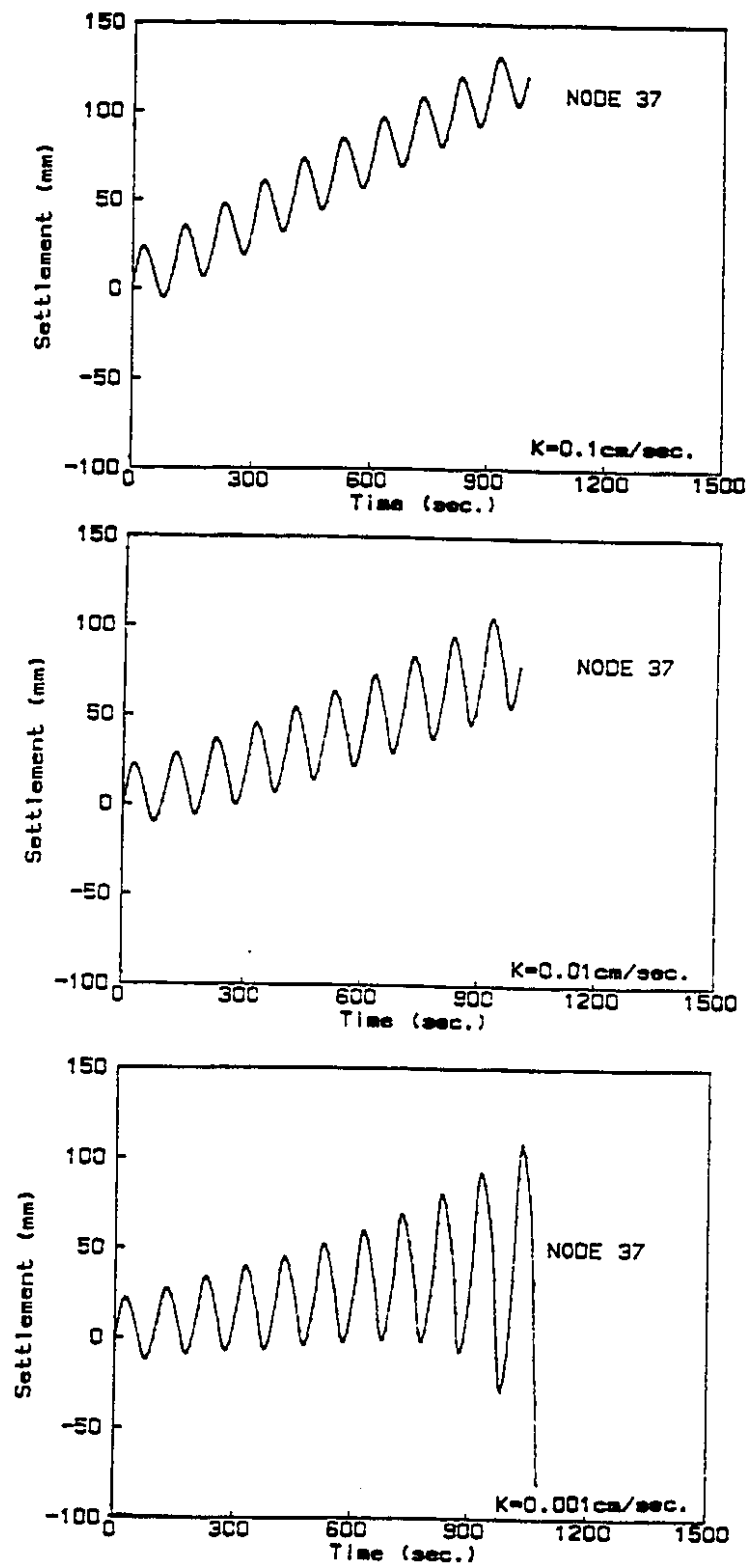Figure 8.6   V. E. Stress vs M. E. Stress   for standing wave case

135

Figure 8.7   Settlement vs Time for standing wave case

136

8.3   RESPONSE OF SEAFLOOR DEPOSITS TO TRAVELLING WAVE

In wave response studies, the seafloor is considered as being subjected to an ocean wave induced plane pressure wave travelling across the surface of the underlying deposits.

Nataraja and Gill (1983) developed a simplified procedure for ocean wave-induced liquefaction analysis and examined a few case histories for evaluation of the simplified procedure. In the simplified procedure, the existing solutions from the theory of elasticity are used to estimate the cyclic shear stress distribution resulting from the passage of a wave train. The existing data on cyclic shear strength of liquefaction under seismic loadings are modified and extended to estimate the cyclic shear strength of liquefaction under wave loading conditions. It can serve as a first step in determining whether a sophisticated analysis is required.

Offshore structures such as large diameter underwater pipelines for nuclear power plants (Christian et al. 1974) and Ekofisk oil storage tank in the North Sea (Lee and Focht, 1975) are two examples of projects where either safety or critical environmental considerations are involved. For such important projects it is usually required to perform sophisticated calculations involving state-of-the-art analytical techniques as well as detailed field and laboratory investigations. The liquefaction susceptibility analyses of the two example cases are carried out in this study. The computer program PCPSTAD has been modified to program PCPTRAV for the travelling wave case, in which the proposed artificial boundary condition is implemented. The second-order approximation (7.5) is used for the lateral artificial boundaries.

It is assumed that in the first stage it takes three wave periods of time to reach the full magnitude while the wave train is forming and travelling simultaneously. Afterwards, the wave is travelling with the constant amplitude. The size of solution domains are taken as one-wave length and two-wave lengths for the Lake Ontario case and the North Sea case, respectively.
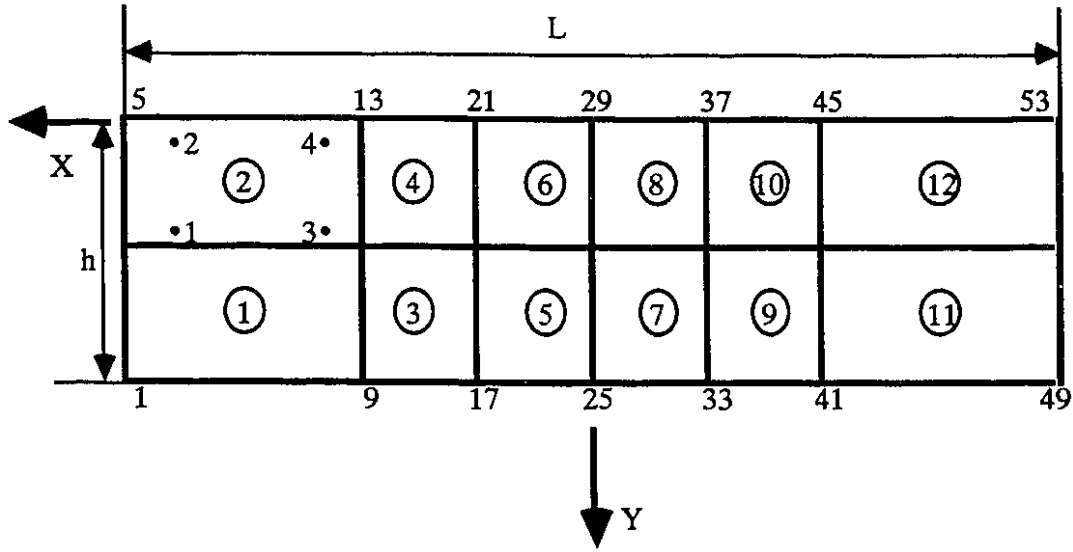
137

Figure 8.8   The finite element mesh for Lake Ontario case

8.3.1 Underwater pipeline in Lake Ontario

The finite element mesh used for the Lake Ontario case is shown in Figure 8.8 whose width is one wave length. The lateral artificial boundaries are set at x=L/2 and x=-L/2.

Plane strain is assumed. The initial and boundary conditions for analysis of travelling wave action are listed below

t=0 $\sigma'_{yy} = (\gamma_s - \gamma_w) \, y$, $\sigma'_{xy} = 0$, $\sigma'_{xx} = \sigma'_{zz} = K_0 \, \sigma'_{yy}$

$$p = 0 \qquad \text{(excess pore water pressure)} \qquad (8.4)$$

y=0 $d\sigma'_{yy} = 0$, $d\sigma'_{xy} = 0$,

$$p = p_0 \cos (Nx - \omega t)$$

$$= p_0 \cos (Nx) \cos (\omega t) + p_0 \sin (Nx) \sin (\omega t)$$

138

$$dp = p_0 \cos (Nx) \,[\, \cos \omega(t + dt) - \cos \omega t \,]$$

$$+ \; p_0 \sin(Nx) \,[\, \sin \omega(t + dt) - \sin \omega t \,]$$

$$p_0 = 0.5 \; \gamma_w \; H \, / \cosh (Nd)$$

$$H = H_{max} \, t \, / \, (3T) \qquad\qquad t \le 3T$$

$$H = H_{max} \qquad\qquad\qquad t > 3T$$

$y=h \qquad \partial p \, / \, \partial y = 0 \,, \qquad\qquad du_x = 0 \,, \qquad du_y = 0$

$x=L/2 \qquad du_x(x,t+dt) = 2u_x(x\text{-}dx,t) - u_x(x\text{-}2dx,t\text{-}dt) - u_x(x,t)$

$\qquad\qquad du_y(x,t+dt) = 2u_y(x\text{-}dx,t) - u_y(x\text{-}2dx,t\text{-}dt) - u_y(x,t)$

$\qquad\qquad dp(x,t+dt) = 2p(x\text{-}dx,t) - p(x\text{-}2dx,t\text{-}dt) - p(x,t) \qquad\qquad (8.6)$

$x=\text{-}L/2 \qquad du_x(\text{-}L/2,\, t+dt) = du_x(L/2,\, t+dt)$

$\qquad\qquad du_y(\text{-}L/2,\, t+dt) = du_y(L/2,\, t+dt)$

$\qquad\qquad dp(\text{-}L/2,\, t+dt) = dp(L/2,\, t+dt)$

where K_0 is the coefficient of earth pressure at rest, T is the wave period and H is the wave height. The wave number $N=2\pi/L$ and the angular frequency $\omega=2\pi/T$.

The following design wave data (Christian et al., 1974), geometrical and material parameters were employed in the numerical analysis:

L =73m.	h = 12m.	d = 12m.
H = 9m.	T = 7sec.	$K_0 = 0.5$
$\gamma_s = 19$ KN/m^3	$\gamma_w = 9.8$ KN / m^3	$n/K_w = 1.2 * 10^{-7}$ m^2 / KN
A = 0.0022	B = 0.05	$\gamma_0 = 5.0$
$\kappa = 0.005$	$\nu = 0.33$	$\eta_0 = 0.004$

	K_z	ϕ_f	ϕ_{cr}	k
loose sand	2000kPa	25^0	25^0	0.01 cm/sec
medium dense sand	4000kPa	39^0	27^0	0.001cm/sec

Two cases, loose sand and medium dense sand, are analyzed. The numerical results for loose sand are shown in Figure 8.9 – 8.16.

Figures 8.9 and 8.10 present variations of the mean effective stress, pore water pressure, vertical effective stress and shear stress with time at Gauss point E4G2. It is clearly shown that all quantities increase their magnitudes in the . This is due to the wave train growing from zero to its full magnitude during e wave periods of time. Afterwards, the wave train remains at a constant ampl. ay be noted the mean effective stress and the vertical effective stress are decreasing with time, and approaching zero only after 5 cycles of surface wave loading. While the pore water pressure is increasing during the same period. It indicates that the condition for liquefaction is indeed developed in the underlying deposits.

Figures 8.11 and 8.12 give the stress paths at Gauss point E4G2. The variation of the vertical effective stress with the mean effective stress is shown in Figure 8.11, in which the curve migrates towards the origin: an indication of liquefaction. The variation of the vertical effective stress with the pore water pressure in shown in Figure 8.12. The reduction of the vertical effective stress is due mainly to a general tendency of the pore water pressure build-up. Figure 8.13 shows the variation of horizontal displacement and vertical displacement with time at Node 13 which is closest to point E4G2, the first liquefied point. The graphs indicate a different deformation trend when compared with the standing wave case under similar circumstances. The initial soil densification is followed by a heave (upward movement) in the standing wave case since the lateral boundaries are

fixed, therefore the upward movement is the most likely motion. However, for the travelling wave case, the lateral boundaries are released by the second-order approximation of the artificial boundary conditions. The horizontal displacement increases noticeably along the direction of wave travel. This indicates a loss of lateral resistance of the soil system during liquefaction.

The accumulation of permanent deformation is described in Figures 8.14-8.16. They show the development of the vertical profiles of horizontal displacement and vertical displacement for cross sections marked by x=0, 9.125, 18.25 m (x=0, L/8, L/4) at different time instants t=21, 28, 35 sec. (3, 4, 5 cycles) respectively.

The numerical results for medium dense sand are illustrated in Figures 8.17–8.25. Figures 8.17 and 8.18 show variation of the mean effective stress, pore water pressure, vertical effective stress and shear stress with time at Gauss point E4G2. Figure 8.19 and 8.20 present the stress paths at Gauss point E4G2. Figure 8.21 gives the variation of horizontal displacement and vertical displacement with time at Node 13. The general tendency appears the same as that in the loose sand case. Liquefaction is also developed but more wave loading cycles (about eight cycles in this case) are required to drive the underlying deposits to liquefy.

The accumulation of permanent deformation is shown in Figures 8.22-8.25 for cross sections marked by x=0, 9.125, 18.25 m (x=0, L/8, L/4) at different moments t=21, 35, 49, 63 sec. (3, 5, 7, 8 cycles), respectively.

The numerical analysis results predict the evidence of liquefaction for both loose sand and medium dense sand in the circumstances of Lake Ontario where, indeed, liquefaction did occur. A single 3.05 m (10 ft) diameter steel pipeline in Lake Ontario has failed several times, apparently because of liquefaction (Christian et al. 1974). It is noted that the soil particles and the water behaved very much like a dense fluid and caused the buried pipeline to float to the surface.

141

8.3.2 Ekofisk tank in the North Sea

The Ekofisk oil storage tank in the North Sea (Lee and Focht, 1975), where the site oceanographic and geotechnical design parameters are well investigated and documented, has successfully withstood 100-year design storm waves without experiencing wave-induced liquefaction.

The finite element mesh used for the North Sea case is shown in Figure 8.26. Its width is two wave lengths. The lateral artificial boundaries are set at $x=L$ and $x=-L$. Plane strain is assumed. The initial and boundary conditions are

$t=0$ $\qquad$ $\sigma'_{yy} = (\gamma_s - \gamma_w) \, y \, , \qquad \sigma'_{xy} = 0 \, , \qquad \sigma'_{xx} = \sigma'_{zz} = K_0 \, \sigma'_{yy}$

$\qquad\qquad\quad$ $p = 0$ $\qquad$ (excess pore water pressure) $\qquad$ (8.4)

$y=0$ $\qquad$ $d\sigma'_{yy} = 0, \qquad d\sigma'_{xy} = 0,$

$\qquad\qquad\quad$ $p = p_0 \cos (Nx - \omega t)$

$\qquad\qquad\qquad$ $= p_0 \cos (Nx) \cos (\omega t) + p_0 \sin (Nx) \sin (\omega t)$

$\qquad\qquad\quad$ $dp = p_0 \cos (Nx) [\cos \omega(t + dt) - \cos \omega t]$

$\qquad\qquad\qquad\quad$ $+ \; p_0 \sin(Nx) [\sin \omega(t + dt) - \sin \omega t]$

$\qquad\qquad\quad$ $p_0 = 0.5 \, \gamma_w \, H \, / \cosh (Nd)$

$\qquad\qquad\quad$ $H = H_{max} \, t \, / \, (3T) \qquad\qquad t \leq 3T$

$\qquad\qquad\quad$ $H = H_{max} \qquad\qquad\qquad t > 3T$

$y=h$ $\qquad$ $\partial p \, / \, \partial y = 0 \, , \qquad du_x = 0 \, , \qquad du_y = 0$

$x=L$ $\qquad$ $du_x(x,t+dt) = 2u_x(x-dx,t) - u_x(x-2dx,t-dt) - u_x(x,t)$

$\qquad\qquad\quad$ $du_y(x,t+dt) = 2u_y(x-dx,t) - u_y(x-2dx,t-dt) - u_y(x,t)$

$\qquad\qquad\quad$ $dp(x,t+dt) = 2p(x-dx,t) - p(x-2dx,t-dt) - p(x,t)$ $\qquad$ (8.7)

x=-L $du_x(-L, t+dt) = du_x(L, t+dt)$

              $du_y(-L, t+dt) = du_y(L, t+dt)$

              $dp(-L, t+dt) = dp(L, t+dt)$

where the symbols are as defined previously.

The following design storm wave data (Lee and Focht, 1975), geometrical and material parameters were employed in the numerical analysis.

L =324m.	h = 25m.	d = 70m.
H = 24m.	T = 15sec.	$K_0 = 0.5$
γ_s = 21.45 kN/m³	γ_w = 9.8 kN / m³	n/K_w =1.2*10⁻⁷ m² / kN
A = 0.0022	B = 0.05	$\gamma_0 = 5.0$
$\kappa = 0.005$	$v = 0.33$	$\eta_0 = 0.004$
$K_z = 14000$ kPa	$\phi_f = 50^0$	$\phi_{cr} = 36^0$
k = 0.01 cm/sec		

The numerical results are shown in Figures 8.27 – 8.37. Figures 8.27 – 8.30 describe the variations of the mean effective stress, pore water pressure, vertical effective stress and shear stress with time at Gauss point E14G2 and E16G4, respectively. In the first stage, all quantities increase their magnitudes in accordance with the wave train development to its full magnitude within the first three wave periods. Afterwards the wave travels with constant amplitude. The mean effective stress and vertical effective stress are gently decreasing for about 500 sec. (33 wave cycles), then fluctuating around certain mean values. The pore water pressure first increases a little, then oscillates about a constant mean value. This implies that the water just enters and leaves the pores of the soil during

143

the wave cycle without affecting the stress regime. The shear stress is almost in a cyclic mode. After a duration of 780 seconds (52 wave-induced cyclic loadings) there is no evidence of liquefaction.

The stress paths at Gauss point E14G2 are given in Figures 8.31 and 8.32. The curves are almost overlapping after 35 wave-induced cyclic loadings indicating a situation generally referred to as cyclic mobility.

Figures 8.33 and 8.34 show the variation of the horizontal displacement and the vertical displacement with time at Nodes 53 and 69, respectively. The general densification tendency with very low rate appears in the vertical displacement. The lateral movements are substantial.

It is noted that the curves representing the effective stresses and pore water pressures at Gauss points E14G2 and E16G4 resemble each other in appearance. The same can be said about the displacements at Node 53 and Node 69. This is as expected since the wave induced responses in the neighborhood should be similar. This may be considered as a verification of the success of the proposed artificial boundary condition.

Figures 8.35 – 8.37 present the vertical profiles of horizontal displacements and vertical displacements for sections marked by x=0, 40.5 and 81m (x=0, L/8 and L/4) at different times of t=300, 600 and 780 seconds (i.e., 20, 40 and 52 cycles), respectively. The permanent deformations are accumulated as the wave loading proceeds.

The numerical analysis successfully predicts that wave-induced liquefaction would be not likely to happen in the North Sea dense sand environment.

loose sand, k=0.01cm/sec. at E4G2.
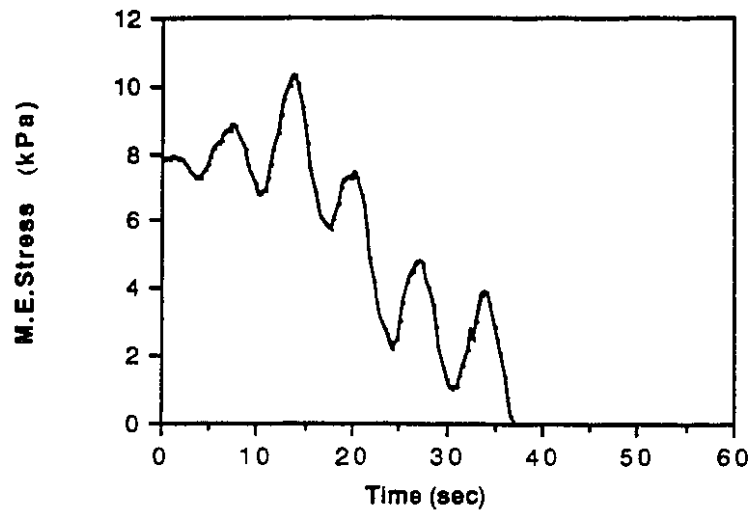
loose sand, k=0.01cm/sec. at E4G2.
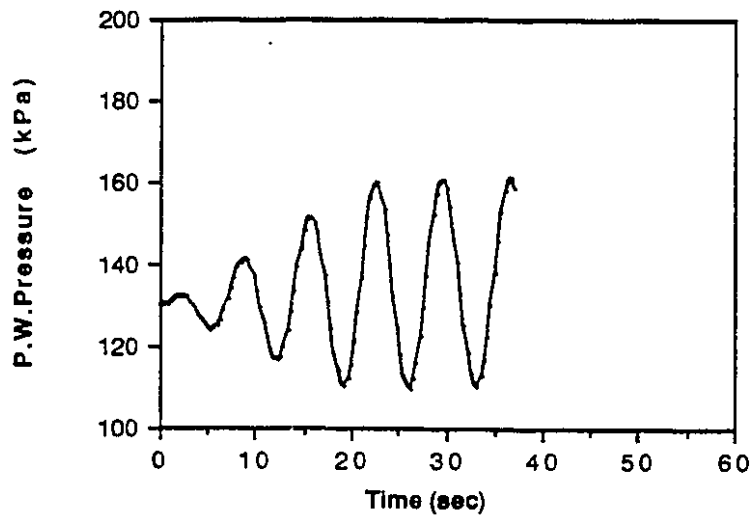
Figure 8.9   M.E.Stress and P.W.Pressure vs Time for Lake Ontario loose sand

145

loose sand, k=0.01cm/sec. at E4G2.

loose sand, k=0.01cm/sec. at E4G2.
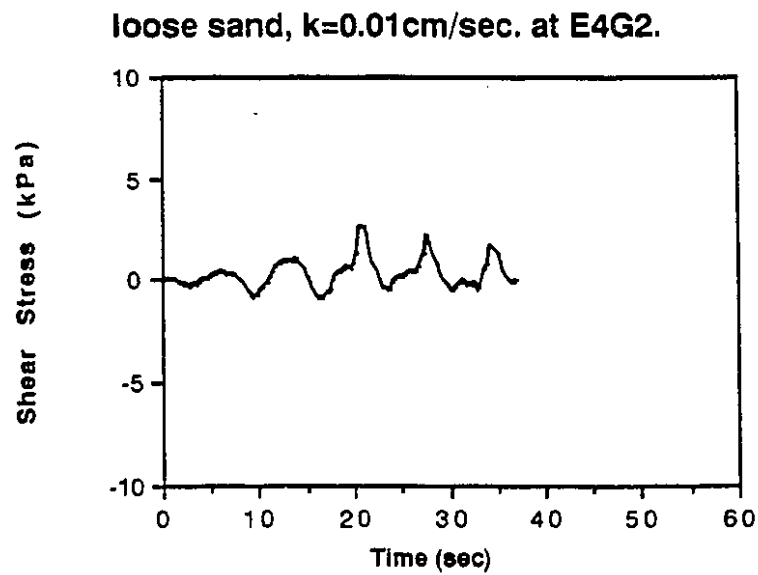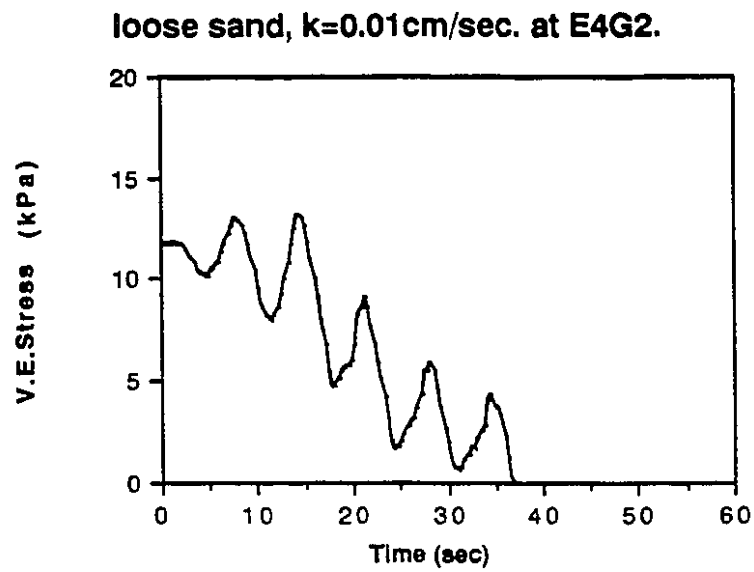
Figure 8.10   V.E.Stress and Shear Stress vs Time for Lake Ontario loose sand

146

M.E.Stress (kPa)

Loose sand, k=0.01 cm/sec. at E4G2.
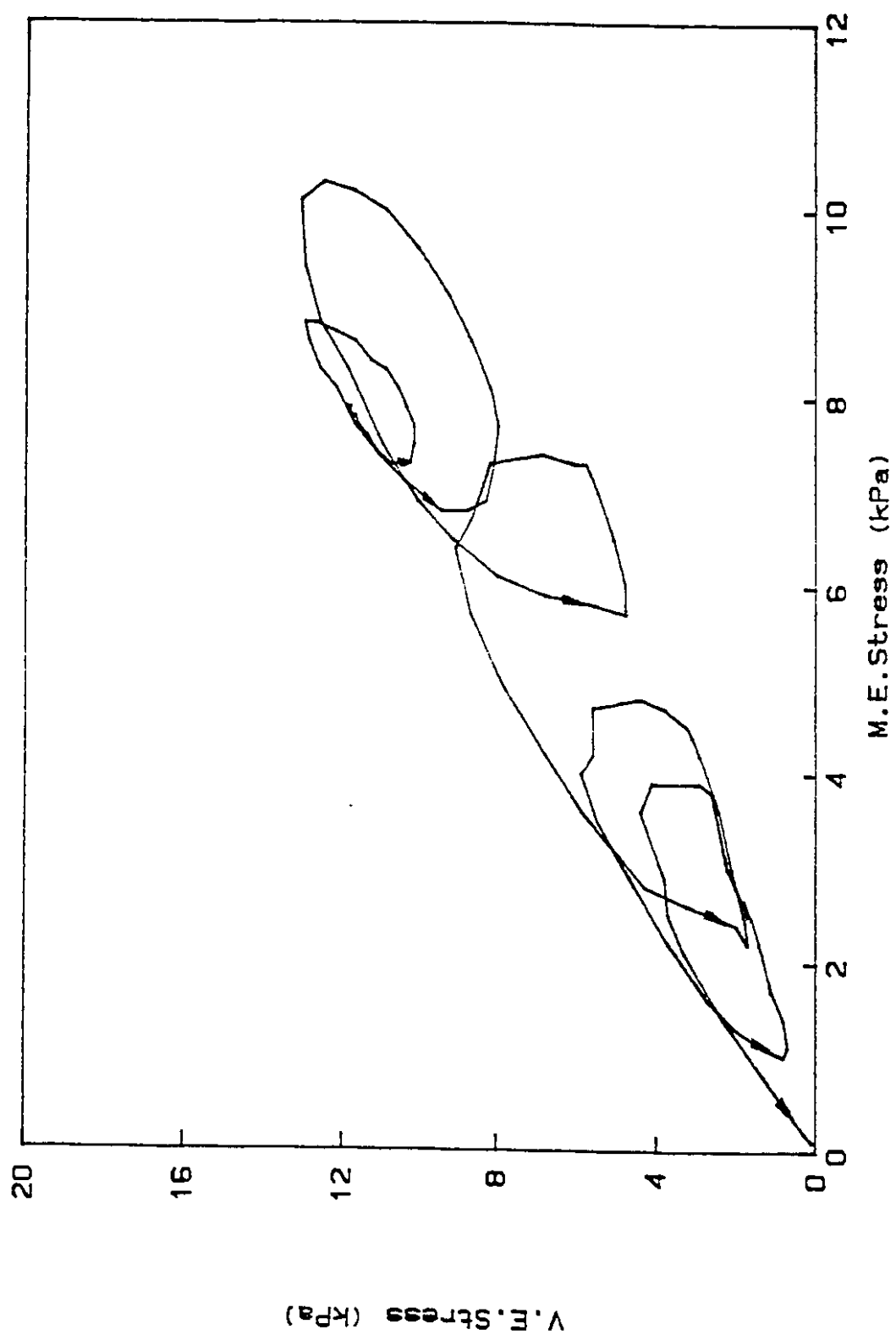
V.E.Stress (kPa)

Figure 8.11 V.E.Stress vs M.E.Stress for Lake Ontario loose sand

147
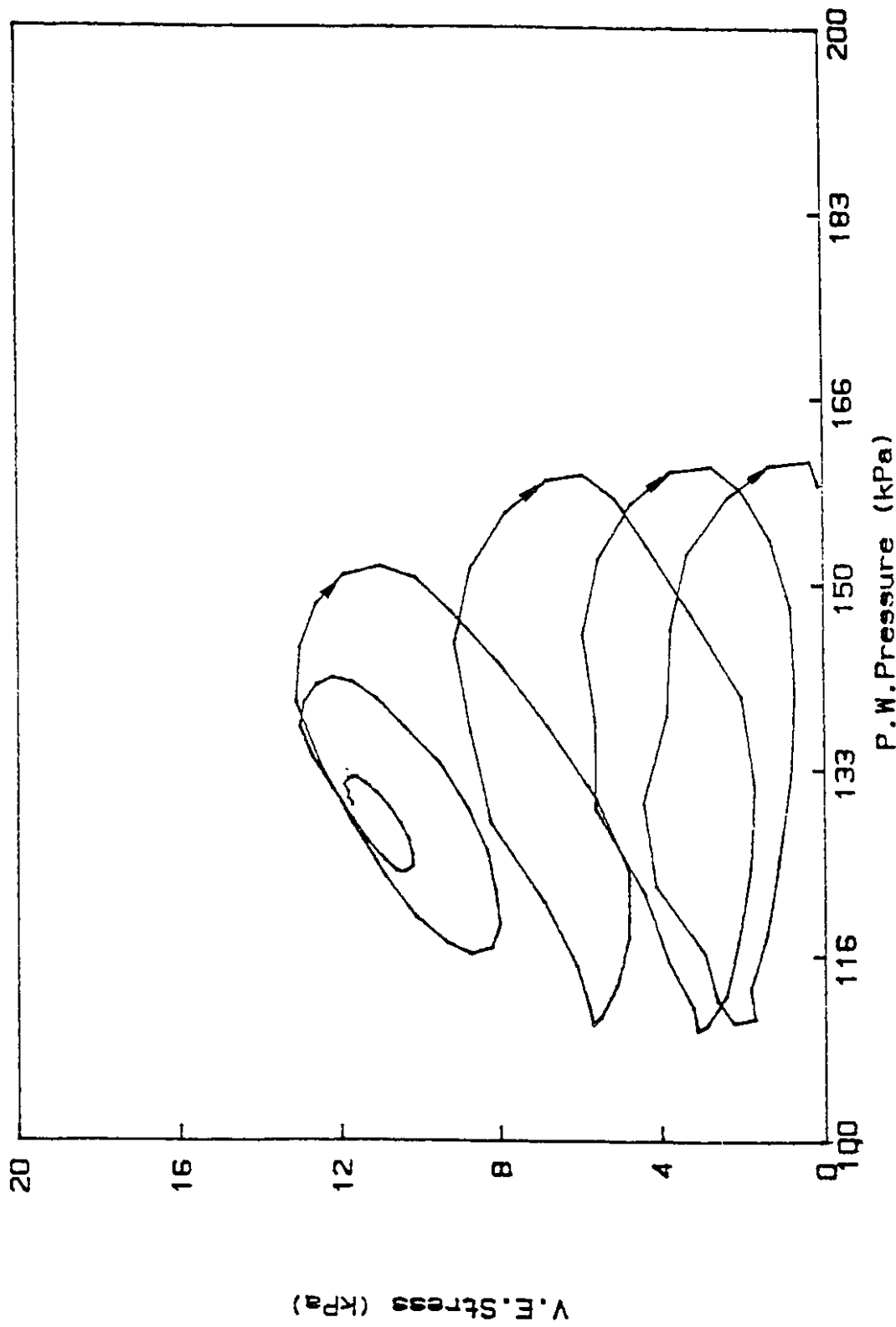
Figure 8.12 V.E.Stress vs P.W.Pressure for Lake Ontario loose sand

Loose sand, k=0.01 cm/sec. at E4G2.

P.W.Pressure (kPa)

V.E.Stress (kPa)

loose sand, k=0.01cm/sec. at Node 13.
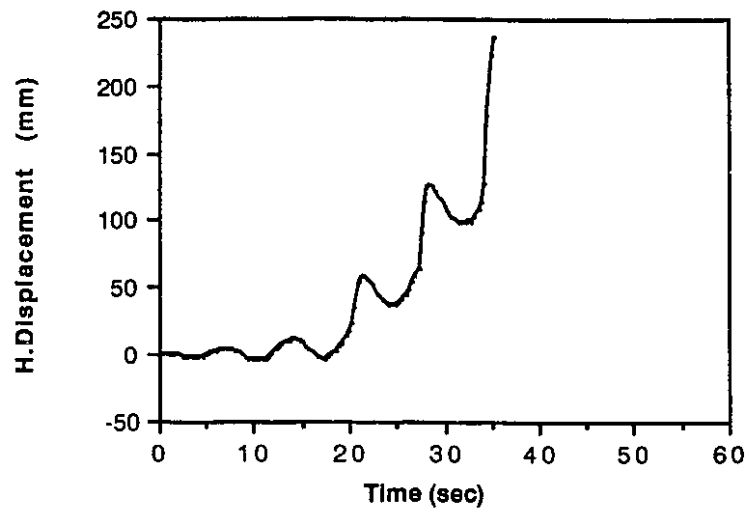
loose sand, k=0.01cm/sec. at Node 13.
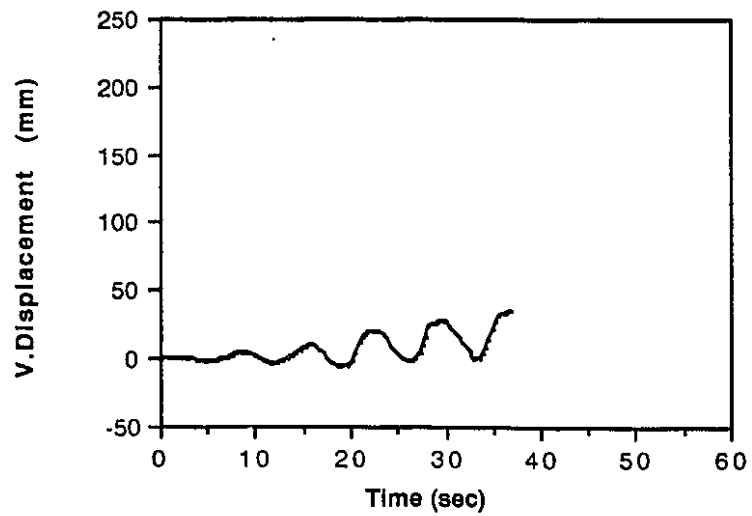
Figure 8.13 Displacement vs Time for Lake Ontario loose sand

149

loose sand, k=0.01cm/sec. at t=21sec.

Legend:
- x=18.25m.
- x=9.125m.
- x=0.0m.

Y-axis: H.Displacement (mm), X-axis: Depth (m)

loose sand, k=0.01cm/sec. at t=21sec.

Legend:
- x=18.25m.
- x=9.125m.
- x=0.0m.

Y-axis: V.Displacement (mm), X-axis: Depth (m)
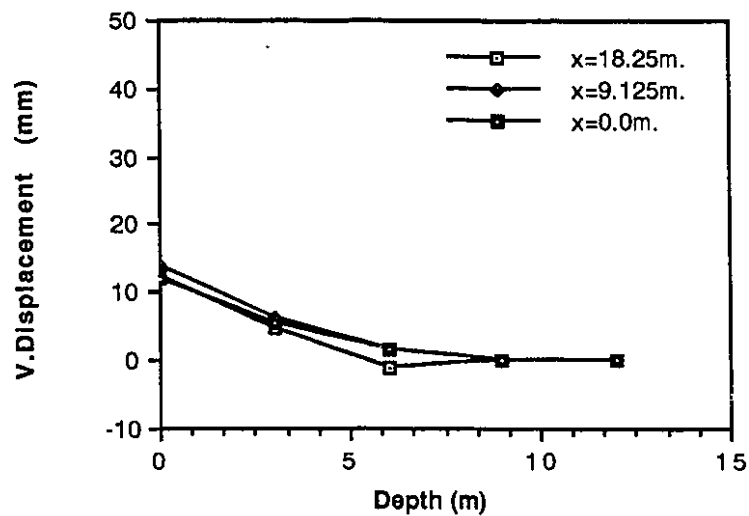
Figure 8.14 Displacement profiles at t=21sec for Lake Ontario loose sand

150

loose sand, k=0.01cm/sec. at t=28sec.

loose sand, k=0.01cm/sec. at t=28sec.
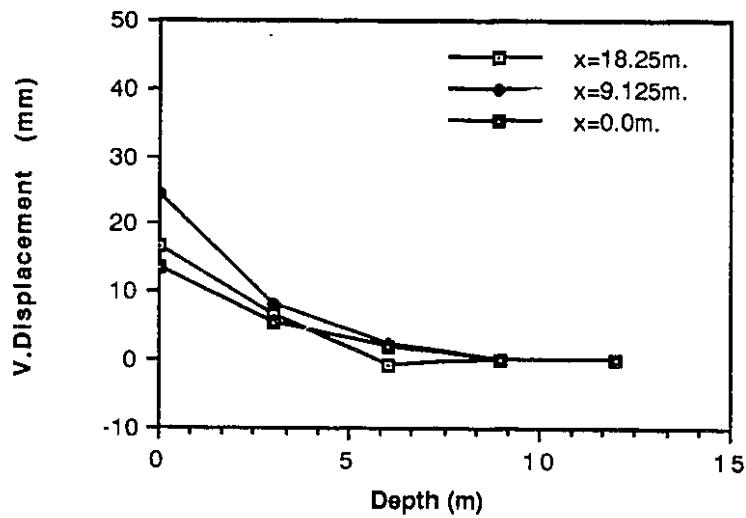
Figure 8.15   Displacement profiles at t=28sec for Lake Ontario loose sand

151

loose sand, k=0.01cm/sec. at t=35sec.

loose sand, k=0.01cm/sec. at t=35sec.
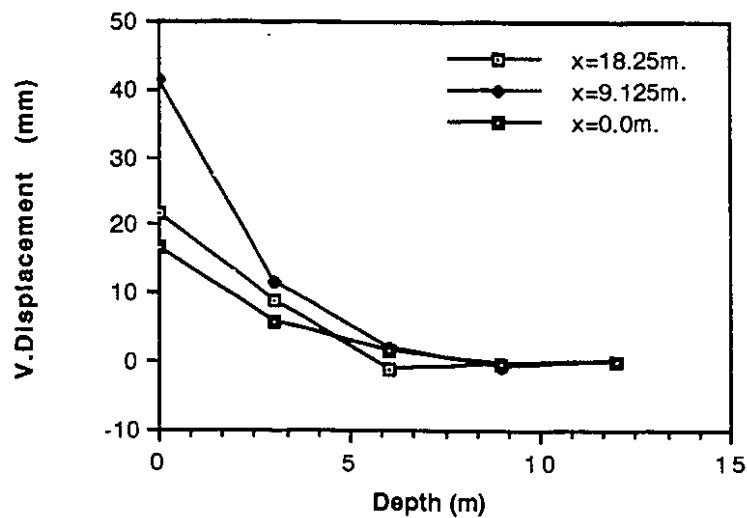
Figure 8.16 Displacement profiles at t=35sec for Lake Ontario loose sand

152

medium dense sand, k=0.001cm/sec. at E4G2.
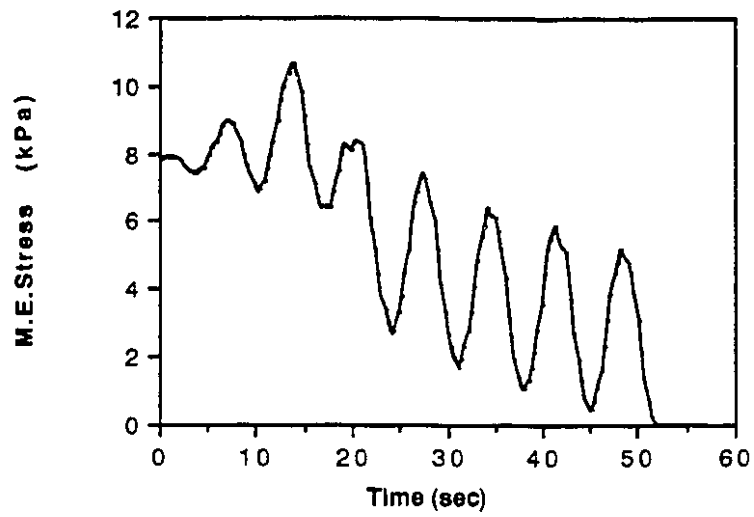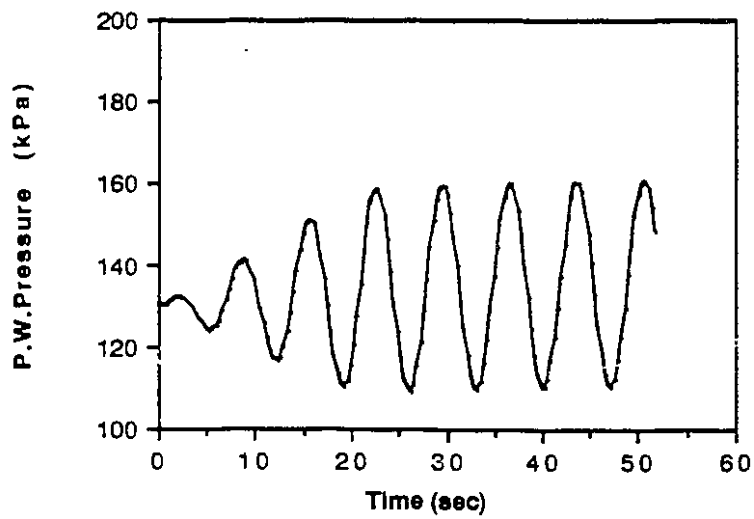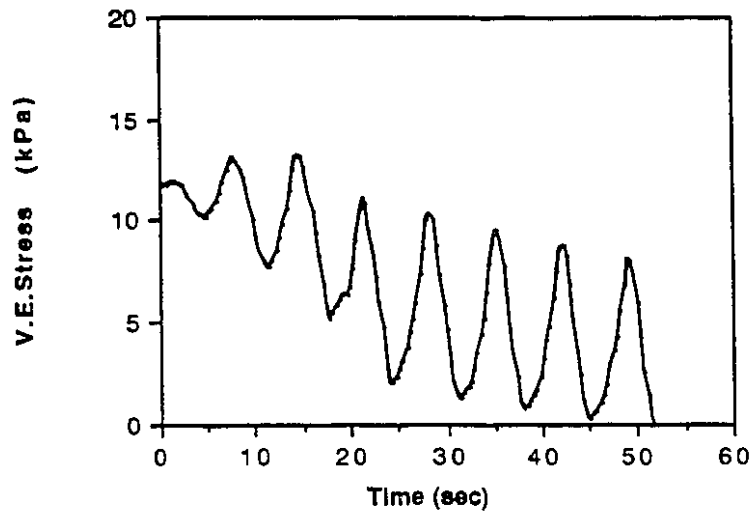

medium dense sand, k=0.001cm/sec. at E4G2.

Figure 8.17 M.E.Stress and P.W.Pressure vs Time for Lake Ontario medium dense sand

153

medium dense sand, k=0.001cm/sec. at E4G2.
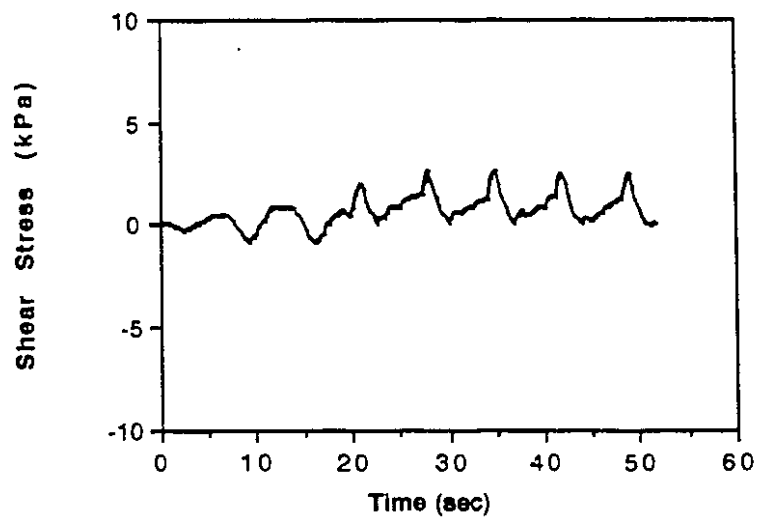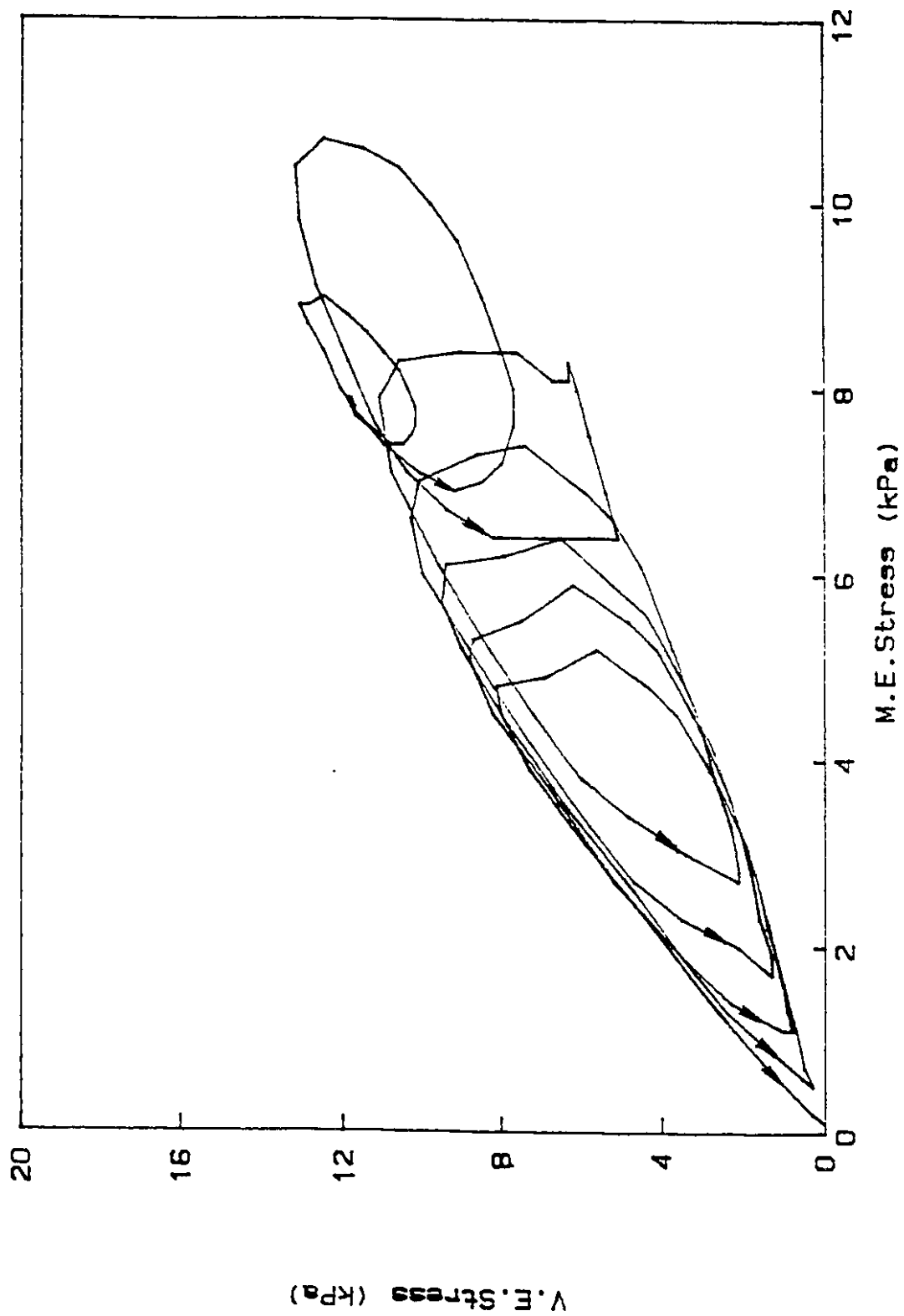

medium dense sand, k=0.001cm/sec. at E4G2.

Figure 8.18 V.E.Stress and Shear stress vs Time for Lake Ontario medium dense sand

154

M.E.Stress (kPa)

Medium dense sand, k=0.001 cm/sec. at E4G2.

Figure 8.19 V.E.Stress vs M.E.Stress for Lake Ontario medium dense sand

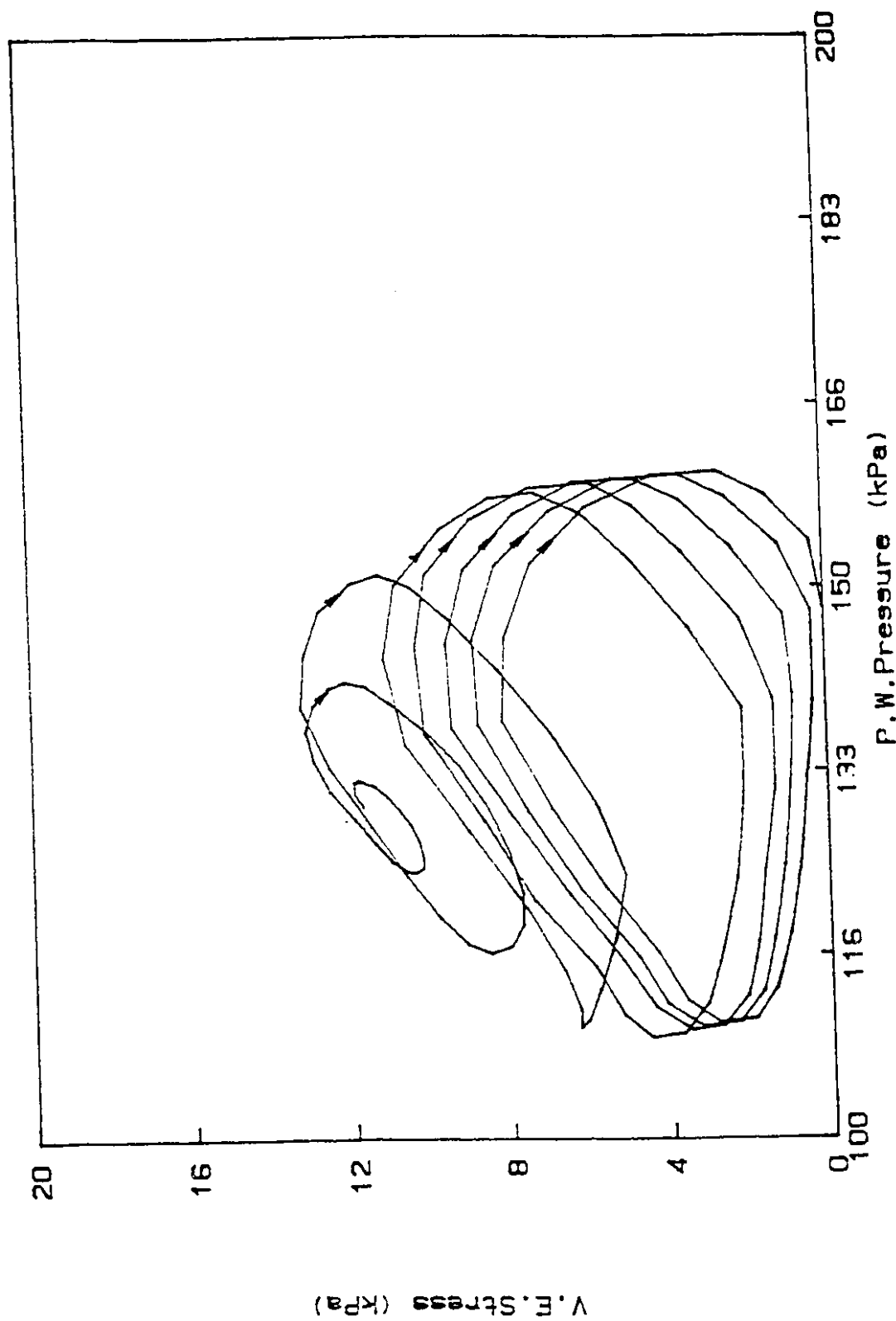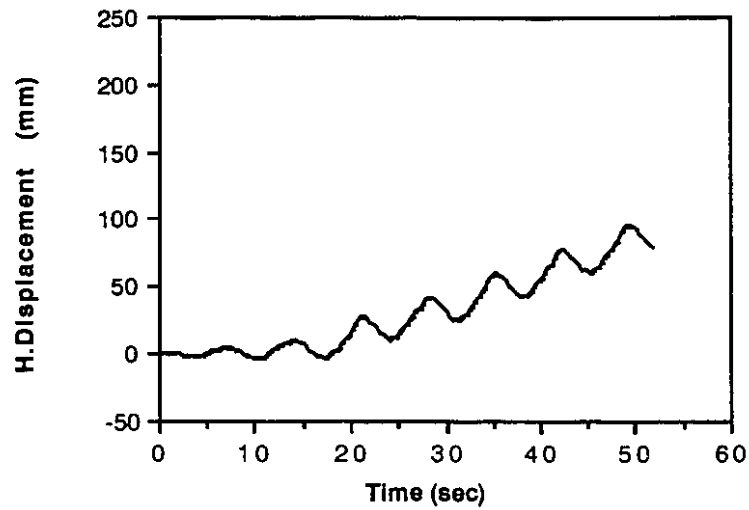V.E.Stress (kPa)

Medium dense sand, k=0.001 cm/sec. at E4G2.

Figure 8.20 V.E.Stress vs P.W.Pressure for Lake Ontario medium dense sand

medium dense sand, k=0.001cm/sec. at Node13.

medium dense sand, k=0.001cm/sec. at Node13.

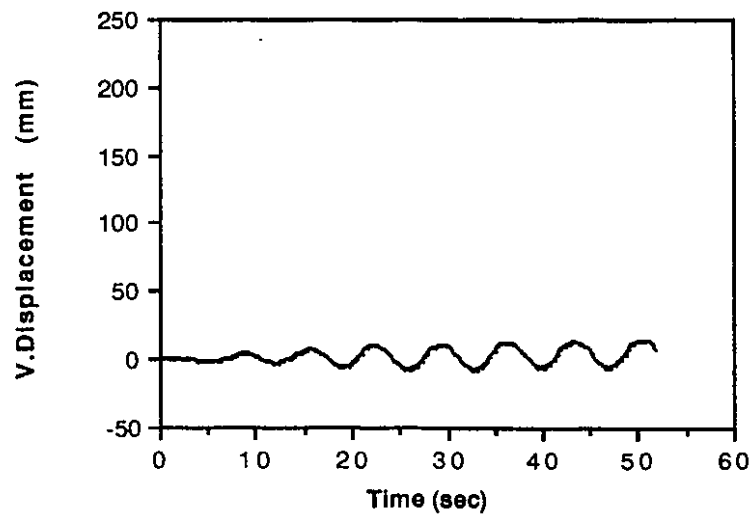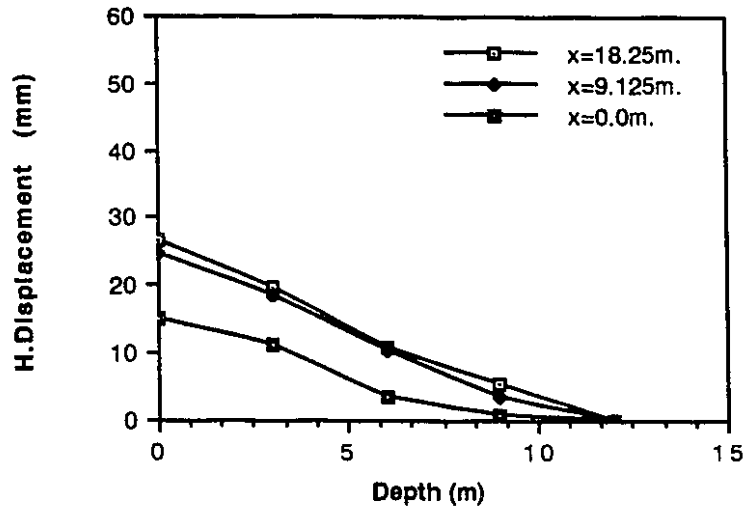Figure 8.21   Displacement vs Time   for Lake Ontario medium dense sand

157

medium dense sand, k=0.001cm/sec. at t=21sec.

medium dense sand, k=0.001cm/sec. at t=21sec.

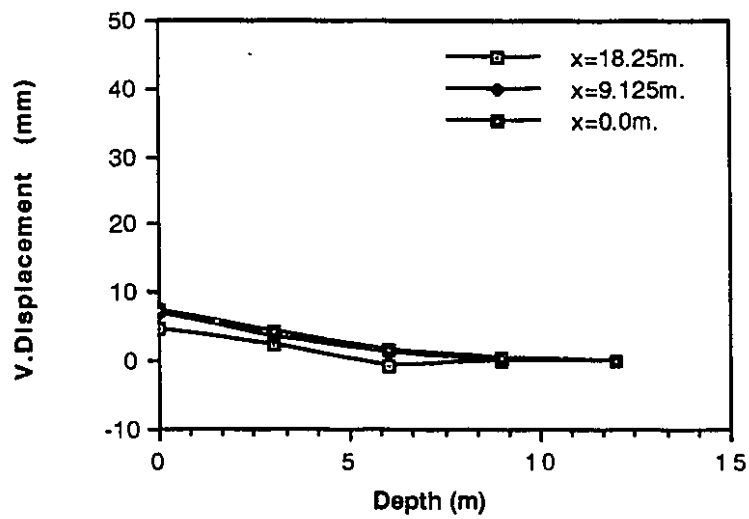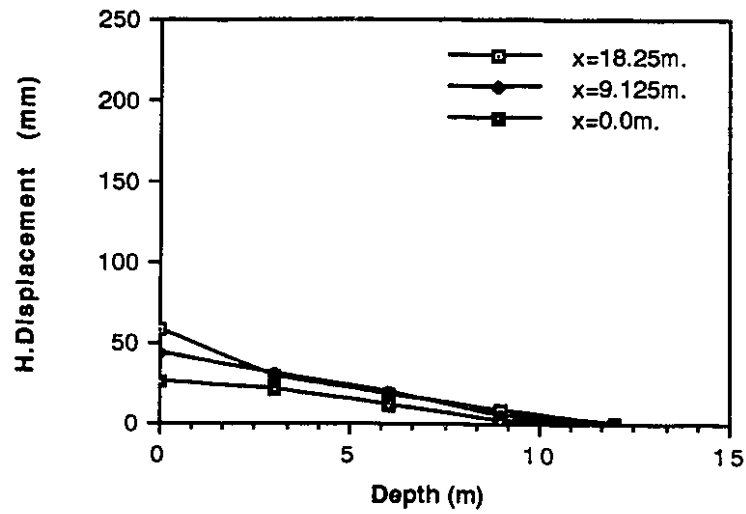

Figure 8.22 Displacement profiles at t=21sec for Lake Ontario medium dense sand

158

medium dense sand, k=0.001cm/sec. at t=35sec.

medium dense sand, k=0.001cm/sec. at t=35sec.

Figure 8.23 Displacement profiles at t=35sec for Lake Ontario medium dense sand

159

medium dense sand, k=0.001cm/sec. at t=49sec.

medium dense sand, k=0.001cm/sec. at t=49sec.
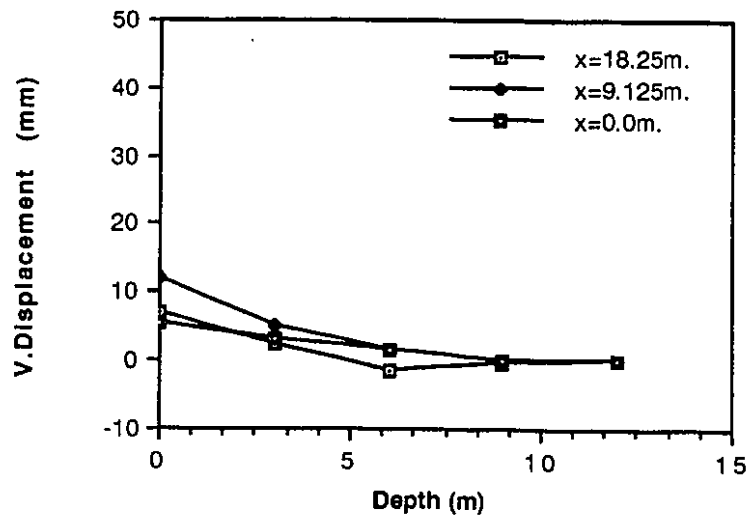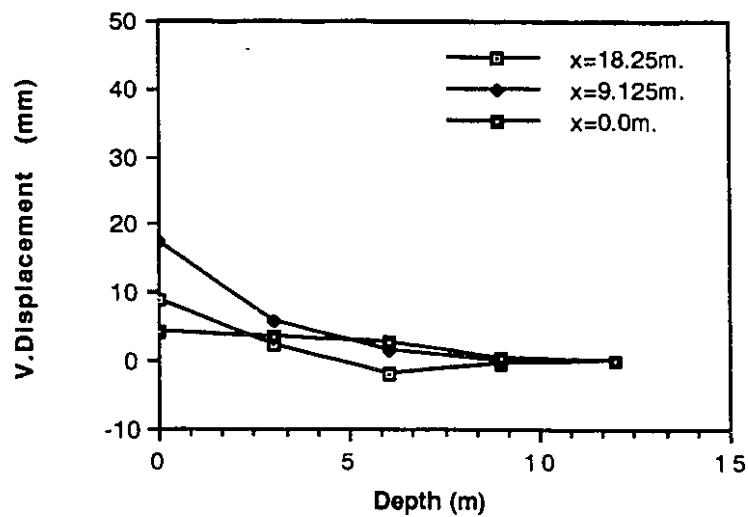

Figure 8.24 Displacement profiles at t=49sec for Lake Ontario medium dense sand

160

medium dense sand, k=0.001cm/sec. at t=63sec.

medium dense sand, k=0.001cm/sec. at t=63sec.
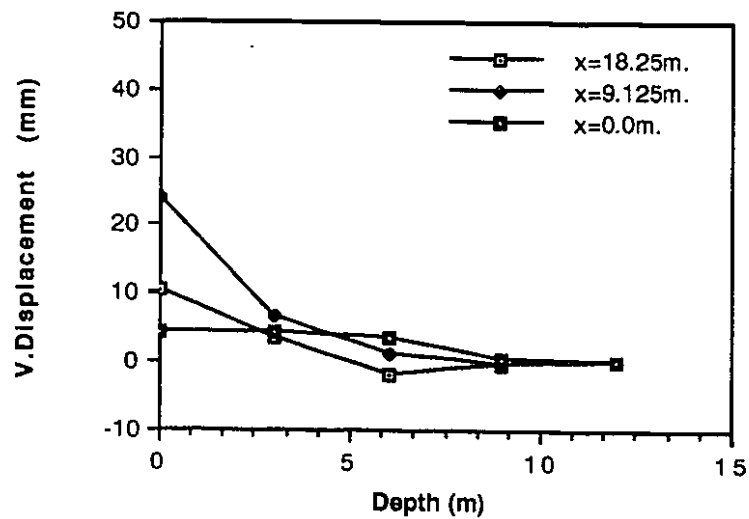
Figure 8.25 Displacement profiles at t=63sec for Lake Ontario medium dense sand

161

Figure 8.26   The finite element mesh for the North Sea case

162

North Sea, dens sand, k=0.01 cm/sec. at E14G2
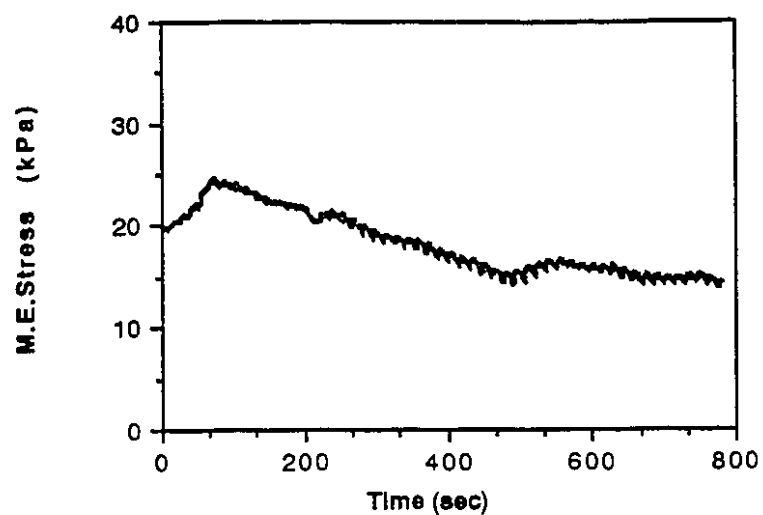
North Sea, dense sand, k=0.01 cm/sec. at E14G2
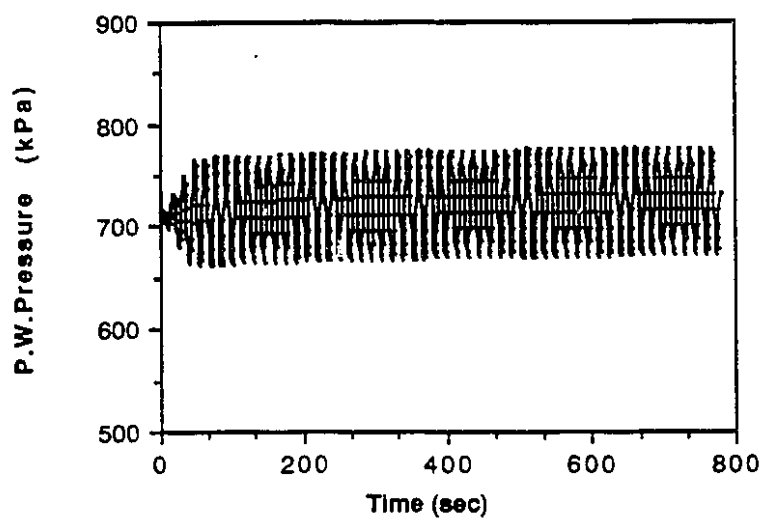
Figure 8.27   M.E.Stress and P.W.Pressure vs Time at E14G2 for the North Sea case

North Sea, dense sand, k=0.01cm/sec. at E16G4.
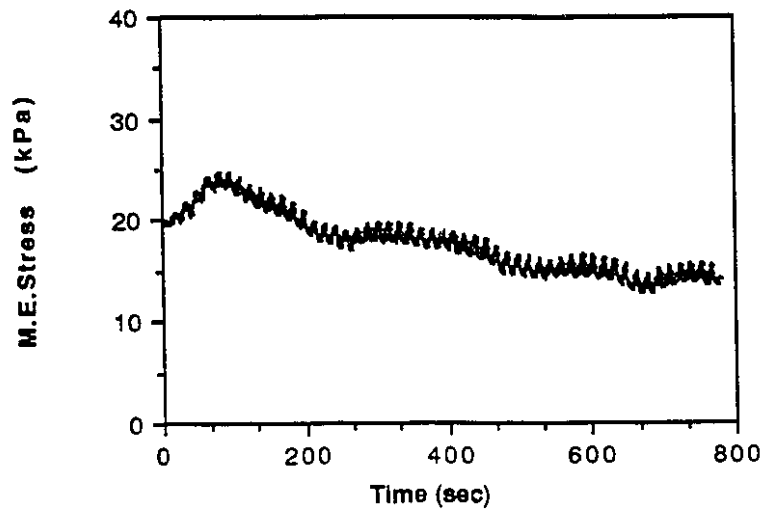
North Sea, dense sand, k=0.01 cm/sec. at E16G4.
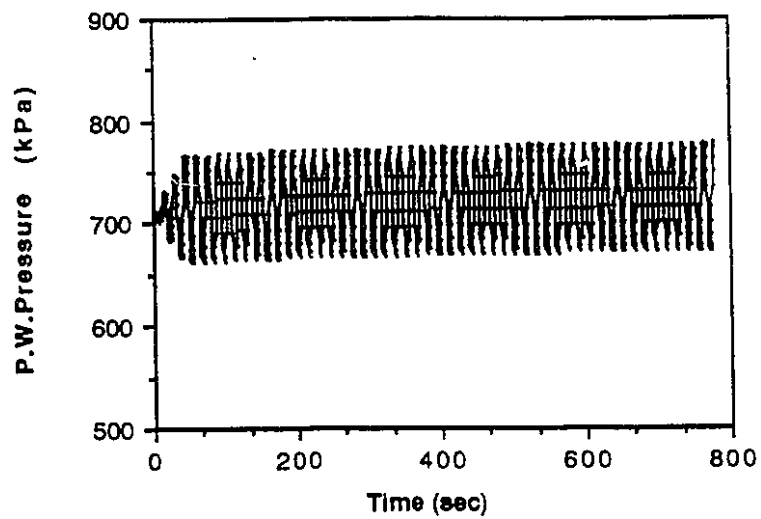
Figure 8.28 M.E.Stress and P.W.Pressure vs Time at E16G4 for the North Sea case

164

North Sea, dense sand, k=0.01 cm/sec. at E14G2.
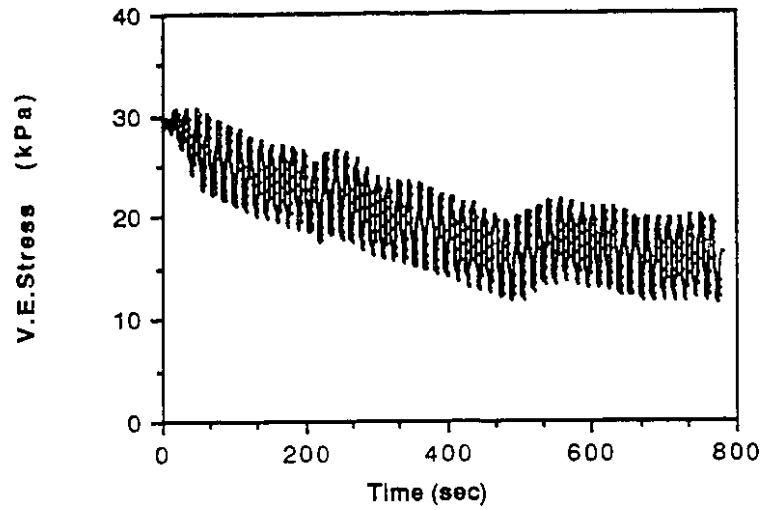
North Sea, dense sand, k=0.01 cm/sec. at E14 G2.
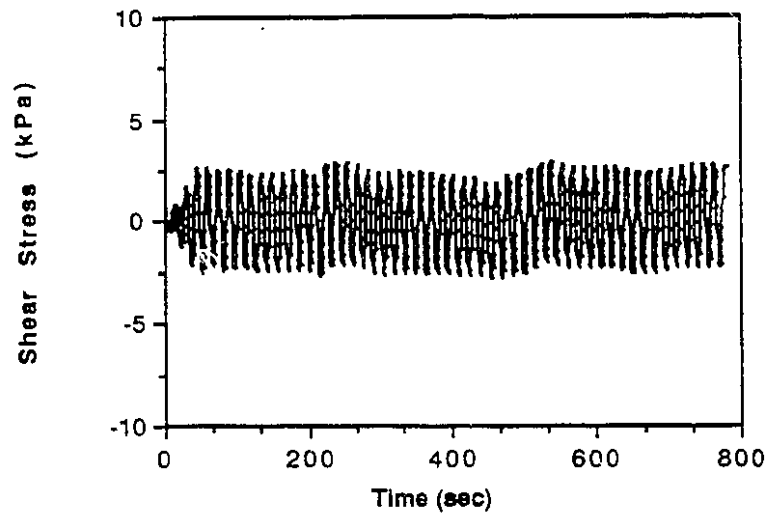
Figure 8.29   V.E.Stress and Shear Stress vs Time at E14G2 for the North Sea case

165

North Sea, dense sand, k=0.01 cm/sec. at E16G4.
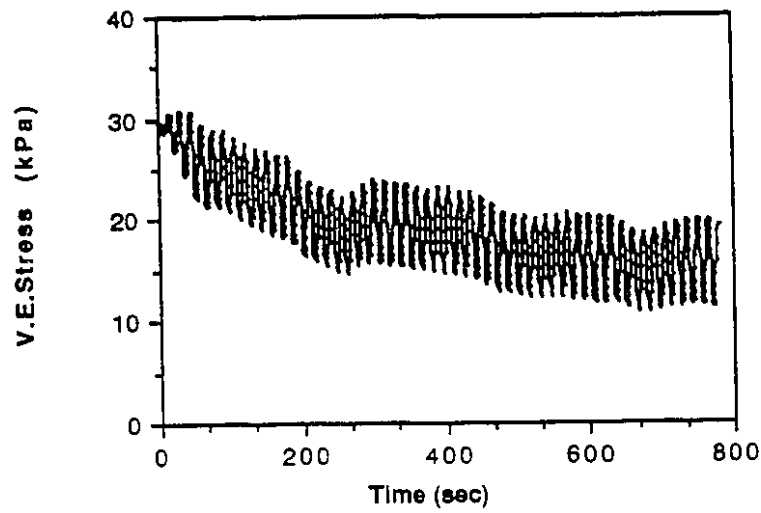
North Sea, dense sand, k=0.01 cm/sec. at E16G4.
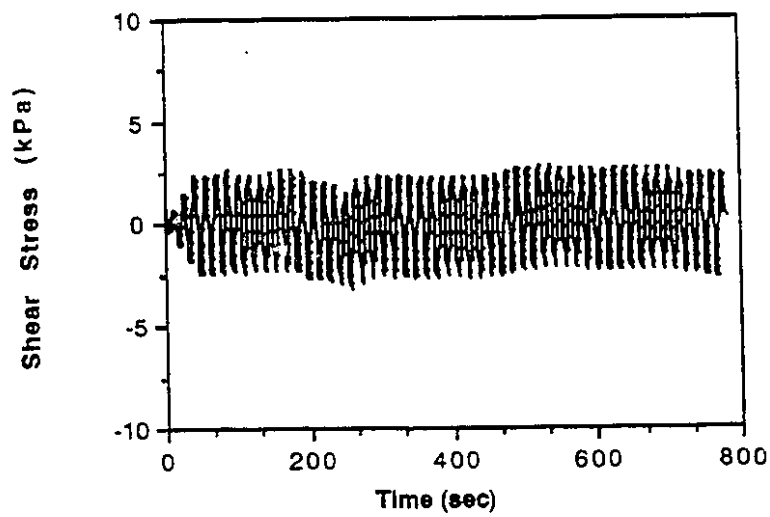
Figure 8.30   V.E.Stress and Shear Stress vs Time at E16G4 for the North Sea case

166
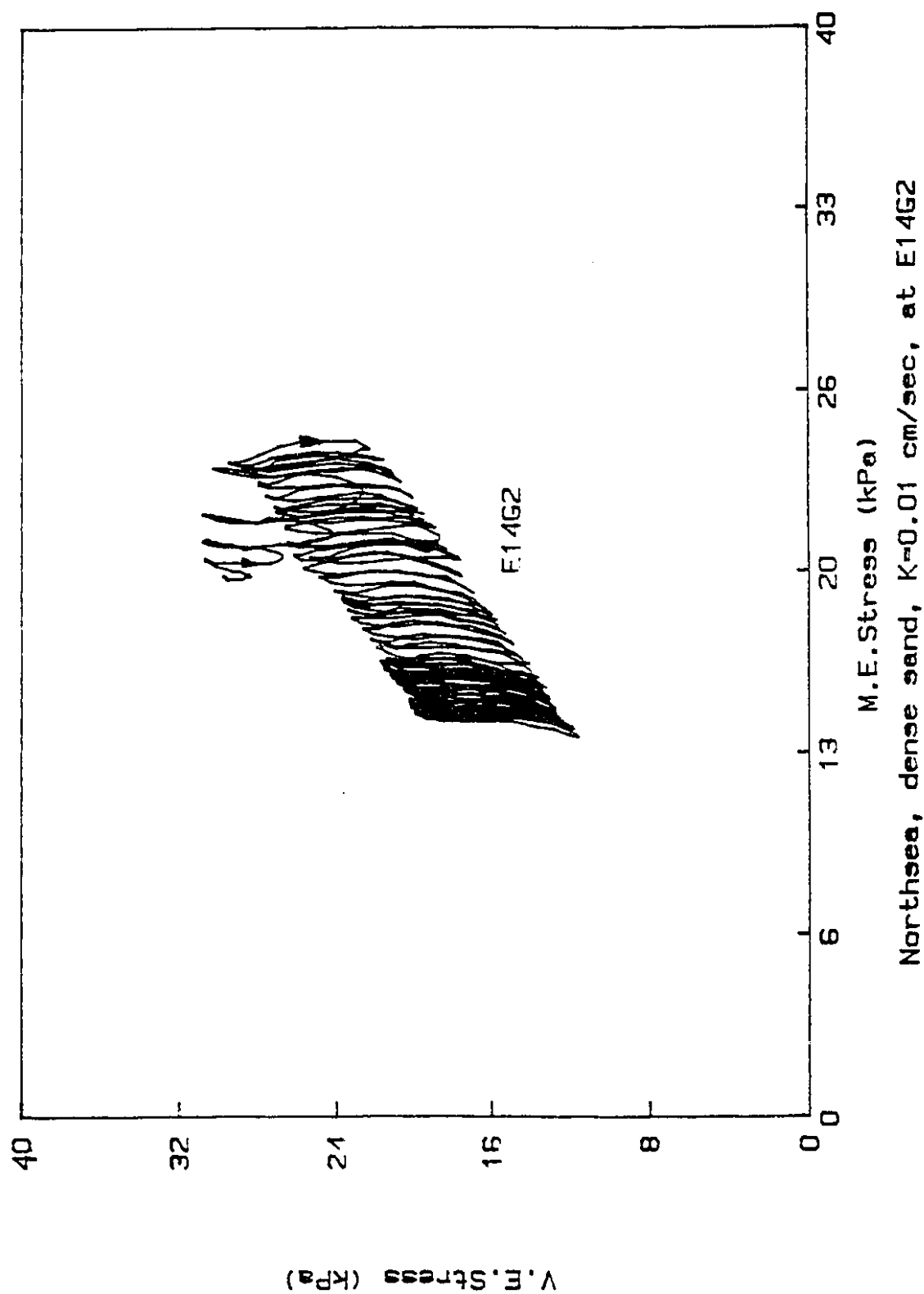
Figure 8.31   V.E.Stress vs M.E.Stress for the North Sea case

P.W.pressure (kPa)
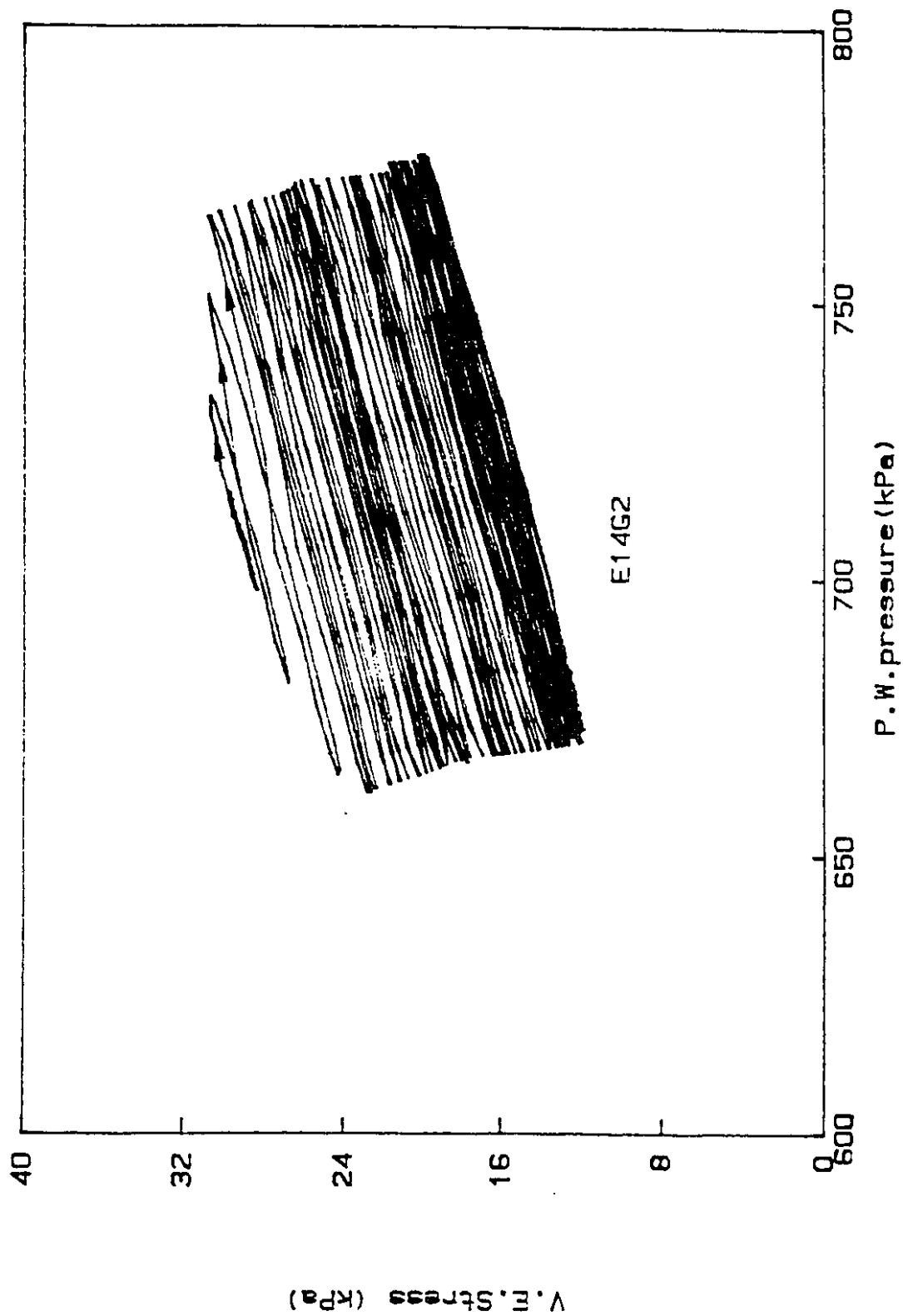
V.E.Stress (kPa)

E14G2

Northsea, dense sand, K=0.01 cm/sec, at E14G2

Figure 8.32   V.E.Stress vs P.W.Pressure for the North Sea case

North Sea , dense sand, k=0.01 cm/sec. at Node 53.
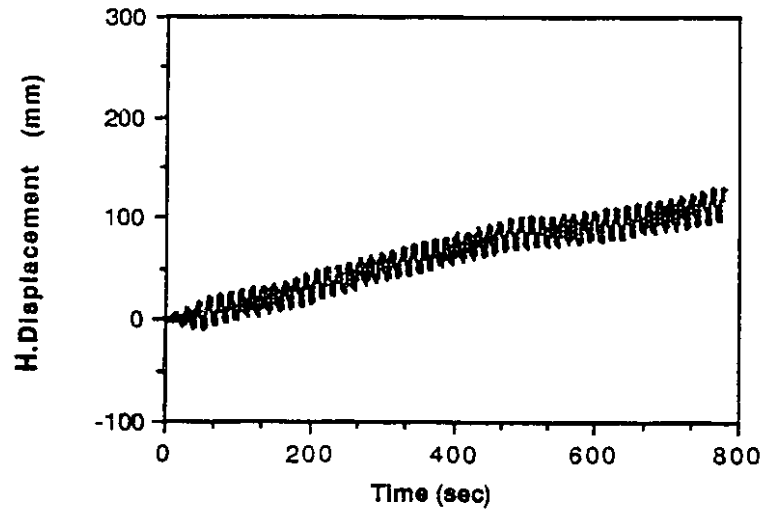
North Sea, dense sand, k=0.01cm/sec. at Node 53.
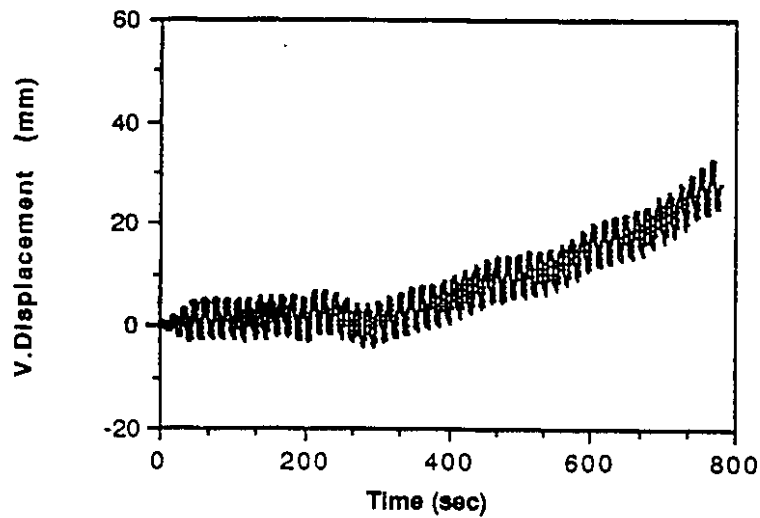
Figure 8.33   Displacement vs Time at Node 53 for the North Sea case

169

North Sea, dense sand, k=0.01 cm/sec. at Node 69.
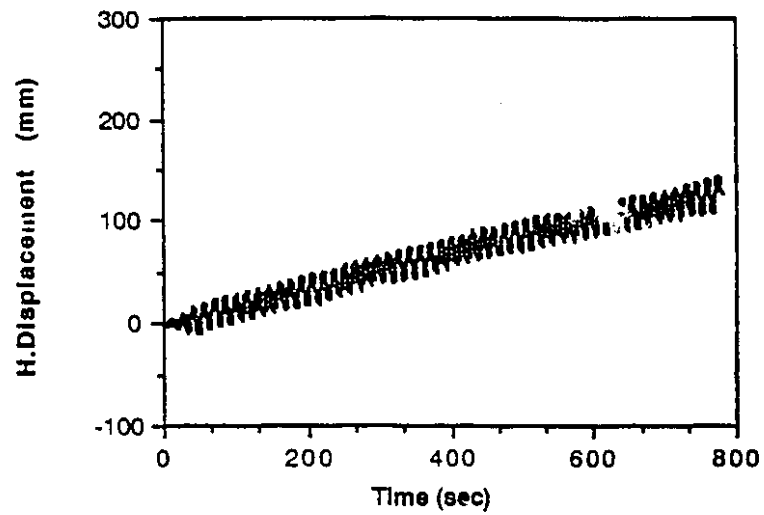
North Sea, dense sand, k=0.01 cm/sec. at Node 69
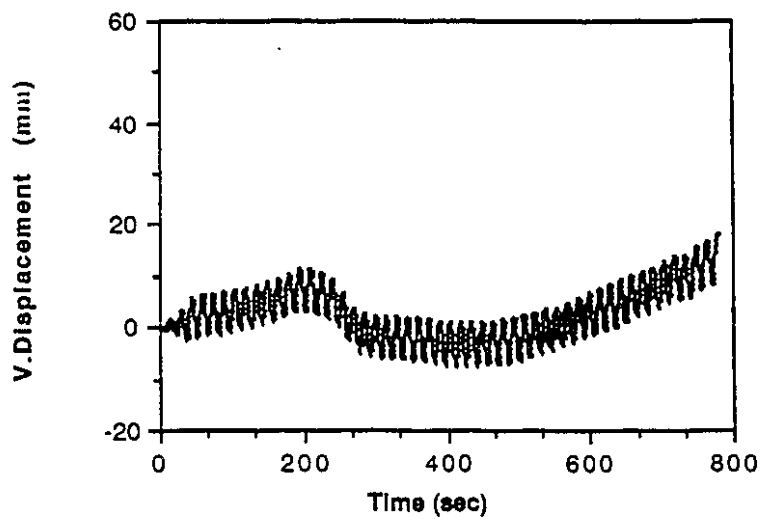
Figure 8.34   Displacement vs Time at Node 69 for the North Sea case

North Sea, dense sand, k=0.01 cm/sec. at t=300sec.
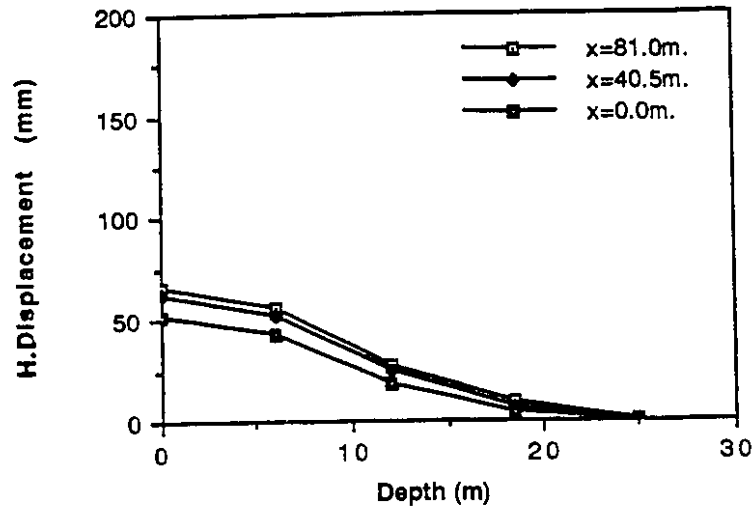
North Sea, dense sand, k=0.01 cm/sec. at t=300sec.
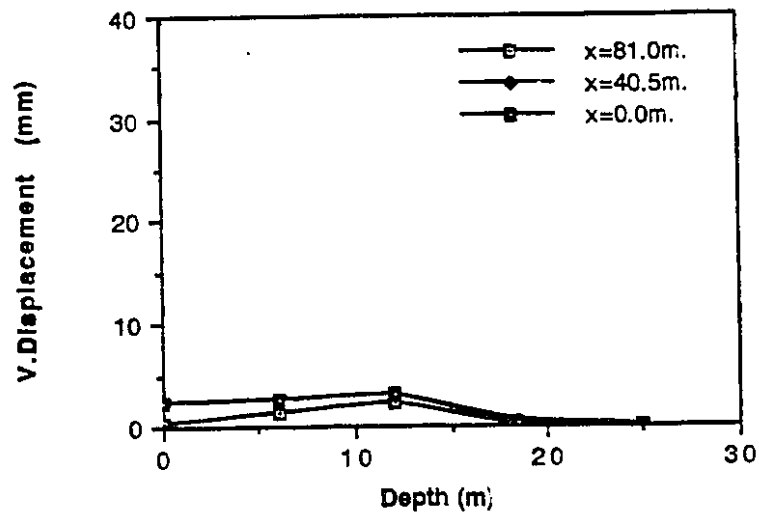
Figure 8.35   Displacement profiles at t=300sec for the North Sea case

North Sea, dense sand, k=0.01 cm/sec. at t=600sec.
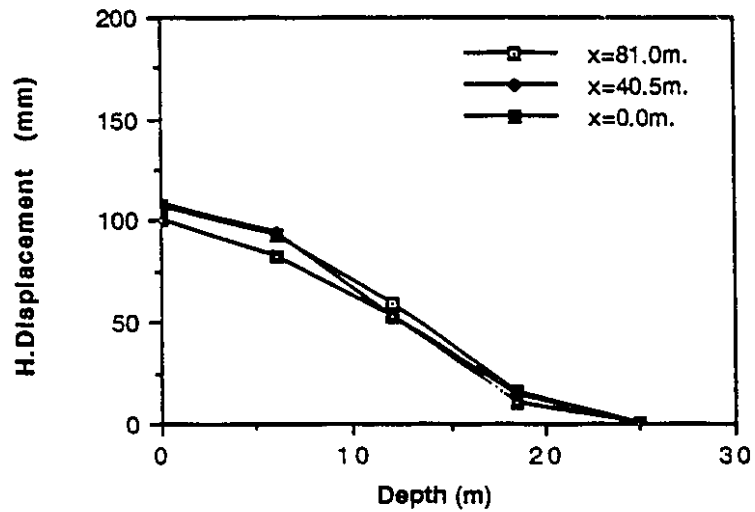
North Sea, dense sand, k=0.01 cm/sec. at t=600sec.
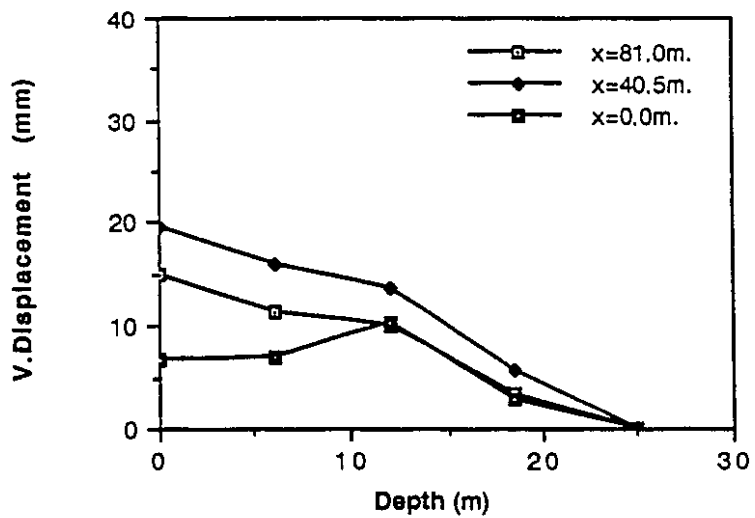
Figure 8.36 Displacement profiles at t=600sec for the North Sea case

172

North Sea, dense sand, k=0.01 cm/sec. at t=780sec.
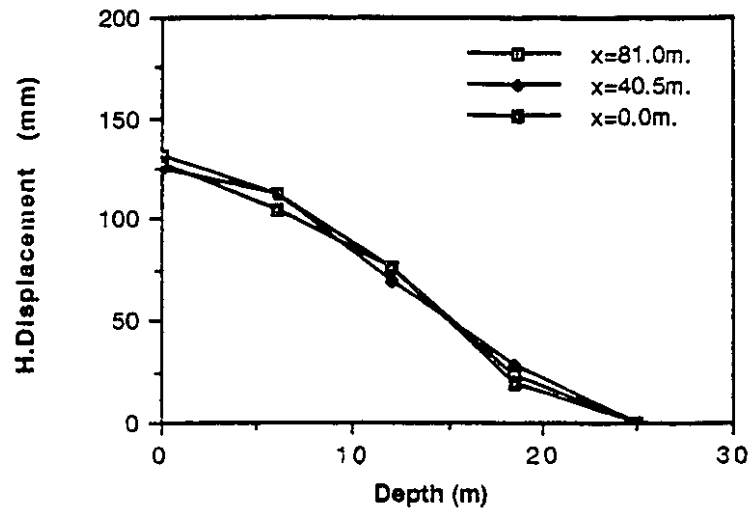
North Sea, dense sand, k=0.01 cm/sec. at t=780sec.
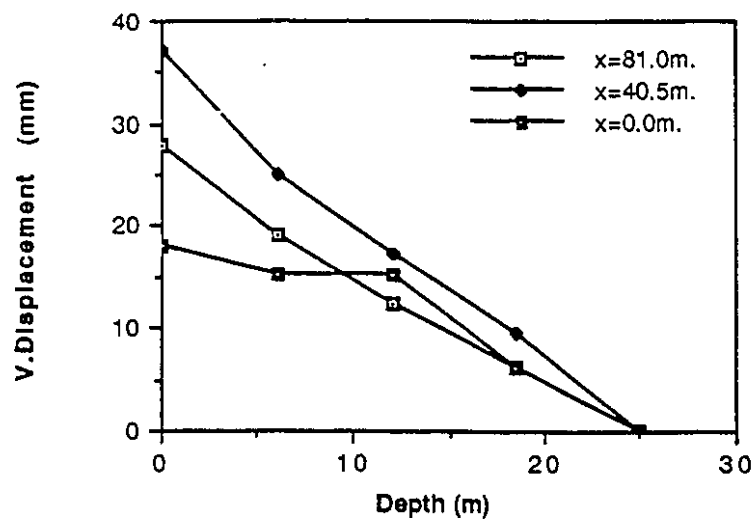
Figure 8.37 Displacement profiles at t=780sec for the North Sea case

173

9

CONCLUSION

9.1 CONCLUDING REMARKS

The ocean wave-induced response of seafloor deposits and liquefaction hazards have received considerable attention in geotechnical and marine engineering. Either safety or critical environmental considerations are involved in the design of pipelines, anchors and offshore structures such as gravity and pile supported platforms.

Until now most analyses of the ocean wave-induced response used very simple models. However, it is possible to develop a more rigorous analysis procedure as presented in this study.

The linear wave theory is introduced for the determination of the wave-induced pressure at the sea bottom (mud line). The seafloor deposit is assumed to be a saturated porous medium which is modelled as a two-phase system consisting of a solid and a fluid phase. The general Biot equations could be derived from the theory of mixture. For slow phenomenon of ocean wave loading, it is reduced to nonlinear transient consolidation equations to serve for analysis of the ocean wave-induced response.

The proposed material constitutive model, based on the generalized plasticity-bounding surface formulation, simplifies the numerical implementation to a very great extent. The non-associated flow rule is adopted. Realistic model parameters from

174

experiments are incorporated in the model. Some comparisons of the numerical model tests with experimental results have been made and the result . . . re considered satisfactory. The simple model is capable of simulating both loose sand and dense sand behavior under monotonic and cyclic loading, drained and undrained conditions.

Time integration of the resulting semi-discrete finite element equations is performed by the Crank-Nicolson method which is unconditionally stable. Incremental iteration of the Modified Newton-Raphson procedure is used to solve the nonlinear system. The numerical procedure adopted is proved to be adequate for solving this coupled nonlinear transient problem of wave-induced response analysis.

A fictitious freedom technique is proposed to treat the different nodal degrees of freedom due to the composition of coupled fields. It has been demonstrated to be quite effective.

Based on Iron's symmetric frontal solver, a non-symmetric frontal solver subroutine is developed in this study to accommodate the asymmetry due to the non-associated plastic flow rule adopted in the material model. It could be used to solve any non-symmetric linear system of equations.

A simple artificial boundary is suggested in this study to deal with the unbounded domain problems. This artificial boundary can be applied to linear or non-linear analysis. It has been used for travelling wave-induced response analysis with success.

An important conclusion obtained from the standing wave induced response analysis is the influence of the coefficient of permeability on the susceptibility of the sand mass to liquefy — for high values of permeability even a loose sand mass need not liquefy. This is in direct contrast to the commonly held view that the liquefaction potential is a function only of the sand density.

Two example cases are studied in detail. The first example examines the seabed response to a wave train at a pipeline site in Lake Ontario (Christian et al., 1974; Nataraja

175

and Gill, 1983), where the deposit was measured to be loose and medium dense. The second example investigates the seafloor behavior under a storm wave at the Ekofisk tank site in the North Sea (Lee and Focht, 1975; Nataraja and Gill, 1983). Here the deposit was reported to be dense. The numerical analyses predict the susceptibility of the two sites to liquefaction which reflects the real situations. It helps build confidence in the numerical procedure adopted in this study and lends it credibility.

Hopefully, with more widespread use of this numerical procedure and additional verification against case histories, as well as extensive experiments and field investigations, this numerical analysis procedure can become 'routine' and made widely available.

It should be noted that the preceding solutions are the free field solutions and must be applied with caution in the vicinity of structures. Since inclusion of the structures in the analysis would make the problem much more complicated, the assessment of a free-field solution is a good first approximation.

Ocean wave-induced response analysis of seafloor deposits and liquefaction susceptibility investigation have necessarily involved many simplifying assumptions. Even so it may still be expensive and time-consuming due to its intrinsic complexity. Hence, good engineering judgement should be exercised.

9.2   FURTHER WORK

1. In the proposed simple model, the relative density or void ratio of the sand does not explicitly appear as a material parameter. It may directly enter the model formulation, say, as one of the state variables to further improve the model performance.

176

2. To extend the application range to clays, the cohesion would have to be added into the model in an appropriate way. Creep type of behavior could also be incorporated by having some viscous terms in the model formulation.

3. For more efficiency and flexibility, the skyline storage technique, the implicit-explicit time integration algorithm and the Quasi-Newton nonlinear iterative procedure could be implemented into the finite element analysis program as options for the user.

4. A seafloor deposit with a sloping surface is another example ready to be analyzed. The finite element computer program may be easily modified to account for a nonhomogeneous seabed situation.

5. The analysis capabilities could be further enhanced by carrying out further research on field equations and algorithmic strategies to allow the calculations to be pursued further after localized liquefaction and possibly up to total liquefaction of the soil deposit.

6. A fully structure-fluid-foundation interaction problem may be formulated. The analysis will be much more expensive and time-consuming. Hence, only very important projects might require such a sophisticated analysis.

REFERENCES

1. Arnold, P. (1973). Finite element analysis - a basis for sea-floor soil movement design criteria, Proceedings, Fifth Annual Offshore Technology Conference, Houston, Tex., Vol.2. Paper No. OCT 1900, pp. 743-752.

2. Atkinson, J. H. and Bransby, P.L. (1978). The Mechanics of Soils – An Introduction to Critical State Soil Mechanics, McGraw-Hill, Maidenhead, 375pp.

3. Bathe, K. J., (1982). Finite Element Procedures in Engineering Analysis, Prentice-Hall, Englewood Cliffs, New Jersey.

4. Bayliss, A., Gunzberger, M. and Turkel, E. (1978). Boundary Conditions for the Numerical Solution of Elliptic Equations in Exterior Regions, ICASE Report No.80-1, NASA, Langley.

5. Beer, G. and Meek, J. L. (1981). Infinite Domain Elements, Int. J. Num. Meth. Engng. Vol. 17. No. 1

6. Besseling, J. F. (1958). A theory of elastic, plastic and creep deformation of an initially isotropic material showing strain hardening, creep recovery and secondary creep, J. Appl. Mech. Vol. 25, Transaction, ASME, Vol. 80, pp. 529.

7. Besseling, J. F. (1963). The complete analogy between the matrix equations and the continuous field equations of structural analysis, International Symposium on Analogue and Digital Techniques Applied to Aeronautics, Liege, Belgium.

8. Bettess, P. (1977). Infinite Elements, Int. J.Num. Meth. Engng. Vol. 11, pp. 53-64.

9.   Bettess, P. and Zienkiewicz, O.C. (1977). Diffraction and refraction of surface waves using finite and infinite elements, Int. J. Num. Meth. Engng. Vol. 11, pp. 1271-1290.

10.   Biot, M. A. (1941). General theory of three-dimensional consolidation, Journal of Applied Physics, Vol. 12, pp. 155-164.

11.   Biot, M. A. (1955). Theory of elasticity and consolidation for a porous anisotropic solid, Journal of Applied Physics, Vol. 26, pp. 182-185.

12.   Biot, M. A. (1956). Theory of propagation of elastic waves in a fluid-saturated porous solid, Part I: Low frequency range and Part II: Higher frequency range, J. Acoust. Soc. of America, Vol. 28, pp. 168-191.

13.   Biot, M. A. (1962). Mechanics of deformation and acoustic propagation in porous media, Journal of Applied Physics, Vol. 33, pp. 1483-1498.

14.   Biot, M. A. (1963). Theory of stability and consolidation of a porous medium under initial stress, J. Math. and Mech., Vol. 12, pp. 521-541.

15.   Bishop, A. W. (1966). The strength of soils as engineering materials, Geotechnique, Vol. 16, pp. 91-130.

16.   Booker, J. R. and Davis, E. H. (1972). A note of a plasticity solution to the stability of slopes in homogeneous clay, Geotechnique, Vol. 22, pp. 509-513.

17.   Booker, J. R. and Small, J. C., (1975). An investigation of the stability of numerical solutions of Biot's equations of consolidation, Int. J. Solids Structures, Vol. 11, pp. 907-917 .

18.   Booker, J.R. And Small, J.C. (1977). Finite element analysis of primary and secondary consolidation, Int. J. Solids Struct, Vol.13 No.2, pp. 137-149.

19.   Bowen, R. M. (1976). Theory of Mixtures in Continuum Physics, Vol. III, ed. by A. C. Eringen, Academic Press, pp. 1-127.

20. Bowen, R. M. (1982) Compressible porous media by use of a theory of mixtures, Int. J. Eng. Sci. Vol. 20, No. 6, pp. 697-735.

21. Castro, G. (1969). Liquefaction of Sand, Thesis presented to Havard University, at Cambridge, Mass., in partial fulfillment of the requirements for the degree of Doctor of Philosophy.

22.. Castro, G. (1975). Liquefaction and cyclic mobility of saturated sands, Journal of the Geotechnical Engineering Division, ASCE, Vol. 101, No. GT6, pp. 551-569.

23. Castro, G. and Poulos, S. J. (1977). Factors affecting liquefaction and cyclic mobility, Journal of the Geotechnical Engineering Division, ASCE, Vol. 103, No. GT6, pp. 501-516.

24. Castro, G., Poulos, S. J. and France, J.W. (1982). Liquefaction induced by cyclic loading, Report by Geotechnical Engineers, Inc., to the National Science Foundation, Washington, D.C., pp. 1-80.

25. Chen, W. F. (1975). Limit Analysis and Soil Plasticity, Elsevier, Amsterdam, 638 pp.

26. Chen, W. F. and Saleeb, A. F. (1986), Constitutive Equations for Engineering Materials, Vol. 2 Plasticity and Modeling, Wiley-Interscience, New York, N.Y.

27. Chow, Y. K. (1981). Dynamic Behaviour of Piles, Ph.D. Thesis, University of Manchester.

28. Chow, Y. K. and I. M. Smith (1981). Static and periodic infinite solid elements, Int. J. Num. Meth. Engng. Vol. 17, No.4.

29. Christian, J. T., Taylor, P. K., Yen, J. K. C. and David, R. E., (1974) Large Diameter Underwater Pipeline for Nuclear Power Plant Designed Against Soil Liquefaction, Proceedings, Sixth Annual Offshore Technology Conference, Houston, Taxas, Paper No. OTC 2094, May, 1974, pp. 597-606.

30. Clayeon, R. and Enquist, B. (1977). Absorbing Boundary conditions for acoustic and elastic wave equations, Bull. Seism. Soc. Am., 67(6), pp. 1529-1540.

31. Clough, R.W. (1960). The finite element method in plane stress analysis, Proceedings of 2nd ASCE conference on Electronic Computation, Pittsburgh.

32. Courant, R. (1943). Variational Methods for the solution of problems of equilibrium and vibrations, Bull. Am. Math. Soc., Vol. 49.

33. Crisfield, M. A. (1987). Consistent schemes for plasticity computation with the Newton-Raphson method, in Computational Plasticity; Models, Software and Application, edited by D. R. J . Owen, E. Hinton and E. Onate, Proceeding of the international Conference, Spain, pp. 133-159.

34. Cundall, P. A., Kunar, R. R., Carpenter, P. C. and Marti, J. (1978). Solution of infinite dynamic problems by finite modelling in the time domain, Conference on Applied Numerical Modelling, Madrid.

35. Dafalias, Y. F. and Popov, E. P., (1975). A model of nonlinearly hardening materials for complev loading, Acta Michanica, Vol. 21, pp. 173-192.

36. Dafalias, Y. F. and Popov, E. P. (1976). Plastic internal variables formalism of cyclic plasticity, Journal of Applied Mechanics, Vol. 98, pp. 645-685.

37. Dafalias, Y. F. and Herrmann, L. R. (1982). Bounding surface formulation of soil plasticity, International Symposium on Soils Under Cyclic and Transient Loading, eds., G. N. Pande and O.C. Zienkiewicz, John Wiley and Sons, Inc., London, U.K., pp. 253-282.

38. Darcy, H. (1856). Les Fontaines Publiques de la ville de Dijon, V. Dalmont, Paris.

39. Desai, C. S. and Gallagher, R. H., Editors (1984). Mechanics of Engineering Materials. Wiley.

181

40. Desai, C. S. and Siriwardane, H. J. (1984). Constitutive Laws for Engineering Materials With Emphasis on Geologic Materials, Prentice-Hall, New York, N.Y.

41. Desai, C. S., Krempl, E., Kiousis, P.D. and Kundu, T., Editors (1987). Proceedings of the second International Conference on Constitutive Laws for Engineering Materials: Theory and Applications, University of Arizona, Tucson, Arizona, Elsevier.

42. DiMaggio, F. L. and Sandler, I. S. (1971). Material Model for Granular Soils, J. Eng. Mech. Div., ASCE, 97 (EM3), pp. 935-950.

43. Drucker, D. C. (1951). A more fundamental approach to plastic stress-strain relations, Proc. First U.S. Natl. Congr. Appl. Mech. ASME., pp. 487-491.

44. Drucker, D.C. and Prager, W. (1952). Soil mechanics and plastic analysis or limit design, Quarterly Journal of Applied Mathematics, Vol. 10, pp. 157-165.

45. Drucker, D. C. (1953). Limit analysis of two- and three-dimensional soil mechanics problems, J. Mech. Phys. Solids, Vol. 1, pp. 217-226.

46. Drucker, D. C., Gibson, R. E. and Henkel, D. J. (1957). Soil mechanics and work hardening theories of plasticity, Trans., ASCE, Vol. 122, pp. 338-346.

47. Drucker, D. C. (1959). A definition of stable inelastic material, Journal of Applied Mechanics, Transactions ASME, Vol. 26, pp. 106-112.

48. Drucker, D. C. (1960). Plasticity, in J. N. Goodier and N.J. Hoff (Editors), Structural Mechanics, Pergamon Press, London, pp. 407-445.

49. Dunham, R. S., Olson, R. E. and Reese, L. C. (1971). Analysis of a potential sea floor slide at Block 70, Gulf of Mexico, report to Shell Oil Company, offshore Division Construction, Southern E & P Region, ODC Report 27, 150pp.

50. Duwez, P. (1953). On the plasticity of crystals, Phys. Rev., Vol. 47, pp. 494.

51. Eisenberg, M.A. and Phillips, A. (1969). A theory of plasticity with non-coincident yield and loading surfaces, Acta Mech. Vol. 11, pp. 247-260.

52. Engquist, B. and Majda, A. (1977). Absorbing boundary conditions for the numerical simulation of waves, Math. Comp., 31 (139), pp. 629-651.

53. Eringen, A. C. and Ingram, J. D. (1965). A continuum theory of chemically reacting media, Part I., Int. J. Eng. Sci., Vol. 3, pp. 197-212.

54. Eringen, A. C. and Ingram, J. D. (1967). A continuum theory of chemically reacting media, Part II., Int. J. Eng. Sci., Vol. 5, pp. 289-322.

55. Eringen, A. C. (1980). Mechanics of Continua, Kreiger Publishing Co., NY.

56. Finn, W. D. L. and Martin G. R. (1979). Analysis of piled foundations for offshore structures under wave and earthquake loading, Proceedings, paper No.38, Second International Conference on Behavior of Off-shore Structures, London, England.

57. Finn, W.D. L., and Lee, K.W. (1979). Seafloor stability under seismic and wave loading, Presented at Soil Dynamics in the Marine Environment, ASCE National Convention and Exposition, held at Boston, Mass.

58. Finn, W.D.L., Iai, S. and Ishihara, K. (1982). Performance of artificial offshore islands under wave and earthquake loading: field data analyses, Proceedings, Offshore Technology Conference, Houston, Tex., May, Vol.1, paper No. OTC 4220, pp. 661-672.

59. Focht, J. A. and Kraft,L. M.(1977). Progress in marine geotechnical Engineering, J. Geotech. Engng. Div., ASCE 103(GT10), pp. 1097-1118.

60. Frossard, E. (1983). Une équation d'écoulement simple pour les materiaux granulaires. Geotechnique, 33 (1), pp. 21-29.

61. Gatmiri, B. (1990). A simplified finite element analysis of wave-induced effective stress and pore pressures in permeable seabeds, Geotechnique, Vol. 40, No.1, pp.15-30.

62. Ghaboussi, J. and Wilson, E. L. (1972). Variational formulation of dynamics of fluid-saturated porous elastic solids, J. Eng. Mech. Div., ASCE, Vol. 98, No. EM4, pp. 947-963.

63. Ghaboussi, J. and Momen, H. (1982). Modelling and analysis of cyclic behavior of sands, International Symposium on Soils Under Cyclic and Transient Loading, G. Pande and O. C. Ziendiewicz, eds., John Wiley and Sons, Inc., London, U.K., pp. 313-342.

64. Ghaboussi, J. and Momen, H. (1982). Stress dilatancy and normalized work for sands, IUTAM Conference on Deformation and Failure of Granular Materials, Delft, Netherlands, pp. 265-274.

65. Ghaboussi, J. and Momen, H. (1984). Plasticity model for inherently anisotropic behaviour of sands, International Journal for Numerical and Analytical Methods in Geomechanics, Vol. 8, pp. 1-17.

66. Green, A. E. and Naghdi, P. M. (1965). A dynamical theory of interacting continua, Int. J. Eng. 3, pp. 231-241.

67. Habib, P. and Luong, M. P. (1978). Soils pulvurulents sous changement cyclique des materiaux et structures sous changement cyclique, Ass. Amicale des Ingenienrs Anciens Eleives de L'Ecole Nationale de ports et Chaussees, Palaiseau, pp. 49-79.

68. Henkel D. J. (1970). The role of waves in causing submarine landslides, Geotech. 20(1), pp. 75-80.

69. Hill, R. (1950). The Mathematical Theory of Plasticity, Clarendon Press, Oxford, England.

70. Horikawa, K (1978). Coastal Engineering, University of Tokyo Press.

71. Hughes, T. J. R. (1984). Numerical implementation of constitutive models: Rate-

independent deviatoric plasticity, in "Theoretical Foundations for Large Scale Computations of Nonlinear Material Behaviour," S. Nemat-Nasser, R. Asaro and G. Hegemier eds., Martinus Nijhoff Publishers, The Netherlands.

72. Ishihara.,K., Tatsuoka, F. and Yasuda, S. (1975). Undrained deformation and liquefaction of sand under cyclic stresses, Soils and Foundations, Vol. 15, No. 1, pp. 29-44.

73. Ishihara, K. and Okada, S. (1978). Yielding of overconsolidated sand and liquefaction model under cyclic stresses, Soils and Foundations, Vol. 18, No. 1, pp. 31-45

74. Ishihara, K. and Yamazake, F. (1980). Cyclic simple shear tests on saturated sand in multi-directional loading, Soils and Foundations, Vol. 20, No. 1, pp. 45-59.

75. Ishihara, K. and Yamada, Y. (1981). Liquefaction tests using a true triaxial apparatus, Proceedings of the 10th International Conference on Soil Mechanics and Foundation Engineering, Stockholm, Vol. 3, pp. 235-238.

76. Ishihara, K. and Okada, S. (1982). Effects of large preshearing on cyclic behavior of sand, Soils and Foundation, Vol. 22, No.3, pp. 109-125.

77. Ishihara, K. (1983). Soil response in cyclic loading induced by earthquakes, traffic and waves, Lecture presented to the Asian Regional Conference on Soil Mechanics and Foundation Engineering, Haifa, Israel.

78. Iwan, W. D. (1967). On a class of models for the yielding behavior of continuous and composite systems, J. Appl. Mech., Vol. 34, pp. 612-617.

79. Jones, R. E. (1964). A Generalization of the direct-stiffness method of structural analysis, AIAA J., Vol. 2.

80. Kausel, E. (1974). Forced vibrations of circular foundations on layered media, Rept. R 74-11, Soils Pub. 336, Struct. Pub. 384, Dept. of Civil Eng., Mass. Inst. of Tech., Cambridge, Mass.

81. Kausel, E., and Peek, R. (1982). Boundary integral method for stratified soils, Res. Rept. R82-50, Dept. Of Civil Eng. Order No.746, Mass. Inst. of Tech., Cambridge, Mass.

82. Kraft, L. M. Jr and Watkins, D. J. (1976). Prediction of wave-induced seafloor movements, Proceedings, Fifteenth Coastal Engineering Conference, Honolulu, Hawaii, ASCE, Vol. 2, Cpt.49, pp. 1605-1623.

83. Krieg, R. D. (1975). A practical two surface plasticity theory, Journal of Applied Mechanics, Transactions, ASME, Vol. 42, pp. 641-646.

84. Lade, P. V. and Duncan, M. J. (1975). Elasto-plastic stress-strain theory for cohesionless soil, International Journal of Geotechnical Engineering Division, ASCE, Vol. 101, No. GT10, pp. 1037-1053.

85. Lade, P. V. and Duncan, M. J. (1976). Stress-path dependent behaviour or cohesionless soil, International Journal of the Geotechnical Engineering Division, ASCE, Vol. 102, No. GT1, pp. 51-68.

86. Lade, P. V. (1977). Elasto-plastic stress-strain theory for cohesionless soil with curved yield surfaces, International Journal of Solids and Structures, Vol. 13, pp. 1019-1035.

87. Lade, P. V. (1979). Stress-strain theory for normally consolidated clay, Proc. 3rd Int. Conf. Numer. Meth. Geomech., Aachen, Germany, Vol. 4, pp. 1325-1337.

88. Lade, P. V. and Nelson, R. B. (1981). Incrementalization procedure for elasto-plastic constitutive model with multiple, simultaneous yield surfaces, Proceedings of the symposium on the Implementation of the Computer Procedures and stress-strain laws in geotechnical engineering, Chicago, pp. 503-518.

89. Lade, P. V. (1982). Three-dimensional behavior and parameter evaluation for an elasto-plastic soil model, Proceedings of the International Symposium on Numerical Models in Geomechanics, Zurich, pp. 33-37.

90. Lee, K. L., and Focht, J. A. (1975). Liquefaction potential of Ekofisk Tank in North Sea, Journal of the Geotechnical Engineering Division, ASCE, Vol. 100, No. GT1, pp. 1-18.

91. Liao, Z. P. and Wong, H. L. (1984). A transmitting boundary for the numerical simulation of elastic wave propagation, Soil Dynamics and Earthquake Engng., Vol. 3 (4), pp. 174-183.

92. Lindman, E. L. (1973). On getting all of the waves out of the box proc. Sixth Conf. on Numerical Simulation of Plasmas, Lawrence Berkeley Laboratory, Berkeley, Calif., pp. 42-45.

93. Lindman, E. L. (1975). Free-space boundary conditions for the time-dependent wave equation, J. of Computational Physics, Vol.18, pp. 66-78.

94. Liu, P. F. (1977). On gravity waves propagated over a layered permeable bed, J. Coastal Engng., Vol.1, pp. 135-148.

95. Lynn, P. P. and Hadid, H. A. (1981). Infinite elements with $1/r^n$ type decay, Int. J. Num. Meth. Engng., Vol 17, No.3, pp. 347-355.

96. Lysmer, J. and Kuhlemeyer, R. L. (1969). Finite dynamic model for infinite media, Journal of Engineering Mechanics Division, Proc., ASCE, EM4.

97. Lysmer, J. and Waas, G. (1972). Shear waves in plane infinite structures, J. Eng. Mech. Div., ASCE, 98(EM1), pp. 85-105.

98. Madsen A. S. (1978). Wave induced pore pressures and effective stresses in porous bed, Geotechnique, Vol. 28, pp. 377-393.

99. Mallard, W. and Dalrymple, R. A. (1977). Water waves propagating over a deformable bottom, Proceedings, Ninth Annual Offshore Technology Conference, Houston, Tex., pp. 141-146.

100. Malvern, L. E. (1969). Introduction to the Mechanics of a Continuous Medium, Prentice-Hall, NJ.

101. Marques, J.M.M.C. (1984). Stress computations in elastoplasticity, Engineering Computations, Vol. 11. pp. 42-51.

102. Martin, P. P., Finn, W. D. L. and Seed, H. B. (1975). Fundamentals of liquefaction under cyclic loading, Journal of the Geotechnical Engineering Division, ASCE, Vol. 101, pp. 428-438.

103. Martin, P. P. and Seed, H. B. (1979). Simplified procedure for effective stress analysis of ground response, Journal of the Geotechnical Engineering Division, ASCE, Vol. 105, pp. 739-758.

104. Masing, G. (1926). Eigenspannungen and Verfestigung beim Messing, Proc. 2nd Int. Congress of Applied Mechanics, Zurich, Switzerland.

105. Medina -Melo, F. J. (1981). Modelling of Soil-Structure Interaction by Finite and Infinite Elements. Ph.D. Thesis, University of California, Berkeley.

106. Moroto, N. (1976). A new parameter to measure degree of shear deformation of Granular material in triaxial compression tests, Soils and Foundations, Vol. 16, No. 4, pp. 1-9.

107. Morse, P.M. and Feshback, H. (1953). Methods of Theoretical Physics, McGraw-Hill Book Company, New York.

108. Moshagen, H. and Tørum, A. (1975). Wave induced pressures in permeable seabeds, Journal of Waterways, Harbor and Coastal Engineering, ASCE, Vol.101, No.WW1, pp. 49-58.

109. Mroz, Z. (1967). On the description of anisotropic hardening. Journal of the Mechanics and Physics of Solids, Vol. 15, pp. 163-175.

110. Mroz, Z., Norris, V. A. and Zienkiewicz, O. C. (1978). An anisotropic hardening model for soils and its application in cyclic loading, International Journal for Numerical and Analytical Methods in Geomechanics, Vol. 2, pp. 203-221.

188

111. Mroz, Z., Norris, V. A. and Zienkiewicz, O. C. (1979). Application of an anisotropic hardening model in analysis of elastic-plastic deformation of soils, Geotechnique, No. 29, pp. 1-34.

112. Mroz, Z. (1980). Hypoelasticity and plasticity approaches to constitutive modeling of inelastic behaviour of soils, International Journal for Numerical and Analytical Methods in Geomechanics, Vol. 4, pp. 45-55.

113. Mroz, Z. and Pietrusz zak, S. (1983). On hardening anisotropy of K_0-consolidated clays, International Journal for Numerical and Analytical Methods in Geomechanics, Vol. 7, pp. 19-38.

114. Mroz, Z. and Pietruszczak, S. (1983). A constitutive model for sand with anisotropic hardening rule, Int. J. Num. Anal. Meth. Geomech., Vol. 7, pp. 305-320.

115. Nataraja, M. S. and Gill, H.S. (1983). Ocean wave-induced liquefaction analysis, Proc., ASCE, Vol. 109, GT4, pp. 573-590.

116. Nova, R. (1982). A constitutive model for soil under monotonic and cyclic loading, in G.N. Pande and O. C. Zienkiewicz (eds.), Soil Mechanics-Transient and Cyclic Loads, Wiley, Chichester, Ch 13, pp. 343-375.

117. Oden, J.T. (1969). A general theory of finite element II: Applications, Int. J. Numer. Methods Eng., Vol. 1, No.3,

118. Ortiz, M. and Popov, E.P. (1985). Accuracy and stability of integration algorithms for elastoplastic constitutive relations, Int. J. Numer. Meth. Engng., Vol. 21, pp. 1561.

119. Owen, D.R.J., Marques, J.M.M.C. and Cesae de sa, J.M.A. (1986). Reliability considerations in the numerical solution of elasto-plastic, visco-plastic and flow problems, In Reliability of Methods for Engineering Analysis, ed. K. J. Bathe and D.R.J. Owen, Pineridge Press, Swansea, pp. 221-254.

120. Palmer, A. C., Editor (1973). Proceedings of the symposium on the Role of Plasticity in Soil Mechanics, Cambridge University, Cambridge, England, 314 pp.

121. Pande, G. N. and Zienkiewicz, O. C., Editors (1980). Proceedings of the International Symposium on soils Under Cyclic and Transient Loading, Balkema, Rotterdam.

122. Pande, G. N. and Pietruszczak, S. (1982). Reflecting surface model for soils, Proc. Int. Symp. on Num. Meth. in Geomechanics, Zurich, Editors, R. Dungar, G. N. Pande and J. A. Studer, Balkema, Rotherdam, pp. 50-64.

123. Park, K. C. (1980). Partitioned transient analysis procedures for coupled - field problems: stability analysis, J. Appl. Mech. ASME, Vol.47, pp. 370-376.

124. Park, K. C. and Felippa, C. A. (1980). Partitioned transient analysis procedures for coupled-field problems: Accuracy analysis, J. Appl. Mech. ASME, Vol. 47, pp. 919-926.

125. Parry, R. H. G., Editor (1972). Roscoe Memorial Symposium: Stress-Strain Behaviour of Soils, Henley-on-Thames, Cambridge University, England, 752pp.

126. Pietruszczak, S. and Stolle, D. F. E. (1987). Modelling of sand behaviour under earthquake excitation, Int. J. Num. Anal. Meth. Geomech. Vol. 11, pp. 221-240.

127. Poorooshasb, H. B. (1961). Properties of Sands and Granular Media in Simple Shear, Ph.D. Thesis, University of Cambridge.

128. Poorooshasb, H. B., Holubec, I. and Sherbourne, A. N. (1966). Yielding and flow of sand in triaxial compression, Part 1, Can. Geotech. J., 3, pp. 179-190.

129. Poorooshasb, H. B., Holubec, I. and Sherbourne, A. N. (1967). Yielding and flow of sand in triaxial compression, Part 2, Can. Geotech. J., 4, pp. 376-397.

130. Poorooshasb, H. B. and Pietruszczak, S. (1985). On yielding flow of sand; a generalized two-surface model, Computers and Geotechnics, Vol. 1, pp. 33-58.

131. Poorooshasb, H. B. and Pietruszczak, S. (1986). A generalized flow theory for sand, Soils and Foundations, Vol. 26 (2), pp. 1-15.

132. Poorooshasb, H. B., Ishihara, K. and Yang Q. S. (1987). Action of standing waves on seabed sands, in Proc. Int. Conf. on Computational Engineering Mechanics, Beijing, pp. 146-151.

133. Poorooshasb, H. B., Yang, Q. S. and Clark, J. I. (1990). Non-linear analysis of a seabed deposit subjected to the action of standing waves, Mathl. Comput. Modelling, Vol. 13, No.4, pp. 45-58.

134. Prevost. J. H. (1977). Mathematical modeling of monotonic and cyclic undrained clay behaviour, Int. J. Numer. Analyt. Meth. Geomech., Vol. 1, pp. 195-216.

135. Prevost. J. H. (1978). Plasticity theory for soil stress behavior, J. Eng. Mech. Div., ASCE, 104(EM5), pp. 1177-1194.

136. Prevost, J. H. (1978). Anisotropic undrained stress-strain behaviour of clays, J. Geotech. Eng. Div., ASCE, 104 (GT8), pp. 1075-1090.

137. Prevost. J. H. (1979). Mathematical modeling of soil stress-strain-strength behaviour, Proceeding of the 3rd International Conference on Numerical Methods in Geomehanics, Aachen, pp. 347-361.

138. Prevost, J. H. (1980). Mechanics of continuous porous media, International Journal of Engineering Science, 18 (5), pp. 787-800.

139. Prevost, J. H. (1981). Constitutive equations for soil media, Proceeding of the NATO Advanced Study Ins., Conference on Numerical Methods in Geomechanics, Vimeiro, Portugal, pp. 79-101.

140. Putnam, J. A., (1949). Loss of wAve energy due to percolation in a permeable sea bottom, Transactions, American Geophysical Union, Vol.30, pp. 349-356.

141. Roscoe, K. H., Scofield, H. N. and Wroth, C. P. (1958). On the yielding of soils, Geotechnique, Vol. 8. No. 1, pp. 22-53.

142. Roscoe, K. H., Schofield, A. N. and Thurairjah, A. (1963). Yielding of clays in state wetter than critical, Geotechnique, Vol. 13, No. 3, pp. 211-240.

143. Roscoe, K. H. and Burland , J. B. (1968). On the generalized stress-strain behaviour of wet clay, Engineering Plasticity, J. Heyman and F. Leckie, eds., Cambridge University Press, Cambridge, England, pp. 535-609.

144. Saini, S.S.,Bettess, P. and Zienkiewicz, O.C. (1978). Coupled hydrodynamic response of concrete gravity dams using finite and infinite elements, Earthquake Engineering and Structural Dynamics, Vol 16, pp. 3ᴄ3-374.

145. Sandhu, R. S. and Wilson, E. L. (1969). Finite-element analysis of seepage in elastic media, J. Eng. Mech. Div., ASCE, Vol.95, pp. 641-652 .

146. Sandhu, R. S., Liu, H. and Singh, K. J. (1977). Numerical performance of some finite scheme for analysis of seepage in porous elastic media, Int. J. Numer. Analyt. Methods in Geomech, Vol.1, No.2, pp. 177-195.

147. Schofield, A. N. and Wroth, C. P. (1968). Critical State Soil Mechanics, McGraw-Hill, Inc., London, England.

148. Seed, H. B. and Lee, K. L. (1966). Liquefaction of saturated sands during cyclic loading, Journal of the Soil Mechanics and Foundation division, ASCE, Vol. 92, No. SM6, pp. 105-134.

149. Seed, H. and Idriss, I. M. (1971). Simplified procedure for evaluating soil liquefaction potential, Journal of the Soil Mechanics and Foundations, Division, ASCE, Vol.97, No. SM9, pp. 1249-1273.

150. Seed, H. B. and Peacock, W. H. (1971). Test procedures for Measuring soil liquefaction characteristics, Journal of the Soil Mechanics and Foundation Division, ASCE, Vol. 97, No. SM8, pp. 1099-1119.

151. Seed, H. B., Lee, K. L., Idriss, I. M. and Makdisi, F. I. (1973). Analysis of the slides in the Sea Fernando dams during the earthquake of February 9, 1971,

Report No. EERC 73-2, Earthquake Engineering Research Center, Univ. of California, Berkeley.

152. Seed, H. B., Martin, P. P. and Lysmer, J. (1976). Pore-water pressure changes during soil liquefaction, Journal of the Geotechnical Engineering Division, ASCE, Vol. 192, No. GT4, pp. 323-346.

153. Seed, H. B. and Rahman, M. S. (1977). Analysis for wave-induced liquefaction in relation to Ocean floor stability, Report on Research Sponsored by the National Science Foundation, Report No. UCB TE-77/02.

154. Seed, H. B. and Rahman, M. S. (1978). WAve-Induced pore pressure in relation to ocean floor stability of cohesionless soils, Marine Geotechnology, Vol.3, No. 2, pp. 123-150.

155. Seed, H.B. (1979). Soil liquefaction and cyclic mobility evaluation for level ground during earthquakes, Journal of the Geotechnical Engineering Division, ASCE, Vol. 105, No. GT2, Proc. paper 14380, pp. 201-255.

156. Shield, R. T. (1955). On Coulomb's law of failure in soils, J. Mech. Phys. Solids, Vol.4, pp. 10-16.

157. Siddharthan, R., and Finn, W. D. Liam (1979). STAB-MAX: Analysis of Instantaneous Instability Induced in Seafloor Sands by Large Waves, Soil Dynamics Group, Faculty of Graduate Studies, University of British Columbia, Vancouver, British Columbia, Canada.

158. Siddharthan, R. (1987). Wave-induced displacements in seafloor sands, International Journal for Numerical and Analytical Methods in Geomechanics, Vol. 11, pp. 155-170.

159. Simo, J.C. and Taylor, R.L. (1985). Consistent tangent operators for rate-independent elastoplasticity Comp. Meth. Appl. Mech. Engng., Vol. 48, pp. 101-118.

160. Simo, J.C. and Taylor, R.L. (1986). A consistent return mapping algorithm for plane strain elastoplasticity, Int. J. Num. Meth. Engng., Vol. 22, pp. 649-670.

161. Sleath, J. F. A. (1970). Wave-induced pressure in beds of sand, Journal of the Hydraulics Division, ASCE, Vol. 96, No. HY2, pp. 367-378.

162. Smith, W. D. (1974). A non-reflecting plane boundary for wave propagation problems, J. Comp. Phys., Vol . 15, pp. 493-503.

163. Sokolovsky, V. V. (1965). Statics of Granular Media, Pergamon Press, New York, N.Y., 232pp.

164. Stroud, M. A. (1971). The Behaviour of Sand at Low Stress Level in the Simple Shear Apparatus, Ph.D. Thesis, University of Cambridge.

165. Tatsuoka, F. and Ishihara, K. (1974). Yielding of sand in triaxial compression, Soils and Foundations, Vol. 14, No. 2, pp. 63-76.

166. Tatsuoka, F. and Ishihara, K. (1974). Drained deformation of sand under cyclic stress reversing direction, Soils and Foundations, Vol. 14, No. 3, pp. 51-65.

167. Tatsuoka, F. (1980). Stress-strain behavior of an idealized anisotropic granular material, Soils and Foundations, Vol. 20, No. 3, pp. 75-90.

168. Tatsuoka, F., Masashige, M. and Sasaki, T. (1982). Cyclic undrained stress-strain behavior of dense sands by torsional simple shear test, Soils and Foundations, Vol. 22, No. 2, pp. 55-70.

169. Terzaghi, K. (1943). Theoretical Soil Mechanics, Wiley, New York.

170. Truesdell, C. and Toupin, R. (1960). The Classical Field Theories, Handbuch der Physik ,Editor, S. Flugge, Springer-Verlage, Berlin, Vol. III/1.

171. Vermeer, P. A. and Verruijt, A. (1981). An accuracy condition for consolidation by finite elements, Int. J. Numer. Analyt. Methods in Geomech., Vol.5, No.1, 1-14.

172. William, K. T. and Wande, E. P. (1975). Constitutive models for the triaxial behavior of concrete, Proc. Int. Ass. Bridge Struct. Engng., Vol. 19, pp. 1-30.

173. Wright, S.G. and Dunham, R. S. (1972). Bottom stability under wave-induced loading, Preprints, Fourth Annual Offshore Technology Conference, Houston, Tex., Vol. 1, Paper No. OCT 1603, pp. 853-862.

174. Wright, S. G. (1976). Analyses for wave induced sea-floor movements, Proceedings, Eighth Annual Offshore Technology Conference, Houston, Tex., Vol.1, Paper No. OCT 2427, pp. 41-53.

175. Yamamoto, T. (1978). Seabed instability from waves, Proc. 10th Annual Offshore Technology Conferences, paper 3262 1, Houston, Texas, 1819-1824.

176. Yamamoto, T. (1981). Wave induced pore pressures and effective stresses in inhomogeneous sea bed foundations, J. Ocean Engng., 8, 1-16.

177. Yang, Q. S. (1986). Computer programming and numerical simulation of cyclic loading tests for the generalized two-surface elastoplastic constitutive model, Internal Report, Civil Engineering Department, Concordia university, 1986.

178. Yang, Q. S., Poorooshasb, H. B. and Yong, R. N. (1987). The general formulations of plasticity in stress-space and in strain-space, in Proceedings of the Second International Conference on Constitutive Laws for Engineering Materials: Theory and Applications, Tucson, U.S.A., Vol. 1, pp. 353-360.

179. Yong, R. N. and Ko, H. Y., Editors (1981). Limit Equilibrium, Plasticity and Generalized stress-strain in Geotechnical Engineering, ASCE, New York, N.Y., 871pp.

180. Yong, R. N. and Selig, E. T., Editors (1982). Application of Plasticity and Generalized Stress-strain in geotechnical Engineering, ASCE, New York., 356pp.

181. Zienkiewicz, O.C. and Cheung, Y.K. (1965). Finite elements in the solution of field problems, Engineer, Vol. 220.

182. Zienkiewicz, O. C. and Newton, R. E. (1969). Couple vibrations of a structure immersed in a compressible fluid, Proc. of the Symposium on Finite Element Techniques, Stuttgart.

183. Zienkiewicz, O. C. and Bettess, P. (1976). Infinite Elements in the Study of Fluid Structure Interaction Problems. Lecture Notes in Physics, Springer Verlag, No. 58, pp. 133-172.

184. Zienkiewicz, O. C. (1977). The Finite Element Method, 3rd edition, McGraw-Hill, London.

185. Zienkiewicz, O. C., Norris, V. A. and Naylor, D. J. (1977). Plasticity and viscoplasticity in soil mechanics with special reference to cyclic loading problems, in Finite Elements in Non-linear Mechanics, Vol. 2, pp. 455-485, Editor, P. G. Bergan et al., Tapir, Trondheim,

186. Zienkiewicz, O. C., Humpheson, C. and Lewis, R. W. (1977). A unified approach to soil mechanics problems (including plasticity and visco-plasticity), in "Finite Elements in Geomechanics", Ch. 4, 151-178, Ed. G. Gudehus, John Wiley and Sons, New York.

187. Zienkiewicz, O. C., Kelly, D.W. and Bettess, P. (1977). The sommerfeld (radiation) condition on infinite domains and its modelling in numerical procedures, Computer Methods in Applied Sciences and Engineering, Third International Symposium, IRIA Laboria, December.

188. Zienkiewicz, O. C., Leung, K. H., Hinton, E., and Chang, C. T. (1980). Liquefaction and permanent deformation under dynamic conditions-numerical solutions and constitutive relations, International Symposium on Soils Under Cyclic and Transient Loading, G. N. Pande and O. C. Zienkiewicz, eds., John wiley and Sons, Inc., London, U. K., pp. 71-103.

196

189. Zienkiewicz, O. C., Chang, C. T. and Bettess, P. (1980). Drained, undrained, consolidating and dynamic behaviour assumptions in soils, Limits of validity, Geotechnique, No. 30, pp. 385-395.

190. Zienkiewicz, O. C. and Bettess P. (1982). Soils and other saturated media under transient, dynamic conditions; General formulation and the validity of various simplifying assumptions, International Symposium on Soils Under Cyclic and Transient Loading, G. N. Pande and O. C. Zienkiewicz, eds., John Wiley and Sons, Inc., London, U.K., pp. 1-16.

191. Zienkiewicz, O. C. (1984). Coupled problems and their numerical solution. Chapter 1, in Numerical Methods in Coupled Systems, Edited by R. W. Lewis, P. Bettess and E. Hinton, John Wiley & Sons Ltd.

192. Zienkiewicz, O. C. and Mroz, Z. (1984). Generalized plasticity formulation and applications to geomechanics, in Mechanics of Engineering Materials, Editor, C. S. Desai and R. H. Gallagher, Wiley, Ch. 33. pp. 655-679.

193. Zienkiewicz, O. C. and Shiomi, T. (1984). Dynamic behaviour of saturated porous media; The generalized Biot formulation and its numerical solution, International Journal for Numerical and Analytical Methods in Geomechanics, Vol. 8, pp. 71-96.